

Reproduced by



CENTRAL AIR DOCUMENTS OFFICE

WRIGHT-PATTERSON AIR FORCE BASE - DAYTON, OHIO

EEL-C

4458

T.I

77510

"NOTICE: When Government or other drawings, specifications or other data are used for any purpose other than in connection with a definitely related Government procurement operation, the U.S. Government thereby incurs no responsibility, nor any obligation whatsoever; and the fact that the Government may have formulated, furnished, or in any way supplied the said drawings, specifications or other data is not to be regarded by implication or otherwise as in any manner licensing the holder or any other person or corporation, or conveying any rights or permission to manufacture, use or sell any patented invention that may in any way be related thereto."

UNCLASSIFIED

ATI No 77,549

C. DO FILE COPY

AF TECHNICAL REPORT No. 5985
(Revised Jan. 1951)

May 1950

STUDIES ON THE VALIDITY OF THE HYDRAULIC
ANALOGY TO SUPERSONIC FLOW

Parts I and II

Massachusetts Institute of Technology

United States Air Force
Air Materiel Command
Wright-Patterson Air Force Base, Dayton, Ohio

AF TECHNICAL REPORT NO. 5985, Part I

May 1950

STUDIES ON THE VALIDITY OF THE HYDRAULIC
ANALOGY TO SUPERSONIC FLOW

Part I

Massachusetts Institute of Technology

United States Air Force
Air Materiel Command
Wright-Patterson Air Force Base, Dayton, Ohio

FOREWORD

This report was prepared by Donald R. F. Harleman under the direction of Dr. Arthur T. Ippen, Professor of Hydraulics, Department of Civil and Sanitary Engineering, Massachusetts Institute of Technology, under USAF Contract Number W33-038-ac-16703. The contract was initiated under the research and development project, identified by Expenditure Order Number 458-413, and it was administered under the direction of the Aircraft Laboratory, Engineering Division, Air Materiel Command, with Mr. Joseph Flatt acting as project engineer.

ACKNOWLEDGEMENT

This study was initiated originally by Dr. Arthur T. Ippen who acted as project supervisor for the Division of Industrial Cooperation of the Massachusetts Institute of Technology. The design and construction phases were carried on by Mr. Donald R. F. Harleman, Research Associate, with the aid of Mr. Charles E. Carver, Research Assistant in the Department of Civil and Sanitary Engineering. Professor Emeritus George E. Russell and Mr. George R. Higgins contributed greatly in the preparation of the report material. During the construction and erection of the channel, valuable cooperation was received from the technical staff of the laboratory.

ABSTRACT

The primary concern of Part I of this research program is the design, construction, adjustment and calibration of a supercritical flow channel best suited for experimental investigations on the hydraulic analogy to supersonic flow.

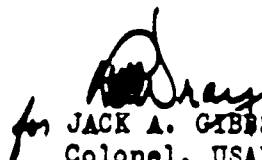
A comprehensive review of previous experimental work both on supercritical flow and on the hydraulic analogy was prepared in order that the design of the channel might benefit from past experience. The construction features of the channel are described in detail.

The instrumentation of the channel together with a description of the method of setting up initial flow conditions is also discussed. It is concluded that the operation of the channel after adjustment and calibration conformed to the original specifications and that it constitutes a useful research facility.

PUBLICATION REVIEW

Manuscript Copy of this report has been reviewed and found satisfactory for publication.

FOR THE COMMANDING GENERAL:

 LT. Col., USAF
for JACK A. GIBBS
Colonel, USAF
Chief, Aircraft Laboratory
Engineering Division

CONTENTS

<u>Section</u>	<u>Page No.</u>
I	Review of Previous Experimental Work 1
	1. A. T. Ippen and R. T. Knapp. Experimental Investigations of Flow in Curved Channels 1
	2. E. Preiswerk. Application of the Methods of Gas Dynamics to Water Flows with a Free Surface 1
	3. Johnson and Witbeck. Water Analogy to Two-Dimensional Air Flow. General Electric Company 2
	4. North American Aviation Inc. Application of the Water Channel - Compressible Gas Analogy 2
	5. Department of Civil and Sanitary Engineering, MIT. Investigations on Hydraulic Shock Waves 4
	6. Mechanical Engineering Department, MIT. Hydraulic Analogy Investigations. Project Meteor 5
	7. H. Rouse, B. V. Bhoota, E-Y. Hsu. Design of Channel Expansions. State University of Iowa 6
	8. California Institute of Technology. Analogy between Surface Shock Waves in a Liquid and Shocks in Compressible Gases 6
	9. National Advisory Committee for Aeronautics. Application of the Analogy between Water Flow with a Free Surface and Two-Dimensional Compressible Gas Flow 7
II	Design, Construction and Calibration of the Supercritical Flow Channel 8
	1. Study of Basic Requirements 8
	2. Design and Construction of the Supercritical Flow Channel 10
	3. Adjustment and Calibration of Channel 17
	4. Instrumentation 18
	5. Method of Obtaining a Desired Froude Number 23
	6. The Deflector Vane for Obtaining Oblique Shock-Waves 28
III	Conclusions 29
	Bibliography - See page 94 and following USAF-TR-5985, PART II

ILLUSTRATIONS

<u>Fig.</u>		<u>Page No.</u>
1	Supercritical Flow Channel - General Assembly	11
2	General View of Supercritical Flow Channel Looking Upstream	12
3	Upstream View of Channel Interior Showing Glass Bottom	13
4	Downstream End Truss Hinge Mounts Showing Discharge Pipe, Ball and Socket Joint and Rubber Coupling to Pump	13
5	Detail of Spindle Lifting Mechanism Showing Micro- Switch Control	13
6	View of Allis-Chalmers Circulating Pump	15
7	View Upstream of Entrance Nozzle with Lifting Mechanism	15
8	Slope Calibration Curve	19
9	Nozzle Calibration Curve	20
10	Point Gage Attached to Crossrail of Traveling Carriage	22
11	Details of Ames-Dial Point Gage	22
12	Comparison of Velocity Distributions Obtained by Various Instruments	24
13	Prandtl Type Pitot Tube Mounted on Traveling Carriage .	25
14	Simple Glass Impact Tube with Carriage Mounting	25
15	Slope and Depth vs Froude Number for Different Rates of Flow	27

SECTION I

REVIEW OF PREVIOUS EXPERIMENTAL WORK

The design of a high velocity water channel which would be best suited for experimental work dealing with the hydraulic analogy is the primary concern of Phase I of this research project. Accordingly, a careful study of previous research was undertaken in order to benefit from suggestions and observations of previous investigators. Abstracts of the pertinent investigations which were studied are presented below.

1. A. T. Ippen and R. T. Knapp. Experimental Investigations of Flow in Curved Channels. (Ref. 1a, 1b, 1c)

In 1935-36, Ippen and Knapp demonstrated for the first time experimentally, the application of the methods of supersonic gas dynamics to hydraulic problems. The fact that the analogy exists had been pointed out by Riabouchinsky (Ref. 2) and von Karman (Ref. 3). Ippen and Knapp undertook a study of the fundamental nature of the curvilinear flow of liquids in an open channel. The basic equipment used in the experimental work consisted of a 12" and later of an 18" channel on a tilting platform 100 feet long. Circular arc curves were inserted into the channel which resulted in transverse disturbances and shock waves crossing the stream periodically and causing alternating depth changes of large magnitude along the walls.

The flow through complex curves specially designed by the method of characteristics to minimize periodic vertical depth changes was also studied but did not lead to practical solutions for such hydraulic structures. Depths of from 1/2" to 4" were used with velocities up to 15 fps. corresponding to Froude numbers from 2 through 5. Satisfactory quantitative agreement between theory and experiment was obtained for water profiles along the side walls up to the point of the first maximum of the depth profile. Beyond this location, the agreement was less satisfactory because damping is neglected in the theory, and the errors due to boundary resistance along the side walls are cumulative.

2. E. Preiswerk. Application of the Methods of Gas Dynamics to Water Flows with a Free Surface. (Ref. 4)

In 1938 Preiswerk extended the theory of the hydraulic analogy for both isentropic flow and flow with shocks and conducted some experiments designed to show the applicability of the analogy to aerodynamic problems. The experiments, while not extensive, served to indicate the usefulness of the analogy as a research tool. A small, fixed slope water channel was used in which supercritical flow was produced by a Laval nozzle designed by the method of characteristics. The nozzle had a throat

of approximately 8 inches and an exit Mach number of 2. The main purpose of the experimental program was to determine the performance of the nozzle under various entrance depths ranging from 4 inches to 1 inch and from 1 inch to 0.3 inches at the exit section.

Satisfactory quantitative agreement for the water surface profiles through the nozzle was obtained at practically all initial depths; however, better agreement was found for the smaller depths. The discrepancies at larger depths are attributed to large vertical accelerations which are neglected by the theory. The influence of bottom and side wall boundary layers upon the flow characteristics of the Laval nozzle was also investigated. The experiments were conducted with a high degree of accuracy, and the results provide substantial verification of the characteristics method in water.

3. Johnson & Witbeck. Water Analogy to Two-Dimensional Air Flow.
General Electric Company. (Ref. 5)

In 1941, the General Electric Company reported the use of a water table in which passages for ram-jets and other aerodynamic devices were to be studied. The working section was approximately one foot wide, and the water was accelerated by means of a dam with a spillway section discharging onto a glass plate. Thus a flow was produced at Mach numbers greater than unity presumably with small depths. The models were located at the foot of the spillway, and the resulting patterns of flow were photographed by means of a shadowgraph method. It was stated that pressure distributions were obtained by painting the model with a water soluble dye which washed off the submerged portion, thus leaving a record of the water depth distribution.

The static pressure was then determined from the square of the depth ratio as required by the analogy. No statement is made as to the accuracy obtained with this method nor are any quantitative data given.

4. North American Aviation Inc. Application of the Water Channel - Compressible Gas Analogy. (Ref. 6)

The North American Aviation Company has used a water channel four feet wide and twenty feet long to conduct a series of tests on the analogy. The water is stationary, and models are towed through the water by means of a travelling carriage. Variations in Mach number are obtained by holding the speed of the carriage constant and varying the depths of the water. Accelerated or decelerated motion of the carriage is also possible.

Advantages and disadvantages of this type of channel are as follows:

a. The depth distribution around the model is necessary for a quantitative application of the analogy. This is simple in the case where the water moves past a stationary model, but quite difficult for the converse case. Two electro-mechanical means are suggested. One is to measure the depths by means of the varying resistance between two stationary vertical electrodes. The second is to measure the position, at instant of contact, of a vertically oscillating electrode. No accurate mechanical method of measuring the water depth or pressure has been found to be feasible, and the electro-mechanical methods had not been fully developed at the time of the report. Should such a device prove feasible, it would, at the most, give water depths relative to the model at only a few points, whereas a large number of points are required for accuracy.

b. Shock wave angles must be measured from pictures photographed from the moving carriage. Since the photographs are usually obtained by the shadowgraph method or other means dependent on the refraction of light rays by a curved water surface, the question arises as to the reliability of these methods. It has been observed that the undular type of oblique jump has a crest of sharp curvature behind the actual wave front. Therefore, wave angles observed by this method are subject to considerable difficulties in interpretation.

In a series of tests made in the North American channel, the effect of static water depth and model size on the shock-wave angle for a given deflection angle were obtained. The static water depth was varied from 0.1 inches to 1.0 inches. Best agreement with theory was obtained in the range 0.2 inches to 0.3 inches, here the ratio $\sin \beta$ (theor.) / $\sin \beta$ (exp.) varied from 95% to 115%. At a static water depth of 1.0 inch this same ratio varied from 130% to 175% depending on the combination of model length and deflection angle. The models used varied in length from 3 inches to 10 inches, and the deflection angles from 3° to 12° . It was not possible to calculate the corresponding Mach numbers as the speeds with which the models were towed through the tank were not given. It is seen that in most cases, the experimental angles were too small which may have been due to the optical method of determination. The report concludes that the optimum water depth is .25 inches which is the depth predicted for minimum effects of capillarity.

c. The advantages obtained from this type of channel are primarily:

(1) the flexibility and ease of determination of the Mach number from the speed of the carriage and the still water depth.

(2) the ease with which transient phenomena may be observed.

An experimental investigation of several techniques for obtaining photographs of shock waves in the water channel was also undertaken by North American (Ref. 7) with best results obtained by the absorption technique. The absorption method is based on the fact that the transmission of light through dye colored water is a function of the water depth. Hence, when waves are formed in the towing basin, which is illuminated from below, the wave crests and troughs will show up as relatively light and dark areas. By photometric measurements on the negative film, it is possible to obtain quantitative information on the contours of the waves. Calibration cells containing known depths of the liquid are placed at the edge of the towing basin, and each picture then carries its own calibration."

5. Department of Civil & Sanitary Engineering, M.I.T. Investigations on Hydraulic Shock Waves. (Ref. 8, 8a, 16a, 16c)

Theoretical as well as experimental investigations on hydraulic shock waves have been carried on by A. T. Ippen at Lehigh University and also at M.I.T. which led to a comprehensive summary of the theory of supercritical flow of water in open channels which corresponds to the two-dimensional supersonic flow of gas. All the findings are contained in Ref. 16a. Specific applications of the theory to the design of channel contractions led to the experiments reported in Ref. 16c which gave in a number of cases good quantitative agreement between theory and experiments for a variety of boundary conditions. For these experiments on channel contractions, a tilting channel 3 feet wide and 10 feet in length was constructed in 1946 in which Barschdorf and Woodbury (Ref. 8) conducted a series of experiments on oblique shock waves in water.

Due to the limitations of the available equipment, the water was accelerated by means of a vertical sluice with a free surface upstream of the gate. Control of the depth was secured by vertical adjustment of the sluice, while uniform flow was obtained by adjusting the slope of the channel by means of jacks at the lower end. The primary tests were made at an initial depth of approximately 0.90 inches and an initial Froude number of 3.86. Oblique shocks were generated by means of movable side walls which produced the required deflection of the flow. Depth profiles of the water surface were obtained with a standard vernier point gage mounted on a travelling carriage. Good quantitative agreement was found for the depth ratio across the shock and the shock wave angle for the various deflection angles at the one Froude number tested.

Several disadvantages of this type of channel were made evident by this research:

1. The range of Froude numbers is limited by the static depth behind the sluice.

2. Surface disturbances are caused by vortices which form in back of the sluice and are carried out into the supercritical flow.

3. The channel had an aluminum floor which prevented lighting from below for photographic purposes.

Much valuable information was obtained for the design of the large supercritical flow channel used in the research described in this report. In addition, many of the experimental techniques used were developed on this small channel, and many changes incorporated in the final channel design were tested here.

6. Mechanical Engineering Department, M.I.T. Hydraulic Analogy Investigations. Project Meteor. (Ref. 9, 10, 11, 12, 31)

During 1946, there was also instituted in the Mechanical Engineering Department under the direction of Dr. A. H. Shapiro a research program dealing with the hydraulic analogy in connection with Project Meteor. To date this program has been the subject of four reports in the form of theses.

Goldman and Meerbaum (Ref. 9) constructed a fixed slope channel of 8 ft. length with a working section approximately 2 ft. by 2 ft. consisting of a glass floor supported on a steel frame. Supercritical flow at a Froude number of 2 was obtained by a 4 foot Laval type nozzle constructed of wood. Photographic technique was investigated for flow around diamond and bullet shaped models approximately 8 inches in length with an initial depth of 2 inches. No quantitative measurements were obtained. Mumford (Ref. 10) replaced the wooden nozzle which had warped, with a metal contour and continued the development of technique. Attempts were made to obtain streamlines by injection of dye, and good results were obtained with the shadowgraph technique of photographing wave patterns.

In 1948, Langtry (Ref. 11) replaced the Laval nozzle by a sluice-type nozzle because of disturbance waves which persisted in the nozzle. The initial Mach number was determined by measuring the stagnation depth at a point in the stream. This device was calibrated by measuring the oblique shock wave produced by a deflecting plate of approximately 6 inches length; the corresponding calculated Mach number was compared to the value obtained from the stagnation depth. Very good agreement was obtained at initial depth of 1/4 inch; however, at initial depth of 3/4 inch, errors ranging from 10% to 40% were observed. The writer believes that the length of the deflector plate was too short to give good results for the higher velocities necessitated by the larger depth. The Phase II report confirms the observation that the initial portion of the shock wave is distorted due to local vertical accelerations and that the length of the deflector plate is of considerable importance in this respect.

The remainder of the experimental work in Ref. 11 consisted of a study of the flow pattern in a supersonic diffuser. Good qualitative results were obtained, and much valuable information was gained on such problems as starting and choking of a supersonic diffuser. Giraud (Ref. 12) continued this work to study supersonic cascade arrangements. A few oblique shock wave contours were measured, but considerable difficulty was encountered in correlating the Mach number calculated from the stagnation depth with the Mach number obtained from the shock angle. Also curvature of the shocks was noticed in the plan views. All measurements were taken within 10 inches of the front edge of the deflector plate. Some experiments of a shock followed by an expansion were again difficult to correlate quantitatively; in this case, the deflector plate was only 1 inch long and about $5/16$ inch in front projection for an initial depth of $1/8$ inch. In general, excellent results were obtained on the qualitative studies of blade arrangements and of starting and choking conditions.

A summary and critical evaluation of the work reported in this article was given by Professor A. H. Shapiro in Ref. 31.

7. H. Rouse, B. V. Bhoota, E-Y. Hsu. Design of Channel Expansions.
State University of Iowa. (Ref. 18d)

The Iowa Institute of Hydraulic Research under its director, Dr. Hunter Rouse, has carried on a research program dealing with supercritical flow in channel expansions. High velocity jets having width-depth ratios of 1, 2 and 4 and Froude numbers up to 8 were used to study the characteristics of flow at abrupt expansions and along gradually expanding boundaries. The water surfaces of the expanding jets were surveyed, and the results were compared to theoretical solutions obtained by the method of characteristics. The conclusion was reached that the elementary wave theory will yield results in essential agreement with experiment as long as the assumptions involved in the theory are approximately satisfied.

8. California Institute of Technology. Analogy between Surface Shock Waves in a Liquid and Shocks in Compressible Gases.
(Ref. 13, 14)

A study of oblique wave intersections has been carried on at the Hydrodynamics Laboratory of the California Institute of Technology under the direction of Knapp and Plesset. In this program two surges of water were released upon a horizontal water table containing initially a static water depth of approximately $1/4$ inch. Depth ratios before and after the shock from 1.2 to 1.9 were used. In all cases studied, there was a definite disagreement between experimental and theoretical values for Mach intersections and some disagreement for regular intersections.

The report recommended that the theory of Mach interactions be revised to account for several noted discrepancies in the assumptions.

9. National Advisory Committee for Aeronautics. Application of the Analogy between Water Flow with a Free Surface and Two-Dimensional Compressible Gas Flow. (Ref. 15)

A research program designed to test the hydraulic analogy for flow around circular cylinders was undertaken by the National Advisory Committee for Aeronautics at Langley Field, Virginia, in 1946. The tests were conducted in a vertical, return-flow water channel with a fixed channel slope of 1° . The working section of length 3 feet and width 2 feet was preceded by a convergent section which accelerated the water. Depth measurements were obtained by a micrometer point gage with a neon lamp to provide a sign of contact between the probe and the water level. Water depths were also obtained by means of static pressure connections in the floor, along the walls and in the circular cylinders. Photographic lighting was provided through the glass floor of the working section.

In all of the tests, the initial Mach number was in the sub-critical range; however, in some of the tests on flow around cylinders, the local Mach number extended into the supersonic range. For the first time, a quantitative comparison of results from a water channel and a wind tunnel was obtained. Good quantitative results were found both numerically and photographically, thus verifying the analogy for the subsonic range up to the sonic velocity.

SECTION II

DESIGN, CONSTRUCTION AND CALIBRATION OF THE SUPERCRITICAL FLOW CHANNEL

1. Study of Basic Requirements

The design of the supercritical flow channel used in this research program was the result of a performance study and analysis of channels previously used in work on supercritical flow studies and on the hydraulic analogy.

The following basic requirements seemed to crystallize as the dominant ones which should govern the type and the dimensions of a water channel most suitable for the work contemplated:

a. Adequate width to permit the study of models of relatively large sizes. Large dimensions are desirable since shock wave fronts in water extend longitudinally for a considerable distance in terms of depth. The distance for the transition from the initial to the final equilibrium condition through a shock front must be made smaller than the distance between successive origins of shock waves on the model boundary, i.e. equilibrium conditions must be attained between successive shock waves or between shock waves and boundary changes.

b. Length of the channel should be such that the working section is far enough downstream of the entrance section to allow the development of the velocity distribution corresponding to uniform flow ahead of the model, while downstream of the model sufficient length must be given to study shock wave patterns.

c. The side walls should be made adjustable to permit the study of flow in non-uniform sections.

d. The bottom should be transparent so that widest scope can be given to lighting and photographing from above or below.

e. A uniform slope of the channel is necessary to secure uniform flow. The slope must be made adjustable to obtain this condition for any desired initial Froude number. Local deflections of the channel bottom must be minimized for the same reason.

f. Flow of any desired Froude number must be readily attainable within a minimum distance without transverse disturbances.

g. The channel interior must be unobstructed and readily accessible over its full width and length for convenience of operation. It thus is also readily converted to towing experiments.

h. A fairly wide range of water depths and of velocities must be provided for in order to permit systematic studies on the influence of viscosity and surface tension.

In accordance with the specifications set forth and with the recommendations of other experimenters (Ref. 15), the dimensions of the channel were chosen as large as possible for the space available in the laboratory. It was decided to make the channel width four feet and the length 45 feet overall so that towing experiments might also be possible. The width chosen is still convenient for depth measurements near the center. The length is adequate to permit an approach section with baffles and a nozzle designed for gradual flow acceleration.

The method by which supercritical flow is obtained is of primary importance. Accordingly, careful consideration had been given to the following methods:

a. A Laval type nozzle has the shortcoming of requiring a different nozzle for each Froude number.

b. A Spillway has the disadvantage that both velocity and depth of flow are difficult to control. Large vertical height would be required to obtain high Froude numbers.

c. The Vertical sluice gate provides relatively flexible adjustment; however, serious surface disturbances due to formation of vortices behind the gate constitute a problem.

d. A Nozzle gives gradual acceleration from an approach section, and the flow emerges as a smooth, high velocity stream. The velocity is easily controlled by means of a throttle valve in the supply line, and the depth is regulated by raising or lowering the lip of the nozzle. A large range of Froude numbers can be readily obtained since the supply system is under pressure to the lip of the nozzle. In accordance with this analysis, the nozzle seemed the most suitable arrangement to produce the supercritical flow desired.

Consideration was also given to towing models in still water. The disadvantages of this method were stated in section I-4, the difficulties being primarily those of adequate instrumentation. However, it is felt that this method has advantages in investigations of certain unsteady flow problems if these difficulties can be overcome. Ultimate use of the channel for towing experiments was therefore considered in its design.

The height of the working section above the floor of the laboratory was planned to allow enough space for photography and lighting through the glass floor. In addition, it was decided to have a two point support over the length of the channel to simplify the tilting mechanism; therefore, the truss supporting the working section had to have a depth sufficient to minimize deflections.

The discharge and slope requirements were such that Froude numbers of approximately 8 or 10 could be obtained. A centrifugal pump having a capacity of 4,000 gallons per minute under a head of 45 feet was available and was found to meet the requirements. A maximum slope of 1 in 10 was decided upon to meet the Froude number specifications and obtain flow with uniform depth. Having set up the basic requirements, the detailed design of the apparatus is next considered.

2. Design and Construction of the Supercritical Flow Channel

A plan and elevation view of the supercritical flow channel and its appurtenances is shown in Fig. 1. Essentially, it consists of the following components:

a. Channel and Supporting Structure

The rectangular channel is approximately 40 feet long, 4 feet wide and one foot in depth. The floor consists of 1/2 inch plate glass over a length of 30 feet. For short distances at either end, 1/4" aluminum plate is employed. The vertical side walls of the channel are made of 1/4 inch aluminum plate attached at intervals of 2-1/2 feet to the top chord of the supporting structure. The channel is supported by two parallel steel trusses, 4-1/2 feet deep; the top chords of which consist of two 10 inch channel sections welded back to back. The top flange of one of the channel sections provides the longitudinal support for the glass and aluminum floor and runs the entire length of the structure.

To provide space for the pump, the top chord is cantilevered at the downstream end, thus permitting the lower chord to be 10 feet shorter. The supporting trusses were designed to limit the deflection under full load of 8 inches of water to 0.025 inches. At five foot intervals, cross ties between the top chords provide supports for the channel floor. Similar ties at the lower panel points support the water supply pipe and diffuser. Lateral bracing in the horizontal and vertical planes insures torsional rigidity of the structure. Care was taken not to obstruct the panels directly beneath the glass floor; accordingly, the top chord lateral bracing was placed only at either end beneath the aluminum floor. Between each 10 foot length of glass, a brass spacing bar 1 inch wide is placed. These bars were incorporated so that it would be possible to attach objects to the floor. All joints between glass and metal were carefully smoothed and sealed against leakage. General views of the channel and supporting structure are shown in Figs. 2 and 3.

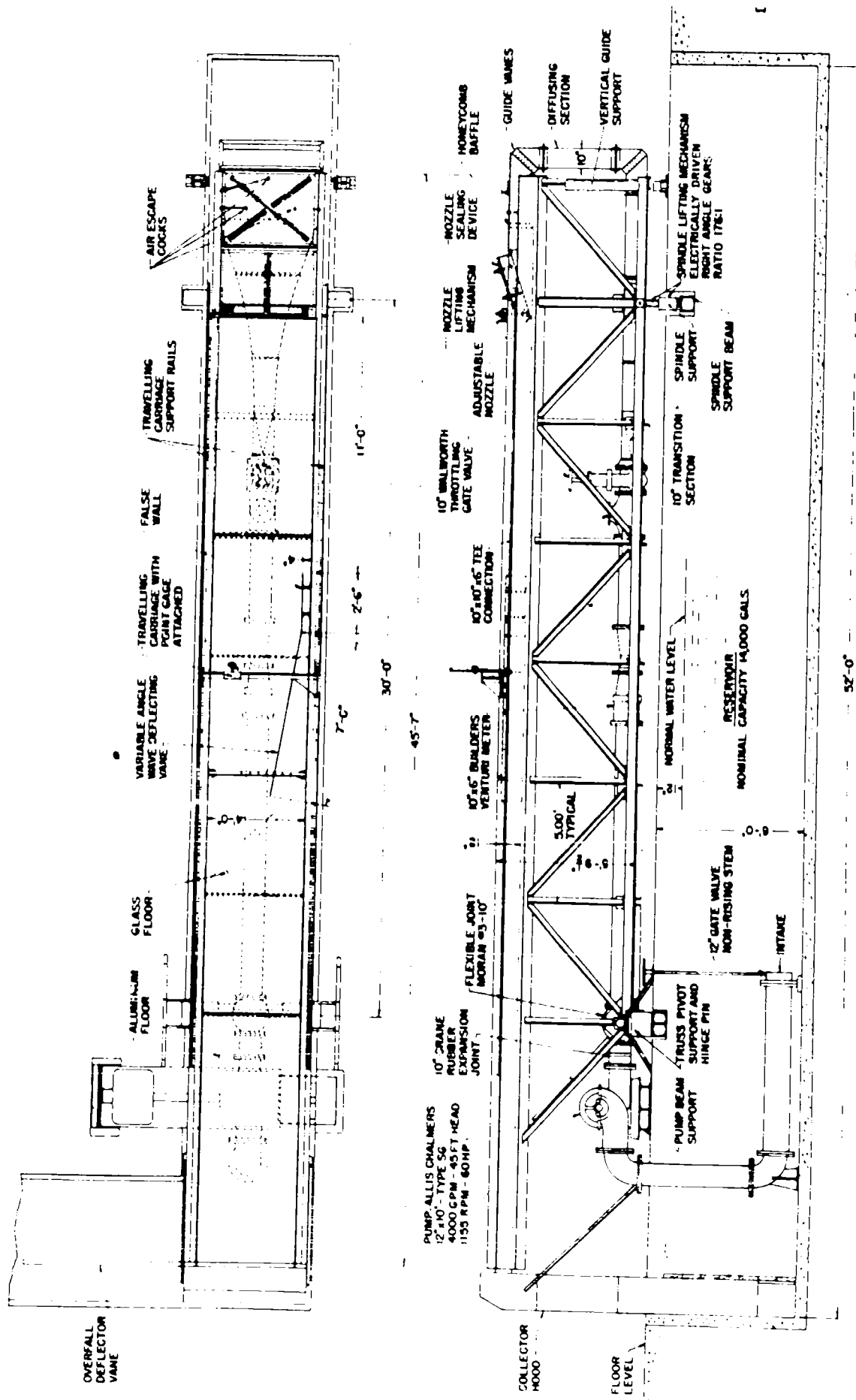


FIG. 1 SUPERCritical FLOW CHANNEL ----- GENERAL ASSEMBLY



Fig. 2. General View of Supercritical Flow Channel Looking Upstream

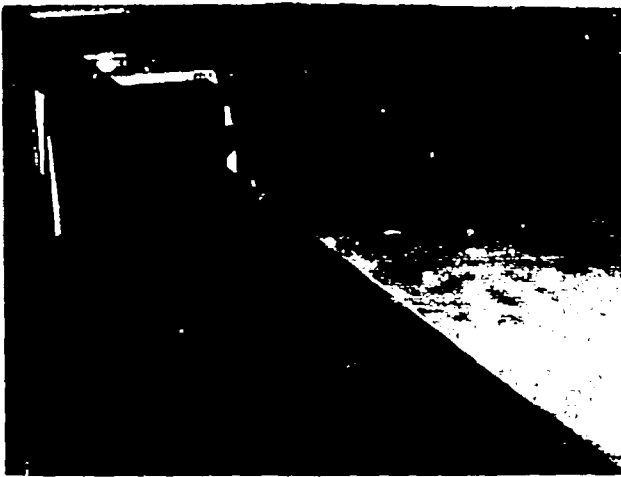


FIG. 3

UPSTREAM
VIEW OF CHANNEL
INTERIOR SHOWING
GLASS BOTTOM.

FIG. 4
DOWNSTREAM END
TRUSS HINGE MOUNTS
SHOWING DISCHARGE
PIPE, BALL AND
SOCKET JOINT AND
RUBBER COUPLING
TO PUMP

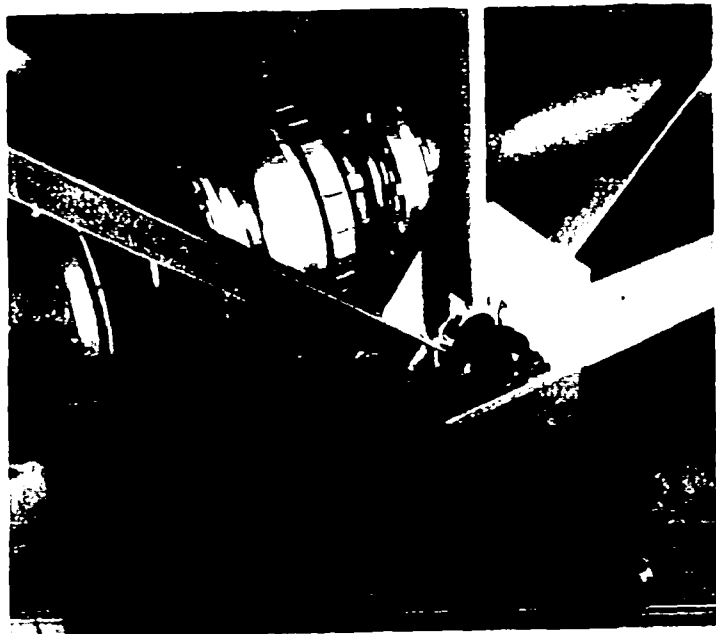


FIG. 5
DETAIL OF SPINDLE
LIFTING MECHANISM
SHOWING MICRO-
SWITCH CONTROL.

b. Channel Tilting Mechanism

Variation of the longitudinal slope of the channel is provided for by means of a tilting mechanism designed as follows:

At the downstream end of the lower chord, the trusses are mounted on hinge pins and bearings and set on blocks mounted on a rigid beam spanning the reservoir as shown in Fig. 4. The upstream support is located at the next to last panel point where two large bronze nuts transfer the weight to three inch steel spindles threaded over their entire length of 53 inches. The steel spindles rest on thrust bearings beneath which are located right angle drives. The vertical shafts of the right angle drives are keyed into the lower end of the spindles, while the horizontal shafts are connected to a 1 H.P. electric reversing motor located between the two spindles. The drives, motor and spindle supports are all mounted on knife edges placed on a supporting beam and in a line at right angles to the longitudinal axis of the channel.

The rotation of the horizontal shaft connected to the motor causes the spindles to rotate at a speed reduction of 176 to 1 through the compound reduction in the right angle drives. Rotation of the spindles causes the nuts which are connected by hinge pins and bearings to the main truss to move up or down, thus changing the slope of the channel. Inasmuch as the nuts must move along a circular arc about the downstream pivot, the tilting of the spindles is provided for by the knife edge mounting mentioned above. A detail view of the tilting mechanism of the channel is shown in Fig. 5. Power from the motor is transmitted to the horizontal shaft by means of a variable speed pulley drive, thus a rate of channel movement of from 2 to 5 inches per minute is possible. Micro switches automatically stop the motion of the channel when it has reached either the level position or its position of maximum slope of 1 to 10.

The actual setting of the channel to a desired slope is accomplished by means of a revolution counter attached to the spindle drive shaft. In order to confine the movement of the channel to a true vertical plane, guides are placed on the outside of each truss at the upper end panel points.

c. Water Supply System

The water supply and storage system is arranged as follows:

A concrete-lined reservoir, 52 feet long, 5 feet wide and 6 feet deep and having a capacity of 14,000 gallons is set into the floor of the laboratory with its top flush with the floor. The longitudinal axis of the channel coincides with that of the reservoir. The pumping equipment is shown in Fig. 6 and consists of a direct motor driven Allis-Chalmers centrifugal pump rated at 4,000 gallons per minute under a



FIG. 6
VIEW OF ALLIS-CHALMERS
CIRCULATING PUMP 45 FT. HEAD
4000 gpm

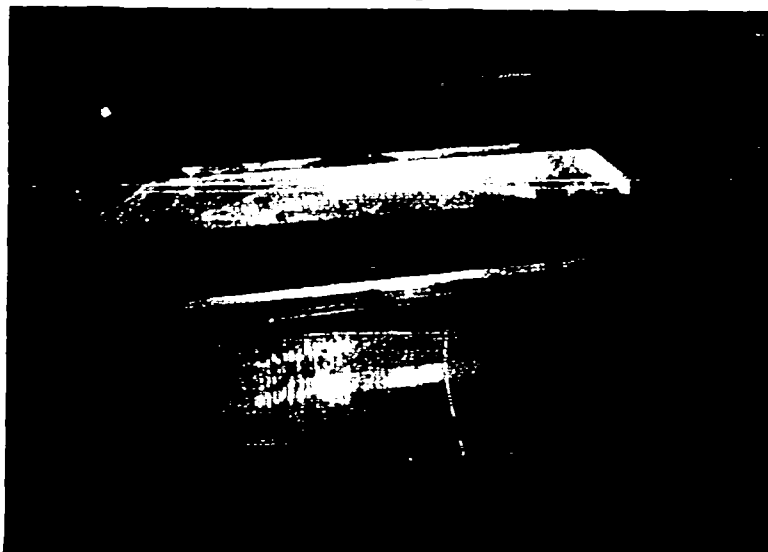


FIG. 7
VIEW UPSTREAM OF ENTRANCE
NOZZLE WITH LIFTING MECHANISM

45 foot head. The pump is bolted to a beam spanning the reservoir underneath the cantilever portion of the truss. The 12" suction pipe extends vertically down into the reservoir and along the bottom of the reservoir to a 12" gate valve. This valve provides a means of holding water in the pump for priming purposes. The horizontal extent of the intake pipe along the reservoir bottom prevents air entrainment which would be caused by having the intake too close to the point at which the water is returned to the reservoir from the downstream end of the channel. The discharge side of the pump is coupled to a 10" rubber expansion joint placed to eliminate vibrations of the pump from being transferred to the trusses. Figure 4 shows the rubber joint coupled to a ball and socket joint set so that its center of rotation coincides with the center line of the hinge pins about which both the channel and the supply pipe rotate during the tilting process.

The supply pipe continues for a distance of 12 feet from the ball joint to a 10" by 6" Venturi meter which is used to meter the flow. Five feet downstream of the Venturi is located a 10 inch throttling valve which controls the rate of flow. Directly connected to the valve is a transition section from a 10 inch circular section to a section 10 inches square. Thereafter the flow is decelerated by a gradually expanding diffuser into a section 10 inches deep and 48 inches wide. To reduce the rate of expansion and to prevent separation and eddying, a streamlined body similar to an airfoil section temporarily divides the flow in the diffuser. The final diffuser area is six times as large as the original, thus velocities are correspondingly reduced. The flow then rises vertically after being turned by a series of guide vanes and is again turned through 90° into the nozzle approach section. The entire water supply system is galvanized to prevent discoloration of the water and subsequent interference with photography.

Completing the supply system and built integrally into the support structure is a nozzle from which water from the diffuser enters the channel. This consists of an approach section designed to accommodate flow baffles and the nozzle which is made of a 1/4 inch aluminum plate extending across the channel. The plate is 10 inches above the channel floor at the hinge and converges to any desired opening at the lip where the stream emerges from the nozzle. Rubber seals prevent leakage between the edge of the nozzle plate and the vertical walls of the channel. The rubber strips are held in place by an arch spring spanning the nozzle. The arch can be made to develop a thrust upon the strips once the plate has been set to a desired opening. The nozzle section was carefully aligned to insure that the emerging stream did not have an initial angularity with respect to the channel walls. The lip of the nozzle is reinforced for stiffness and is set parallel to the glass floor insuring in all positions a uniform depth of flow. The rotation of the plate about its hinge controls the amount of nozzle opening, and the

motion of the plate is accomplished by means of a hand-operated screw mechanism. This consists of three vertical spindles, clearly seen in Fig. 7, operated by miter gears mounted on a common horizontal shaft. A revolution counter attached to the shaft reads zero when the lip is in contact with the floor and registers 228 counts for each one inch vertical rise of the plate. This permits duplication of any given nozzle setting.

The water from the channel is returned to the reservoir at the extreme downstream end of the channel by means of a collector hood mounted vertically and independently of the channel.

3. Adjustment and Calibration of Channel

a. Adjustment

Inasmuch as it was desirable that the channel be geometrically accurate in all its positions, it was assembled with much care. The two hinge points were carefully aligned and set at the same level. The glass floor plates immediately over the hinges were then leveled transversely by means of an engineer's level. The floor at the upper end of the channel was then set at this same level by means of the spindle mechanism, thus establishing the position of zero slope. Then on each of the glass panels, the elevations of 15 points were checked, and the glass set horizontal by means of fiber shims.

To insure longitudinal straightness and a constant width of 48 inches in the channel, an engineer's transit was set up at the lower end and on the center line. The aluminum wall plates were then set at equal distances from line of sight, i.e. the center line by means of a steel rule placed between the inside of the wall plates and the line. Vertical alignment was obtained through the use of a sensitive spirit level. When in proper position, the wall plates were rigidly bolted to the top chord of the trusses by means of spacers, gusset plates and angles.

Test runs made soon after completion of the channel showed the presence of vibrations in the structure. These were traced to the collector hood at the lower end of the channel which had been mounted integrally with the channel. The hood was detached and mounted on the laboratory floor. Vibrations then were negligible. Test runs also indicated the probable existence of a spiral flow in the supply pipe as the water left the pump. As this could affect the readings of the Venturi meter, straightening vanes were placed in the pipe just beyond the universal joint.

It was also observed that vortices appeared in the flow as the water emerged from the nozzle lip. To eliminate these disturbances, baffles were installed in the nozzle approach where it joined the nozzle. The core of an automobile radiator was cut in half and jointed together to form a continuous baffle, 10 inches high by 48 inches wide extending across the section. Not only did it eliminate objectionable vortices, but it also reduced depth fluctuation to a negligible amount.

b. Calibration

Several weeks were spent in calibration tests of the channel. Longitudinal slopes were calibrated against readings of the revolution counter attached to the spindle drive-shaft. At increments of 500 or 1000 counts of the counter, elevations of the channel floor were determined at three chosen points by an engineer's level. From these the main channel slope was computed. The slope vs. readings of the revolution counter was found to have a perfectly linear relation (Fig. 8). Subsequently in operating the channel, it was possible to set the channel to any desired slope by means of the counter reading. Likewise the amount of the nozzle opening was calibrated against readings of the counter attached to the operating shaft. Figure 9 shows this relation.

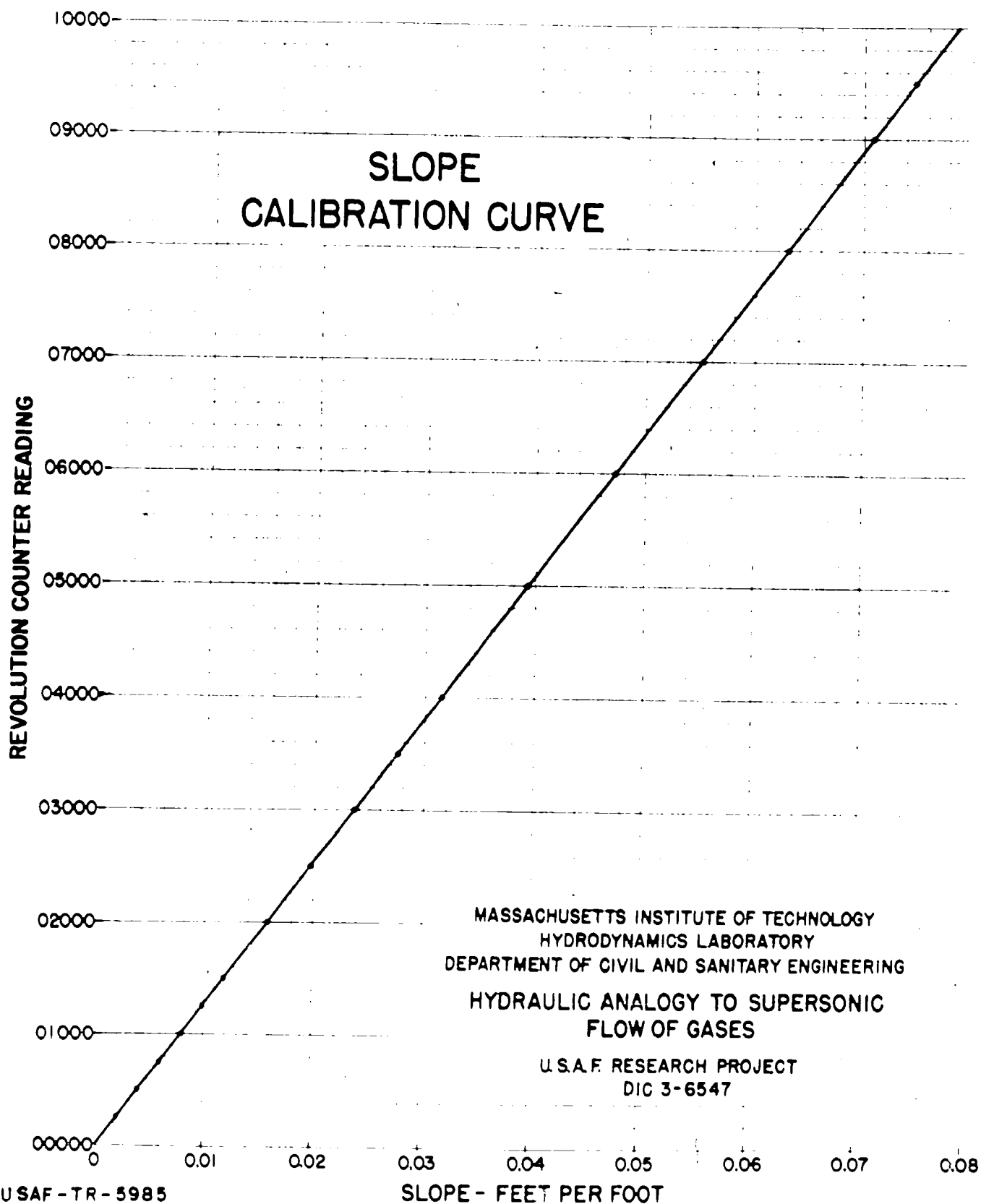
4. Instrumentation

a. Point Gage and Carriage

In order to provide suitable and quick means for the measurement of flow depths in any portion of the channel, a travelling carriage carrying a point gage was constructed.

Steel rails, circular in section and 1-1/4 inch in diameter, were mounted outside the channel walls on the top flanges of the channels forming the top chords of the trusses. These are supported on adjustable screws and were made parallel to the channel floor by means of a precise level. They were adjusted also to parallelism with the channel walls. The travelling carriage which spans the channel runs the length of the channel on these rails. At both ends of the carriage vertical supports carry ball bearing rollers resting on the rails. The rollers on the left side of the carriage, four in number, are set in pairs at an angle of 90°, thus holding the carriage to the track and insuring rigidity. Two rollers with horizontal axes support the right end of the carriage and both ends are provided with clamping devices by which the carriage may be locked to the rails.

The main member of the carriage consists of a horizontal 5 inch aluminum channel carrying three rails, likewise of aluminum, that serve as supports and guides for a transverse carriage to which the point gage is attached. This carriage is supported vertically on roller bearings



USAF-TR-5985
PART I

FIG.8

NOZZLE CALIBRATION CURVE

REVOLUTION COUNTER READING

00800

00700

00600

00500

00400

00300

00200

00100

00000

MASSACHUSETTS INSTITUTE OF TECHNOLOGY
HYDRODYNAMICS LABORATORY
DEPARTMENT OF CIVIL AND SANITARY ENGINEERING
HYDRAULIC ANALOGY TO SUPERSONIC
FLOW OF GASES

U.S.A.F. RESEARCH PROJECT
DIC 3-6547

NOZZLE OPENING-INCHES

0 0.5 1.0 1.5 2.0 2.5 3.0

USAF-TR-5985
PART I

FIG. 9

while others at the top and bottom act as guides and hold the carriage securely to the rails. The latter were carefully machined and so aligned that all roller bearings are simultaneously in contact with the tracks. The cross-carriage is equipped with a clamping device which engages a fourth horizontal rail.

Located centrally on this same carriage is a mounting to carry the point gage. Its design permits the easy removal of the gage and the substitution of a Pitot tube. It also allows the point gage to be rotated on its vertical axis and to be kept in a vertical position as the slope of the flow channel is altered. The point gage embodies a novel idea in that an Ames dial, having a 10 inch travel and recording to 0.01 of an inch, is substituted for the more common decimal scale and vernier. The main stem of the point gage carries a rack which, meshing with gears in the dial box, transfers vertical movements of the gage to the dial. Figures 10 and 11 show the point gage and traveling carriage.

In reading water depths, the point of the gage is lowered to the channel floor and the adjustable dial rotated to its zero reading under the indicating hand. The point is then raised to the water surface, and the depth read directly from the dial. The lateral location of the point gage is read from a tape having its free end attached to the point-gage carriage, while the other is fastened to the carriage support. Spring winding of the tape keeps it taut at all times.

b. Pitot Tubes

The measurement of velocity distributions in the channel and the checking of the Venturi meter coefficient called for the use of Pitot tubes. Early experimental runs indicated that the form should be such as to function accurately in flow sections of small depth and high velocity. A Leupold and Stevens Pitot-static tube having an outside diameter of 5/16 inch was first tried out but found to be too large for measurements close to the boundaries. It was used, however, in checking the coefficient of the Venturi meter which was done at a much larger depth of flow (3.5 inches) than was later used in studying wave profiles. Its coefficient of 1.01 was determined by comparative measurements made with a Prandtl tube having a coefficient of 1.00. The latter had a diameter of 0.24 inch which permitted observations to be made fairly close to the boundaries. It was used in all subsequent velocity determinations.

Near the close of the experimental work on wave formations, it was decided to check the accuracy of results obtained by the Prandtl tube. For this purpose, two other tubes were constructed both of which were plain impact tubes. One was made of glass, the other of stainless steel. Both were 1/8 inch in diameter with a conical nose and impact opening approximately 1/16 inch in diameter. The glass tube was mounted

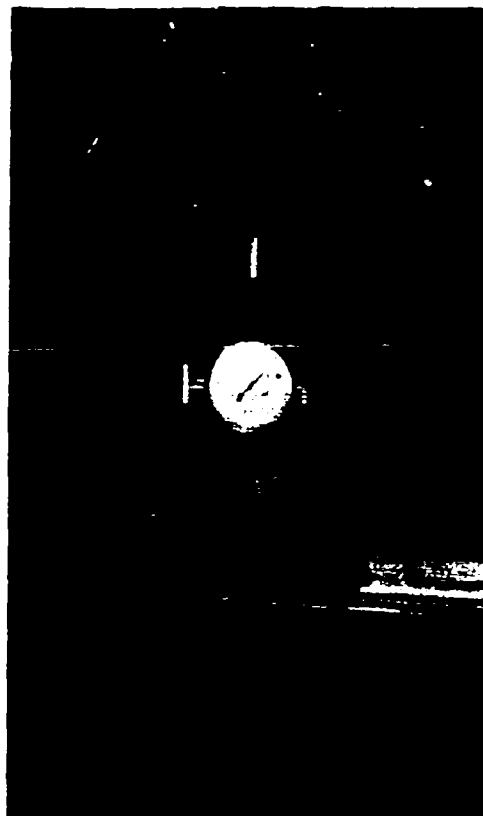
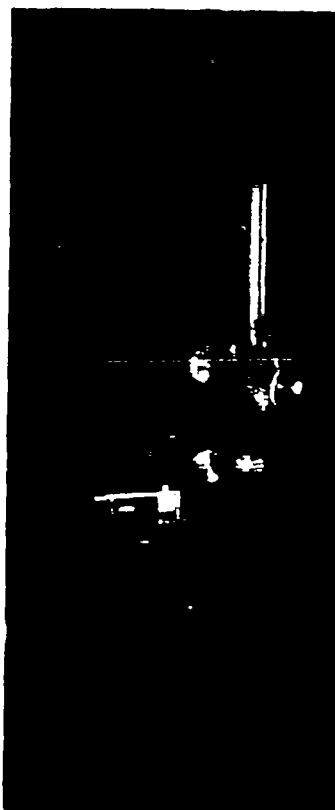


FIG II
DETAILS OF AMES-DIAL POINT GAGE

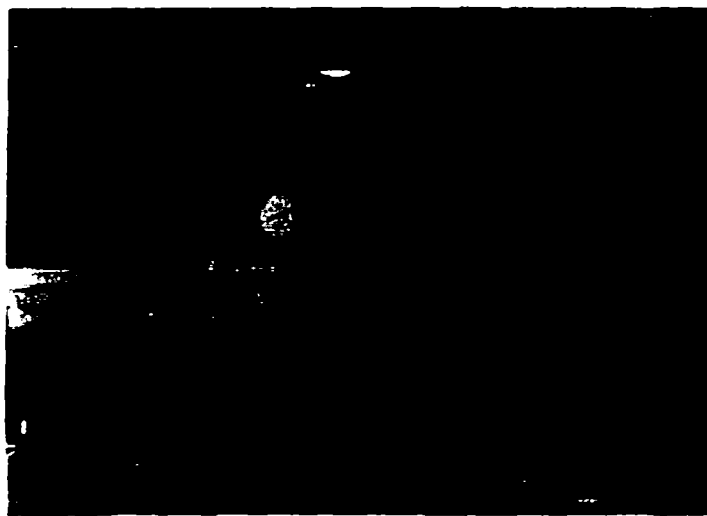


FIG IO
POINT GAGE ATTACHED TO CROSSRAIL
OF TRAVELING CARRIAGE

like the Prandtl tube on the travelling carriage. The stainless steel tube, however, was inserted upward, in an inverted position, through one of the brass strips separating the glass plates of the bottom. This position was for the purpose of permitting measurements close to the water surface without having the stem of the tube interfere with near-surface velocities.

Observations with all three tubes were made at a single station for a constant rate and depth of flow, and the results plotted. These are shown in Fig. 12. Although the impact tubes indicated velocities slightly larger than the Prandtl tube, the percentage differences were small. It was decided to accept the results of the Prandtl tube since the coefficients of the plain impact tubes were uncertain. It should be stated that a coefficient of 1.00 was used for all three tubes for the comparison in Fig. 12. Photographs of the Prandtl tube and glass impact tubes are shown in Figs. 13 and 14.

c. The Venturi Meter

The effective mean velocities and depths had to be determined by Pitot tube traverses and by point gage to eliminate channel wall effects and to obtain the effective Froude numbers as pointed out in a later section. Therefore, the measurement of total rate of flow was unnecessary except for the purpose of duplicating desired flow conditions in the channel. A 10 inch by 6 inch Venturi meter was provided in the supply line for the latter reason.

The Venturi meter coefficient, 0.983, was obtained from "Fluid Meters, Their Theory and Application", Part 1, A.S.M.E. Report, 1937, 4th Edition. Flow-rates based on this coefficient were found to check closely with those based on Pitot tube measurements simultaneously made in the channel.

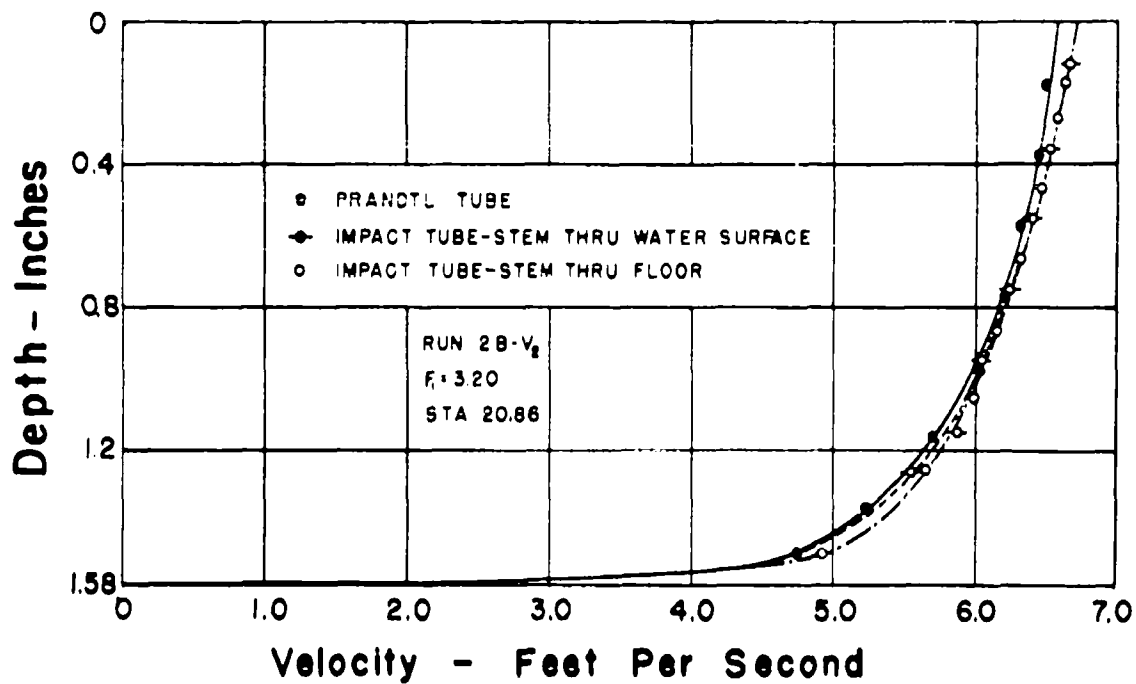
The flow-rate, in cubic feet per second, corresponding to a differential head, Δh , in fact, as read from the gages is given by the following expressions:

$$Q = 1.659 \sqrt{\Delta h} \quad \text{using the air-water manometer} \quad (1)$$

$$Q = 5.875 \sqrt{\Delta h} \quad \text{using the mercury-water manometer} \quad (2)$$

5. Method of Obtaining a Desired Froude Number

The flow-rate in a given channel is a function of the water depth and channel slope. Calculations of the slopes necessary to produce a given Froude number (hence velocity) at different depths were



\bar{V} (Prandtl Tube) = 5.97 fps

\bar{V} () = 6.05 fps

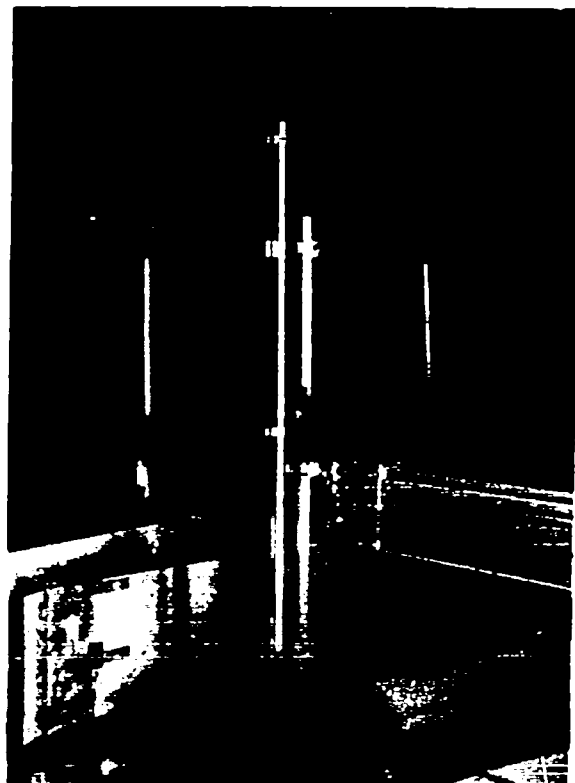
\bar{V} () = 6.08 fps

COMPARISON OF VELOCITY DISTRIBUTIONS
OBTAINED BY VARIOUS INSTRUMENTS
FIG. 12



FIG. 13
PRANDTL TYPE
PITOT TUBE
MOUNTED ON
TRAVELING
CARRIAGE.
DETAIL OF 6"
LEAD VANE
AHEAD OF
DEFLECTOR VANE.

FIG. 14
SIMPLE GLASS
IMPACT TUBE
WITH CARRIAGE
MOUNTING.



made to facilitate the initial adjustment of the channel. For this purpose the commonly accepted Manning formula for open-channel flow,

$$V = \frac{1.486R^{1/6}}{n} \sqrt{RS}$$

was employed, wherein

V = velocity in feet per second

R = hydraulic radius in feet

S = channel slope = sine of angle of inclination

n = roughness coefficient

From standard values of n , a value of 0.008 was taken and later found to be substantially correct for the smooth glass and aluminum channel. For this value of n , the above equation was used to determine the curves for constant depth as a function of slope and Froude number shown in Fig. 15 so that for any desired depth and Froude number, the channel slope could be read. Also curves of constant discharge were plotted in the same graph as a function of Froude number and depth which gave at once the discharge for the desired depth and Froude number. Initial adjustment of the flow conditions were therefore quickly made, and final adjustment necessary to produce truly uniform flow were reduced to a minimum.

With this procedure completed, the velocity distributions over a few depths across the flow section are determined by means of the Pitot tube, and the corresponding curves are plotted. The mean velocities are then determined by planimeter. The average of these is used to compute a first value of the Froude number. This value, and that of the existing depth, are usually found to be fairly close to the desired values, and the channel slope and nozzle opening need to be changed little to correct the discrepancies. Vertical velocity curves in some eight or nine locations are then again obtained and plotted. From them the transverse curve of mean velocities for the entire section is plotted and planimetered to obtain the final mean. The value of the resulting Froude number is the final one.

This method of setting up the flow to obtain a desired Froude number at a given depth was found to be very satisfactory. It was possible to obtain the same flow characteristics at any time by simply setting the differential gage, channel slope and nozzle opening at the recorded values.

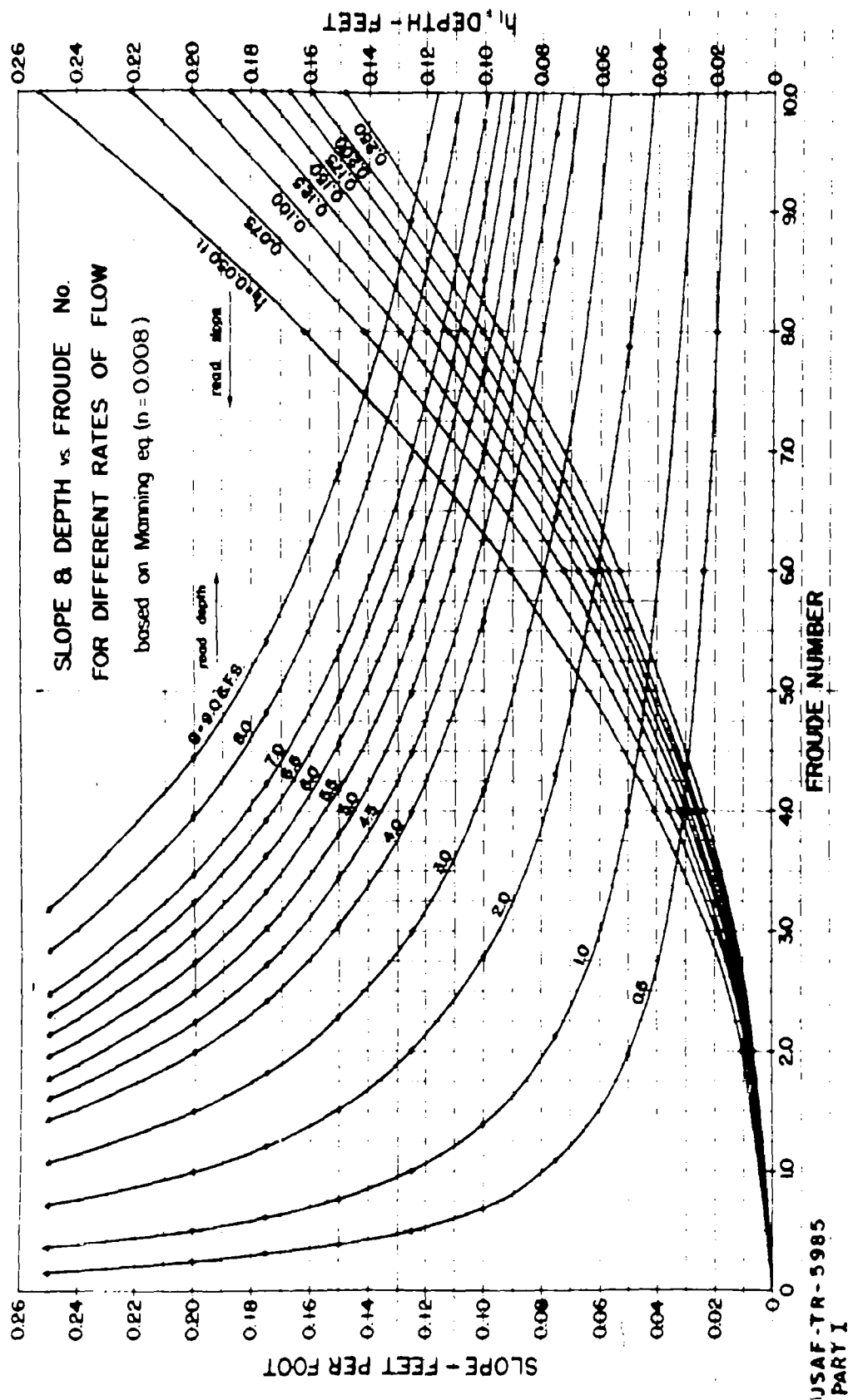


FIG.15

6. The Deflector Vane for Obtaining Oblique Shock-Waves

To produce oblique shock-waves, a variable-angle deflecting vane was installed in the channel at a point 11 feet downstream from the nozzle opening. It consisted of two parts:

1. the movable deflecting vane, 7 feet long by 10 inches high, set vertically, and
2. a short stationary lead-vane, 2-1/2 feet long and 10 inches high, attached to the channel wall by angles and gusset plates.

The face of the latter was parallel to, and 4 inches from, the wall. To it the deflector vane was joined by specially designed hinges which permitted the deflector to be moved through a wide angle with a sharp break and tight joint between it and the lead vane. The lead vane was replaceable with vanes of shorter length, and provision was made to obtain flow deflection without a lead vane. The primary purpose of the lead vane was to initiate a boundary layer in the flow ahead of the deflector.

The deflector vane can be set to various angles from 3° to 21° in increments of three degrees by means of a vertical pin located near the downstream end of the vane. The pin passes through holes in a cross member spanning the channel, thence through a bracket attached to the vane and then engages accurately spaced holes in one of the brass bars on the channel floor. Measurements after installation indicated that the angles obtained by this method were accurate within five minutes. Both lead vane and deflector were made of 1/4 inch aluminum plate reinforced for stiffness.

SECTION III

CONCLUSIONS

It was found that the supercritical flow channel after the initial period of adjustment and calibration conformed to the original specifications set forward at the beginning of section II. Relatively little time was spent on adjustments, and all major features of the channel remained as originally designed.

A number of items in the design were conditioned by the available space in the laboratory and by the equipment on hand since many materials were still in short supply at the time of construction. However, these factors did not necessitate the sacrifice of any of the specifications originally set.

It is expected that the channel will be used to advantage for purposes beyond the scope of the research reported in Part II of this program, and these possibilities were considered throughout the design.

AF TECHNICAL REPORT NO. 5985, Part II

May 1950

STUDIES ON THE VALIDITY OF THE HYDRAULIC
ANALOGY TO SUPERSONIC FLOW

Part II

Massachusetts Institute of Technology

United States Air Force
Air Materiel Command
Wright-Patterson Air Force Base, Dayton, Ohio

FOREWORD

This report was prepared by Donald R. F. Harleman under the direction of Dr. Arthur T. Ippen, Professor of Hydraulics, Department of Civil and Sanitary Engineering, Massachusetts Institute of Technology, under USAF Contract Number W33-038-ac-16703. The contract was initiated under the research and development project, identified by Expenditure Order Number 458-413, and it was administered under the direction of the Aircraft Laboratory, Engineering Division, Air Materiel Command, with Mr. Joseph Flatt acting as project engineer.

ACKNOWLEDGEMENT

This study was initiated originally by Dr. Arthur T. Ippen, who acted as project supervisor for the Division of Industrial Cooperation of the Massachusetts Institute of Technology. The experimental and analytical work was carried on by Mr. Donald R. F. Harleman, Research Associate, with the assistance of Mr. Charles E. Carver and Mr. George R. Higgins, Research Assistants, in the laboratory. Professor Emeritus, George E. Russell, contributed greatly in the analysis of experimental results and in the preparation of the report material.

ABSTRACT

An experimental program designed to verify the theory of oblique shocks in water constitutes the primary concern of this investigation. Additional experiments are carried out to determine factors affecting the frictional distortion of the basic wave form and to determine the influence of non-uniform velocity distribution and boundary layer development.

The hydraulic analogy for supersonic flow with shocks is presented. Two possible modifications in the analogy are proposed which promise improvements in the method of obtaining quantitative aerodynamic information from water measurements for the simple shock wave patterns investigated.

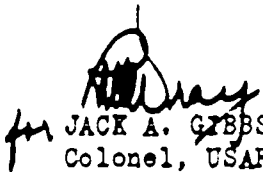
Definite conclusions derived from the present study are as follows:

- (1) there is satisfactory agreement between theory and experiment for oblique shock waves in water.
- (2) non-uniform velocity distribution inherent in this experimental method has a negligible influence upon the results.
- (3) the size of model used in experiments in water has an important effect upon the results, and large ratios of longitudinal dimensions to depth should be employed.
- (4) the practical limits of the analogy are consistent with the range in which supersonic flow theory applies.
- (5) optimum use of the water channel as a research tool requires intimate knowledge of its hydraulic characteristics combined with a judicious interpretation of results.

PUBLICATION REVIEW

Manuscript Copy of this report has been reviewed and found satisfactory for publication.

FOR THE COMMANDING GENERAL:


for JACK A. GIBBS
Colonel, USAF
Chief, Aircraft Laboratory
Engineering Division

CONTENTS

<u>Section</u>		<u>Page</u>
I	Theoretical Summary of the Hydraulic Analogy . . .	1
	1. Introduction to Flow through a Normal Compression Shock or Jump	1
	2. Normal Hydraulic Jump	4
	3. Normal Compression Shock in Gas	5
	4. Investigation of the Analogy	8
	5. Flow through an Oblique Hydraulic Jump	10
	6. Constant Specific Energy Flow	13
	7. Oblique Compression Shocks	17
	8. Isentropic Flow	19
II	Possible Modifications in the Analogy for Quantitative Application	21
	1. Introduction	21
	2. Correlation of Water-Air Data by Direct Analogy.	21
	3. First Modification of the Direct Analogy . . .	22
	4. Second Modification of the Direct Analogy . . .	25
III	Experimental Program and Procedure	34
	1. Experimental Series I - Determination of β and h_2/h_1 for given F_1 and θ	34
	2. Experimental Series II - Influence of length of lead vane and of initial depth for const. F_1 .	37
	3. Experimental Series III - Depth profiles related to length of lead vane	42
	4. Experimental Series IV - Experimental Determination of F_2	42

CONTENTS

<u>Section</u>		<u>Page</u>
IV	Analysis of Experimental Data	44
	1. Method of Determining the Shock-Wave Characteristics	44
	a. Determination of Initial Froude Number	44
	b. Determination of Depth Ratio Across Shock	44
	c. Determination of Shock Wave Angle	47
	d. Determination of Froude Number Behind Shock	58
	2. Correlation of Oblique Jump Characteristics with Hydraulic Theory	60
	3. Effect of Initial Depth and Velocity Distribution on the Shock Characteristics	71
	4. Effect of Initial Side-Wall Boundary Layer	81
	5. Effect of Surface Tension	85
	6. Discussion of Shock-Wave Shape	85
	7. Correlation of Experimental Results with Aerodynamic Theory	88
	a. Mach Number Assumed Equal to Froude Number	88
	b. On Basis of Modified Analogy.	89
V	Summary of Conclusions	97
	Bibliography	98

TABLES

<u>Table</u>		
I	Summary of Gas-Water Flow Direct Analogy	21
II	Theoretical Correlation of Air-Water Data by First Modification of the Analogy	24
III	Summary of Experimental Series I	35
IV	Summary of Experimental Series II	43
V	Summary of Experimental Series III	43
VI	Comparison of Methods for Determination of F_2	60
VII (a-k)	Hydraulic Correlations Summarized	61-70
VIII (a-d)	Air Correlations Summarized	90-93

ILLUSTRATIONS

<u>Fig.</u>		<u>Page</u>
1	Definition Sketch of Hydraulic Jump and Gas Compression Shock	2
2	Definition Sketch of Normal Jump	11
3	Definition Sketch of Oblique Jump	11
4	Flow Parameters across Oblique Shocks in Water for Various Initial Froude Numbers	14-15
5	Characteristics Diagram for Expansion or Constant Energy Flow of Water	18
6	Theoretical Correlation between Analogous Water and Air Characteristics	23
7	Ratio of Froude Number to Mach Number for Similar Geometry of Flow	27
8	Comparison of F_1 and M_1 for Similar Geometry of Flow	29-30
9	Theoretical Comparison of Modified Analogy for Successive Shocks	31
10	Theoretical Comparison of Modified Analogy for Combined Shock and Expansion Waves	32
11	Plan View of Test Section Showing Deflector Vane . .	36
12	Photographs of Shock Waves $F_1 = 4.18$	38-39
13	Photographs of Shock Waves $F_1 = 3.20$	40-41
14	Velocity Distribution for Determination of Initial Froude Number. Run B	45
15	Velocity Distribution for Determination of Initial Froude Number. Run G	46
16 (a-j)	Shock Wave Profiles	48-57
17	Section through Shock Wave Showing Method of Determining Shock Front	58
18	Velocity Profiles and Contours behind Shock Front . .	59
19	Hydraulic Correlation: Comparison of Experimental and Theoretical Values for Oblique Shock-Wave Angles in Water	72

ILLUSTRATIONS

<u>Fig.</u>		<u>Page</u>
20	Hydraulic Correlation: Comparison of Experimental and Theoretical Depth Ratio across an Oblique Shock in Water	73
21	Hydraulic Correlation: Comparison of Experimental and Theoretical Values for Froude Number Behind an Oblique Shock in Water	74
22	Definition Sketch: Effect of Velocity Distribution on Shock Waves	71
23	Comparison of Experimental Velocity Distribution with Boundary Layer Equations	76
24	Comparison of Velocity Distributions Before and After Shock Front	78
25	Effect of Initial Depth on Shock Characteristics	79
26	Effect of Initial Depth Variation on Shock Characteristics for Constant Froude Number and Deflection Angle	80
27	Effect of Length of Lead Vane on Depth Profiles, along Deflector Wall, at Initial Depth $h_1 = 0.90"$	82
28	Effect of Length of Lead Vane on Depth Profiles, along Deflector Wall, at Initial Depth $h_1 = 1.50"$	83
29	Comparison of Wall Profiles for Various Lengths of Lead Vane	84
30	Classification of Jump Form by Use of Froude Numbers Normal to Wave Front	87
31	Air Correlation: Comparison of Hydraulic Experiments with Aerodynamic Theory by Direct Analogy. Wave Angle	94
32	Air Correlation: Comparison of Hydraulic Experiments with Aerodynamic Theory by Direct Analogy. Density Ratio	95
33	Comparison of Theoretical and Experimental Values of F_1 and M_1 to produce Similar Geometry of Flow	96

NOTATIONS

a	=	local sonic velocity
C	=	celerity of a small gravity wave
c_v	=	specific heat at constant volume
c_p	=	specific heat at constant pressure
e	=	base of natural logarithms
E_w	=	internal energy per unit weight for liquids
E_g	=	internal energy per unit mass for gases
F	=	Froude number = V/\sqrt{gh}
g	=	gravitational acceleration
h	=	water depth
H	=	specific flow energy for water
I	=	enthalpy
M	=	Mach number = V/a
p	=	static pressure
P	=	force due to hydrostatic pressure
r	=	radius of curvature of free liquid surface
R	=	universal gas constant
S	=	entropy or slope of free surface
T	=	absolute temperature
U	=	local velocity
V	=	average velocity of flow
w	=	weight per unit volume
β	=	shock wave angle with respect to original flow direction
γ	=	ratio of specific heats
η	=	momentum correction factor
θ	=	deflection angle of flow
ρ	=	mass density
σ	=	surface tension of liquid

Subscript 1 refers to conditions in front of shock wave
 Subscript 2 refers to conditions in back of shock wave
 Subscript n refers to direction normal to shock wave

SECTION I

THEORETICAL SUMMARY OF THE HYDRAULIC ANALOGY

1. Introduction to Flow through a Normal Compression Shock or Jump

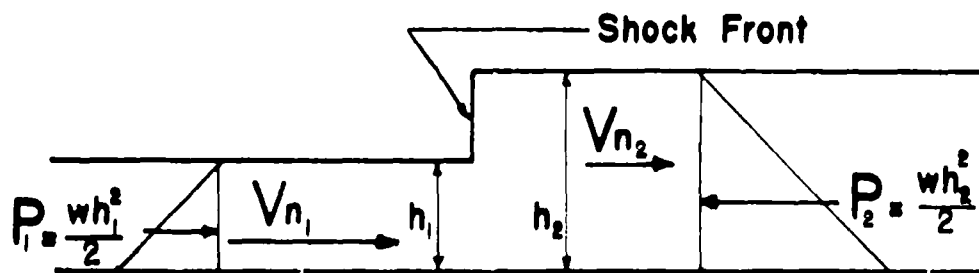
The analogy for the special flow condition of the normal compression shock or right-angle hydraulic jump is presented as background for the more general flow in which oblique shocks occur (see section I-5). The analogy for isentropic flow or constant energy flow without discontinuities and the analogy for flows involving shocks are fundamentally quite different. The isentropic flow analogy has been extensively investigated both theoretically and experimentally by Preiswerk (Ref. 1), N.A.C.A. (Ref. 15) and others. (See summary in Phase I report, section I) The isentropic analogy depends upon disturbances or changes in the flow being propagated as long waves of small amplitude while the shock-wave analogy is based upon the principles of conservation of matter, momentum and energy.

The type of flow to be considered is essentially one-dimensional both in hydrodynamics and gas dynamics. Specifically in:

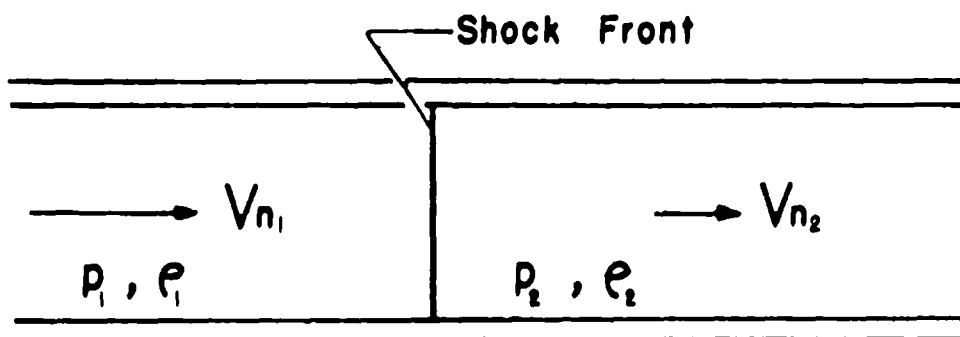
Hydrodynamics: A parallel uniform flow of liquid having a free surface in a horizontal channel of infinite width is assumed. Variations in the velocity occur only in the X direction. The flow is frictionless; in practice, the implications of this requirement are met indirectly by sloping the channel in the direction of flow until boundary resistance is balanced by gravity forces. Thus, initially, flow of uniform depth and constant velocity is obtained.

Gas Dynamics: Flow in a duct of constant section is assumed without friction or heat transfer; that is, the gas flow is non-viscous and adiabatic. Variations in the flow take place only in the X direction.

If, as in Fig. 1, the existence of a normal hydraulic jump and a normal compression shock are postulated, the continuity, momentum and energy equations show that such flows are possible. In the following development the subscript 1 refers to conditions in front of the shock while subscript 2 refers to conditions behind the shock. V_n is the velocity normal to the shock; h the depth of the liquid; p and ρ the pressure and density; E_w the internal energy per unit weight for liquid; and E_g the internal energy per unit mass for gas. Where equations for gas and liquid bear the same number, they are distinguished by subscripts w for liquid and g for gas.



HYDRAULIC JUMP



GAS COMPRESSION SHOCK

FIG.1

Continuity

$$h_1 V_{n1} = h_2 V_{n2} \quad (1_w)$$

$$\rho_1 V_{n1} = \rho_2 V_{n2} \quad (1_g)$$

Momentum

$$\frac{1}{2} g (h_2^2 - h_1^2) = h_1 V_{n1} (V_{n1} - V_{n2}) \quad (2_w)$$

$$p_2 - p_1 = \rho_1 V_{n1} (V_{n1} - V_{n2}) \quad (2_g)$$

Energy

$$\frac{V_{n1}^2}{2g} + h_1 + E_{w1} = \frac{V_{n2}^2}{2g} + h_2 + E_{w2} \quad (3_w)$$

$$\frac{V_{n1}^2}{2} + \frac{p_1}{\rho_1} + E_{g1} = \frac{V_{n2}^2}{2} + \frac{p_2}{\rho_2} + E_{g2} \quad (3_g)$$

The formal analogy is obtained by comparing the three fundamental equations. The two continuity conditions are identical if h is equivalent to ρ , then

$$h_2/h_1 \sim \rho_2/\rho_1 \quad (4)$$

The momentum conditions are identical if h is equivalent to ρ and $g \frac{h^2}{2}$ is equivalent to p , then

$$(h_2/h_1)^2 \sim p_2/p_1 \quad (5)$$

These two conditions imply a relation for the gas between p and ρ of the form

$$p_2/p_1 = (\rho_2/\rho_1)^2 \quad (6)$$

From the perfect gas relation, $p = \rho RT$, it is seen that

$$h_2/h_1 \sim T_2/T_1$$

The speed of propagation of an infinitesimally small pressure wave is the speed of sound and is equal to $a = \sqrt{\gamma p/\rho}$.

If p is replaced by $g \frac{h^2}{2}$, ρ by h , and $\gamma = 2$ from the relation indicated by Eq. (6), then $a \sim \sqrt{gh}$ and the sonic velocity is analogous to the celerity $c = \sqrt{gh}$ of a vanishingly small gravity wave. Accordingly, the Mach number $M = \frac{V}{a}$ and the Froude number $F = \frac{V}{\sqrt{gh}}$ are also analogous. The energy conditions are identical if h is equivalent to p/ρ ; this requirement is satisfied by Eqs. (4) and (5) and does not result in any new relationship. The energy equations also imply that E_w

is equivalent to E_g . The exact analogy exists then only for a gas which satisfies the pressure density relation given by Eq. (6) provided that the internal energy terms for liquid and gas are shown to be equivalent. These conditions will be investigated in detail after the necessary equations for hydraulic jumps and compression shocks have been developed.

2. Normal Hydraulic Jump

Considering first the hydrodynamic problem of the normal hydraulic jump (Fig. 1) in uniform parallel flow, it is convenient to choose coordinates stationary with respect to the jump thereby reducing the problem to one of steady flow. It is seen from Eqs. (1w), (2w) and (3w) that if V_{n1} , h_1 and E_{w1} are given, the three unknowns V_{n2} , h_2 and E_{w2} can be determined by means of the three equations. However, since the internal energy term appears only in the energy equation, h_2 and V_{n2} can be calculated when h_1 and V_{n1} are given by use of the continuity and momentum relations alone. Thus, solving Eq. (2w) for V_{n1} and eliminating V_{n2} by Eq. (1w)

$$V_{n1} = \sqrt{\frac{1}{2}(gh_1)\left(\frac{h_2}{h_1}\right)\left(1 + \frac{h_2}{h_1}\right)} \quad (7)$$

or in terms of the initial Froude number $F_{n1} = \frac{V_{n1}}{\sqrt{gh_1}}$, the depth ratio across the jump becomes,

$$\frac{h_2}{h_1} = \frac{1}{2} \left(\sqrt{8F_{n1}^2 + 1} - 1 \right) \quad (8)$$

This equation and the results of the energy equation next considered completely determine the flow conditions for a hydraulic jump and show the existence of this phenomenon previously postulated. The increase in internal energy across the jump can be calculated from Eq. (3w) by eliminating V_{n1} and V_{n2} by means of Eqs. (1w) and (2w) then,

$$E_{w2} - E_{w1} = \Delta E_w = \frac{(h_2 - h_1)^3}{4h_1 h_2}$$

$$\frac{\Delta E_w}{h_1} = \frac{(h_2/h_1 - 1)^3}{4h_2/h_1} \quad (9)$$

An inspection of this equation shows that if h_2/h_1 is less than unity, there must be a decrease in internal energy. For an incompressible fluid, this requires a decrease in entropy, a violation of the second

law of thermodynamics, thus a hydraulic drop of the shock type is physically impossible. Since $h_2/h_1 \geq 1$ Eq. (8) shows that $F_{n1} \geq 1$ and a hydraulic jump can occur only in supercritical flow. Eq. (9) also shows that the gain in internal or loss of initial "flow" energy

(defined as $\frac{V_{n1}^2}{2g} + h_1$) is relatively small. For a 100% depth change

$h_2/h_1 = 2$, the "lost" energy is 5% of the initial "flow" energy. Further energy consideration will be discussed after the necessary equations have been developed for the compression gas shock. The simplifications and limitations implied in the derivation of the hydraulic jump are summarized below.

a. The flow is steady.

All quantities are independent of time.

b. The flow is frictionless.

There are no non-conservative or viscous forces.

c. The flow is incompressible.

Density of the liquid is constant.

d. The pressure on the free surface of the liquid is constant.

e. The pressure distribution is hydrostatic.

f. Surface tension forces are negligible.

3. Normal Compression Shock in Gas

Choosing coordinates making the shock stationary with respect to the duct in which it occurs, the fundamental equations are derived by a consideration of continuity, momentum and energy in a manner similar to that used for the hydraulic jump. The energy Eq. (3g) may be re-written in terms of enthalpy

$$\frac{V_{n1}^2}{2} + I_1 = \frac{V_{n2}^2}{2} + I_2 \quad - \quad (10)$$

where I , the enthalpy or total heat content is given by $I = \frac{P}{\rho} + E = c_p T$ where c_p is the specific heat at constant pressure and T is the absolute temperature. Eq. (10) then becomes

$$\frac{V_{n1}^2}{2} + c_p T_1 = \frac{V_{n2}^2}{2} + c_p T_2 \quad - \quad (11)$$

A consideration of Eq. (1g) (2g) and (11) shows that four variables ρ , V_n , p and T are now involved and that an additional equation is needed.

The perfect gas relation

$$p = R \rho T = \frac{\gamma-1}{\gamma} c_p \rho T \quad - (12)$$

constitutes the additional relation and thus if ρ_1 , V_{n1} , p_1 and T_1 are specified for a given gas ρ_2 , V_{n2} , p_2 and T_2 can be calculated. The fact that four equations are necessary for the gas problem while only three appear in the hydrodynamic problem is explained by noting that an analogous "perfect gas relation" for an incompressible fluid is embodied in the momentum equation under the assumption of hydrostatic pressure conditions. (The relation between pressure and depth is $p = \rho h$ (density being constant) and the corresponding total hydrostatic pressure force over a vertical section is $P = \frac{\rho h^2}{2}$).

Substituting the perfect gas relation (Eq. 12) into the momentum equation (2g) and eliminating ρ_2 by means of the continuity equation (1g) there results,

$$V_{n1}(V_{n1} - V_{n2}) = \frac{\gamma-1}{\gamma} c_p \left[\frac{V_{n1}}{V_{n2}} T_2 - T_1 \right] \quad - (13)$$

Eliminating T_2 by means of the perfect gas relation (12) and rearranging in terms of the initial Mach number,

$$M_{n1} = \frac{V_{n1}}{a_1} = \frac{V_{n1}}{\sqrt{\gamma p_1 / \rho_1}} = \frac{V_{n1}}{\sqrt{(\gamma-1) c_p T_1}} \quad - (14)$$

where a_1 is the local sound velocity,

$$\text{gives:} \quad \frac{V_{n2}}{V_{n1}} = \frac{(\gamma-1) M_{n1}^2 + 2}{(\gamma+1) M_{n1}^2} = \frac{C}{C_2} \quad - (15)$$

The temperature ratio may be obtained by combining Eq. (15) with the energy (Eq. 11)

$$\frac{T_2}{T_1} = \frac{[2\gamma M_{n1}^2 - (\gamma-1)] [(\gamma-1) M_{n1}^2 + 2]}{(\gamma+1)^2 M_{n1}^2} \quad - (16)$$

the corresponding pressure ratio results from the perfect gas relation (12) and Eq. (16)

$$\frac{p_2}{p_1} = \frac{2\gamma M_{n1}^2 - (\gamma-1)}{\gamma+1} \quad - (17)$$

thus

$$\frac{T_2}{T_1} = \left(\frac{P_2}{P_1}\right)\left(\frac{\rho_1}{\rho_2}\right) \quad - (18)$$

The Rankine-Hugoniot pressure-density relations are obtained by combining Eq. (16) and (17),

$$\frac{P_2}{P_1} = \frac{\left(\frac{\gamma+1}{\gamma-1}\right) \frac{\rho_2}{\rho_1} - 1}{\left(\frac{\gamma+1}{\gamma-1}\right) - \frac{\rho_2}{\rho_1}} \quad - (19a)$$

and

$$\frac{\rho_2}{\rho_1} = \frac{1 + \left(\frac{\gamma+1}{\gamma-1}\right) \frac{P_2}{P_1}}{\left(\frac{\gamma+1}{\gamma-1}\right) + \frac{P_2}{P_1}} \quad - (19b)$$

For an adiabatic flow process the change in entropy, S , is given by

$$\Delta S = S_2 - S_1 = (C_v) \ln \left(\frac{P_2}{P_1}\right) \left(\frac{\rho_1}{\rho_2}\right)^\gamma \quad - (20)$$

Therefore in a constant entropy or isentropic process $\Delta S = 0$, then

$$\left(\frac{P_2}{P_1}\right) \left(\frac{\rho_1}{\rho_2}\right)^\gamma = 1 \quad \text{or} \quad \frac{P_2}{P_1} = \left(\frac{\rho_2}{\rho_1}\right)^\gamma \quad - (21)$$

Inasmuch as the pressure density relations obtained in the shock analysis, Eq. (18) and (19), are not of this simple form, a change in entropy must be expected for flow through a shock. The change in entropy across a shock is found from Eq. (20) by substituting Eq. (16) and (17)

$$\frac{\Delta S}{C_v} = \ln \left(\frac{2\gamma M_{n1}^2 - (\gamma-1)}{\gamma+1} \right) \left(\frac{(\gamma-1) M_{n1}^2 + 2}{(\gamma+1) M_{n1}^2} \right)^\gamma \quad (22)$$

an inspection of this equation indicates that for ΔS to be positive M_{n1} must be larger than unity. Therefore, a shock can occur only in a supersonic stream.

Let $M_{n1}^2 = 1 + m$, then Eq. (22) becomes

$$\frac{\Delta S}{C_v} = \ln \left(1 + \frac{2\gamma}{\gamma+1} m \right) \left(1 + \frac{(\gamma-1)}{(\gamma+1)} m \right)^\gamma \frac{1}{(1+m)^\gamma} \quad (23)$$

For Mach numbers close to 1, i.e. small values of m , Eq. (23) may be expanded in a power series in m .

$$\frac{\Delta S}{C_v} = \frac{2\gamma(\gamma-1)}{(\gamma+1)^2} \frac{m^2}{3} + \dots \quad (24)$$

or since $\gamma = \frac{c_p}{c_v}$ and $R = c_p - c_v$ where R is the gas constant

$$\frac{\Delta S}{R} = \frac{2\gamma}{(\gamma+1)^2} \frac{(M_{h_1}^2 - 1)^2}{3} + \dots \quad (25)$$

Thus for weak shocks, the entropy increase is of the third order with respect to the shock strength. It becomes zero and therefore isentropic as M_{h_1} approaches unity. Equation (25) may be compared to Eq. (9) which was developed for the change in internal energy for the hydraulic jump. For values of h_2/h_1 close to unity the internal energy changes also with the cube of the jump height.

The assumptions inherent in the foregoing gas flow analysis are as follows:

- a. The flow is steady; all quantities are independent of time.
- b. The flow is frictionless and adiabatic.
- c. The gas is polytropic; i.e. internal energy is a function of temperature alone.

4. Investigation of the Analogy

With the fundamental equations for the hydraulic jump and the compression shock thus established, it is necessary to return to the development of the analogy. [Eq. (4), (5) and (6)] It has been shown that the exact analogy exists for a gas which satisfies the pressure-density relation

$$\left(\frac{p_2}{p_1}\right) = \left(\frac{\rho_2}{\rho_1}\right)^2 \quad (\text{Eq. 6})$$

provided also that any changes in internal energy for the liquid and gas are equivalent. The first condition, that of the pressure-density relation, may be examined by means of Eq. (18), (19) and (20). Equation (20) may be rewritten in exponential form

$$\left(\frac{p_2}{p_1}\right) \left(\frac{\rho_1}{\rho_2}\right)^\gamma = e^{\Delta s/c_v} \quad (26a) \quad \text{and Eq. (6) yields}$$

$$\left(\frac{p_2}{p_1}\right) \left(\frac{\rho_1}{\rho_2}\right)^2 = 1 \quad (26b)$$

Therefore, the exact analogy applies for a gas having a ratio of specific heats, $\gamma = 2$ and for a shock across which $\Delta S = 0$. Neither condition is fulfilled by real gases, air has a value for $\gamma = 1.40$, and it has been shown that for flows involving shocks a change of entropy must occur. The degree to which the change of entropy affects the analogy for a hypothetical gas of $\gamma = 2$ for Mach numbers close to

unity is shown by setting $\gamma = 2$ and expanding $e^{\Delta S/c_v}$ in Eq. (26a),

thus

$$\left(\frac{p_2}{p_1}\right)\left(\frac{\rho_1}{\rho_2}\right)^2 = 1 + \frac{\Delta S}{c_v} + \dots \quad \text{substituting for}$$

$$\frac{\Delta S}{c_v} \quad \text{from Eq. (24), with } \gamma = 2,$$

$$\left(\frac{p_2}{p_1}\right)\left(\frac{\rho_1}{\rho_2}\right)^2 = 1 + .148 (M_{n_1}^2 - 1)^2 + \dots \quad (27)$$

while for $\gamma = 1.40$

$$\left(\frac{p_2}{p_1}\right)\left(\frac{\rho_1}{\rho_2}\right)^{1.4} = 1 + 0.162 (M_{n_1}^2 - 1)^2 + \dots \quad (28)$$

these values are to be compared to

$$\left(\frac{p_2}{p_1}\right)\left(\frac{\rho_1}{\rho_2}\right)^\gamma = 1.$$

Considering, now, the equivalence of the internal energy terms appearing in Eqs. (3w) and (3g), it can be seen that for water all of the change in internal energy ΔE must go into energy of turbulence and ultimately into heat. Thus, this portion of the total energy can have no further influence on the flow conditions. In the case of gases, the change of internal energy has an effect on both the temperature and density in accordance with:

$$\Delta E_g = T \Delta S - \frac{p}{\Delta \rho}$$

Thus, only a portion of the change in internal energy is used to increase the entropy of the system while the remainder affects the dynamic properties of the flow. Therefore, the energy conversions are not exactly equivalent. Section II of this report deals with the correlation of air-water data for flow with shocks.

5. Flow through an Oblique Hydraulic Jump

The equations developed for the normal jump and compression shock in the previous section may be readily generalized to include flows in which oblique shocks and jumps occur. The derivation and statements regarding the analogy are unchanged by this generalization.

It is convenient to again consider the shock wave as fixed with respect to the coordinate system with the fluid moving obliquely through it. Such a field of flow can be obtained from a normal hydraulic jump by superimposing on the whole system a constant velocity V_{t1} and V_{t2} (where $V_{t1} = V_{t2}$) parallel to the jump front and normal to the original direction of flow given by V_{n1} and V_{n2} , as shown in Fig. 2. The resultant flow field is pictured in Fig. 3b wherein the flow has been oriented so that V_1 becomes the initial flow direction and V_2 the direction of flow turned through the angle θ after passing through the jump. The continuity, momentum and energy Eqs. (1w), (2w), (3w) are unaffected by the transformation, and the notation as used for the normal jump also conforms to that used in this section. Considering only the mechanical shock conditions, that is, continuity and momentum, there are two equations and two unknowns (V_{n2} , h_2) when V_{n1} and h_1 are specified. The inclusion of oblique shocks brings two additional variables into the analysis: β the angle between the shock wave and the original direction of flow and θ , the deflection angle through which the flow is turned. Only one additional independent equation is obtained from the geometry of the vector diagram:

$$\frac{\tan \beta}{\tan(\beta - \theta)} = \frac{V_{n1}}{V_{n2}} \quad (29)$$

θ may be specified and β computed from Eq. (29). Since it is inconvenient to work with the velocity components V_{n1} and V_{n2} , V_1 and V_2 will henceforth be used as determined from the geometry,

$$V_1 = \frac{V_{n1}}{\sin \beta} \quad (30)$$

and

$$V_2 = \frac{V_{n2}}{\sin(\beta - \theta)} \quad (31)$$

However, in most cases, the equations relating the variables are obtained in a more useful form if instead of the velocity V_1 and V_2 the Froude numbers before and after the jump are used.

$$F_1 = \frac{V_1}{\sqrt{gh_1}} \quad (32)$$

and

$$F_2 = \frac{V_2}{\sqrt{gh_2}} \quad (33)$$

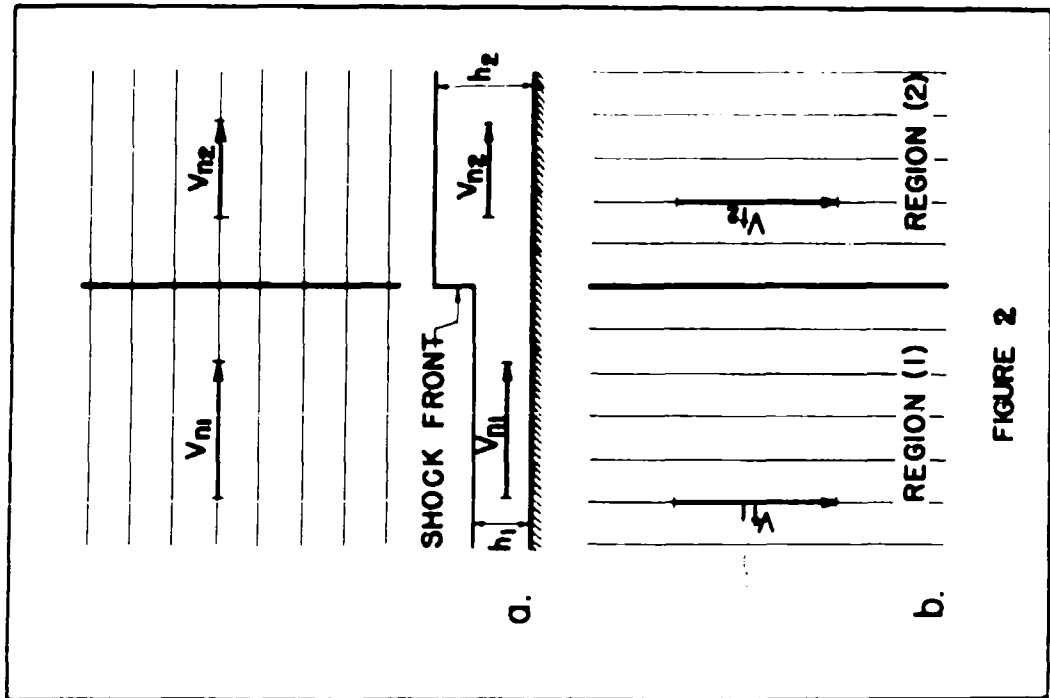


FIGURE 2

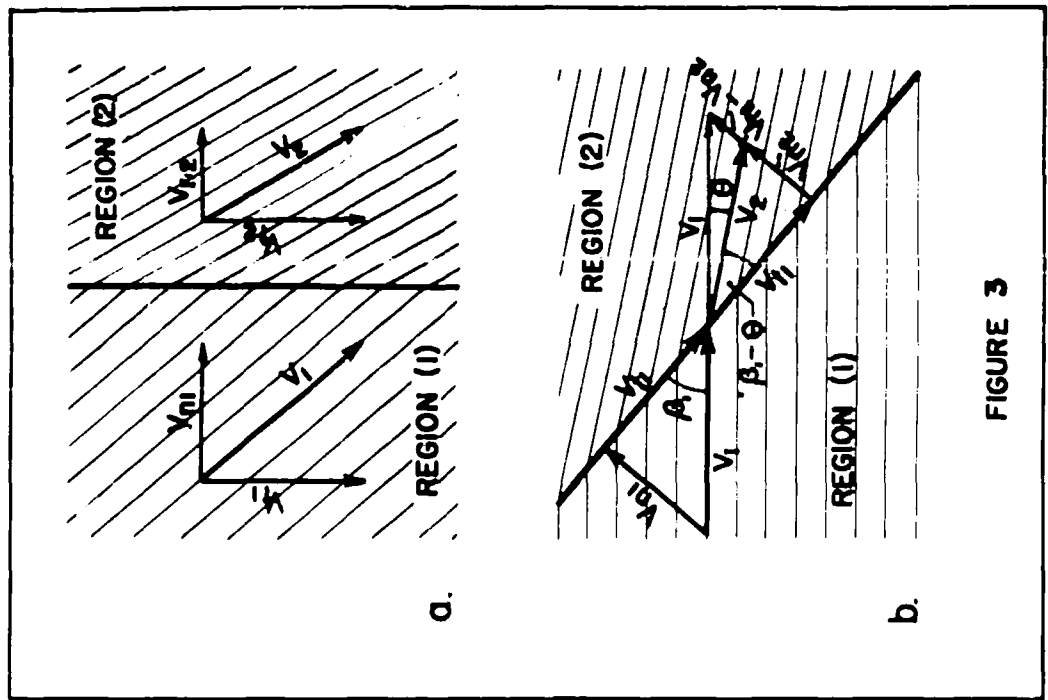


FIGURE 3

From Eq. (7),

$$V_{n1} = V_1 \sin \beta_1 = \sqrt{v_2 (gh) \frac{h_2}{h_1} \left(1 + \frac{h_2}{h_1}\right)}$$

or

$$\sin \beta_1 = \frac{1}{F_1} \sqrt{\frac{1}{2} \frac{h_2}{h_1} \left(1 + \frac{h_2}{h_1}\right)} \quad (34a)$$

thus the fundamental relation between β_1 , F_1 & $\frac{h_2}{h_1}$ is obtained. For convenience in later developments, the two alternate forms are also given here.

$$F_1 = \frac{1}{\sin \beta_1} \sqrt{\frac{1}{2} \frac{h_2}{h_1} \left(1 + \frac{h_2}{h_1}\right)} \quad (34b)$$

$$\frac{h_2}{h_1} = \frac{1}{2} (\sqrt{1 + 8 F_1^2 \sin^2 \beta_1} - 1) \quad (34c)$$

A combination of the geometric Eq. (29) and continuity (1w) results in a relation for depth ratio across the shock in terms of β_1 and θ ,

$$\frac{h_2}{h_1} = \frac{\tan \beta_1}{\tan(\beta_1 - \theta)} \quad (35)$$

Equations (34a) and (35) can be equated to obtain a form involving F_1 , β_1 and θ , thus,

$$\tan \theta = \frac{\tan \beta_1 (\sqrt{1 + 8 F_1^2 \sin^2 \beta_1} - 3)}{(2 \tan^2 \beta_1 - 1) + \sqrt{1 + 8 F_1^2 \sin^2 \beta_1}} \quad (36a)$$

which when solved for F_1 , becomes

$$F_1 = \frac{1}{\sqrt{8 \sin^2 \beta_1}} \cdot \sqrt{\left[\frac{\tan \theta (1 - 2 \tan^2 \beta_1) - 3 \tan \beta_1}{\tan \theta - \tan \beta_1} \right]^2 - 1} \quad (36b)$$

The Froude number F_2 after the shock can be obtained from Eq. (7), eliminating V_{n1} by the continuity Eq. (1w), and eliminating V_{n2} by means of the geometric relation (31), resulting in

$$F_2 = \frac{h_1/h_2}{\sin(\beta_1 - \theta)} \sqrt{\frac{1}{2} \left(1 + \frac{h_2}{h_1}\right)} \quad (37a)$$

or in terms of F_1 and h_2/h_1 ,

$$F_2 = \sqrt{\frac{h_1}{h_2} \left[F_1^2 - \frac{1}{2} \frac{h_1}{h_2} \left(\frac{h_2}{h_1} - 1 \right) \left(\frac{h_2}{h_1} + 1 \right)^2 \right]} \quad (37b)$$

A graphical plot of certain of these relationships becomes necessary when any analysis is to be carried out. For instance, it is very often necessary to find the shock angle β , for a given initial Froude number F_1 and deflection angle Θ . Inasmuch as Eq. (36) cannot be solved explicitly for β a graph is desirable to avoid trial and error solutions. A convenient four quadrant plot is presented in Fig. 4 which relates all of the variables for liquid flow across an oblique jump. For a given F_1 and Θ ; β , h_2/h_1 and F_2 are easily determined. Figure 4, therefore, represents in a cartesian plot the information for water which is usually contained in the familiar Busemann shock-polar diagram for gases. In analyses involving relatively few shocks, the cartesian plot is normally easier to use. It should be pointed out that most of the relationships developed in this section and therefore Fig. 4 can be used for flow analysis where shocks are present, which result in a decrease of the available flow energy.

6. Constant Specific Energy Flow

Supercritical flow fields or portions thereof in which changes in flow conditions without jumps are accomplished can be treated as cases in which the "flow" energy remains constant, as long as boundary resistance may be neglected. The following additional specification is then satisfied:

$$\frac{V^2}{2g} + h = H = \text{constant} \quad (38)$$

where H is called the specific energy and is referred to the bottom boundary of the channel. Inasmuch as the theory of characteristics is extensively treated in the literature, only a brief development for liquids will be given here in order to have the necessary equations available in this notation. The theory of characteristics may be developed in a condensed manner by writing the momentum equation in differential form:

$$g h(dh) = h V_n(dV_n)$$

or

$$(dV_n) = g \frac{(dh)}{V_n} \quad (39)$$

The geometric relation for an infinitesimally small change in the flow geometry may be obtained from Fig. 3b by replacing Θ by $\Delta \Theta$ and the

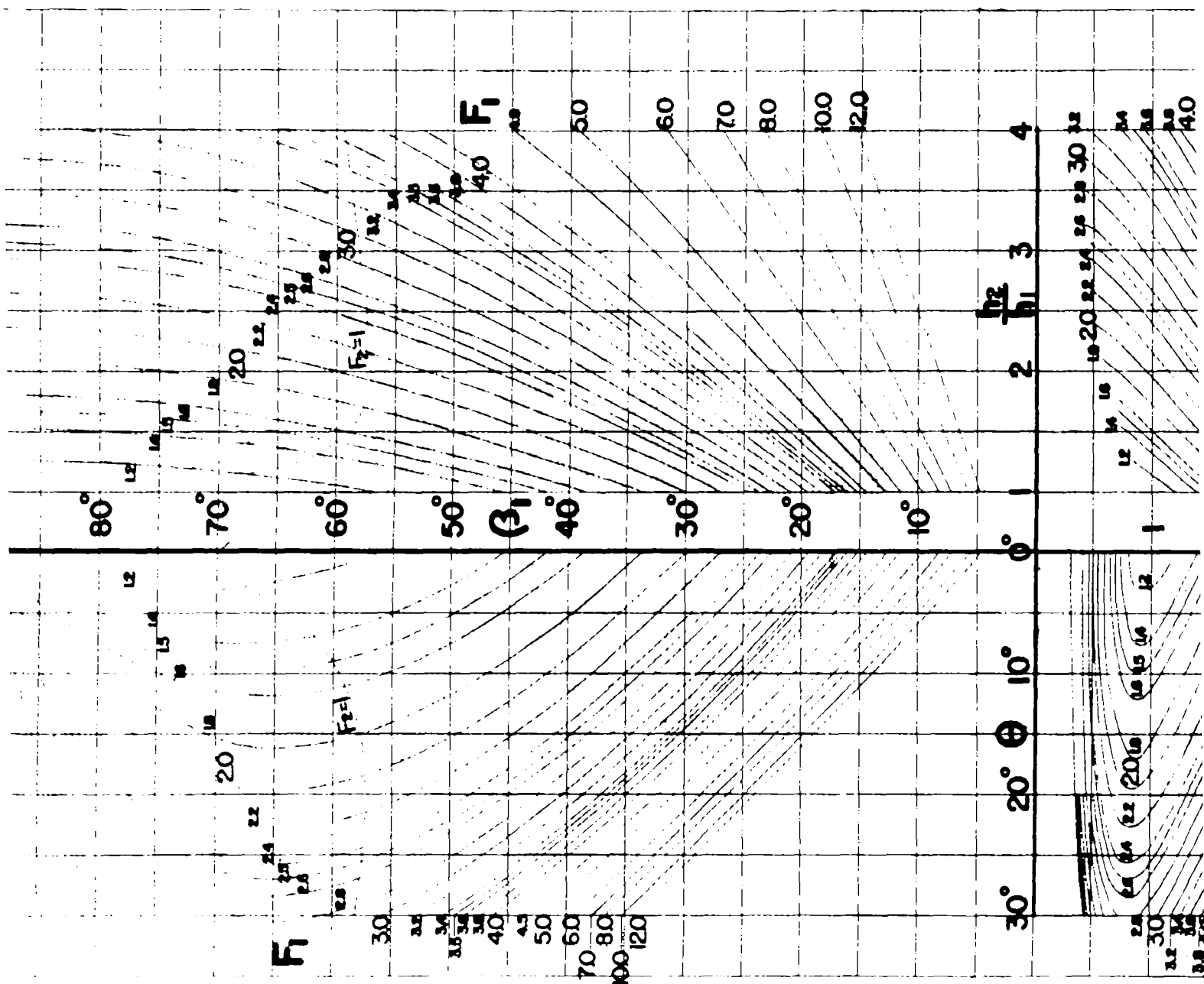


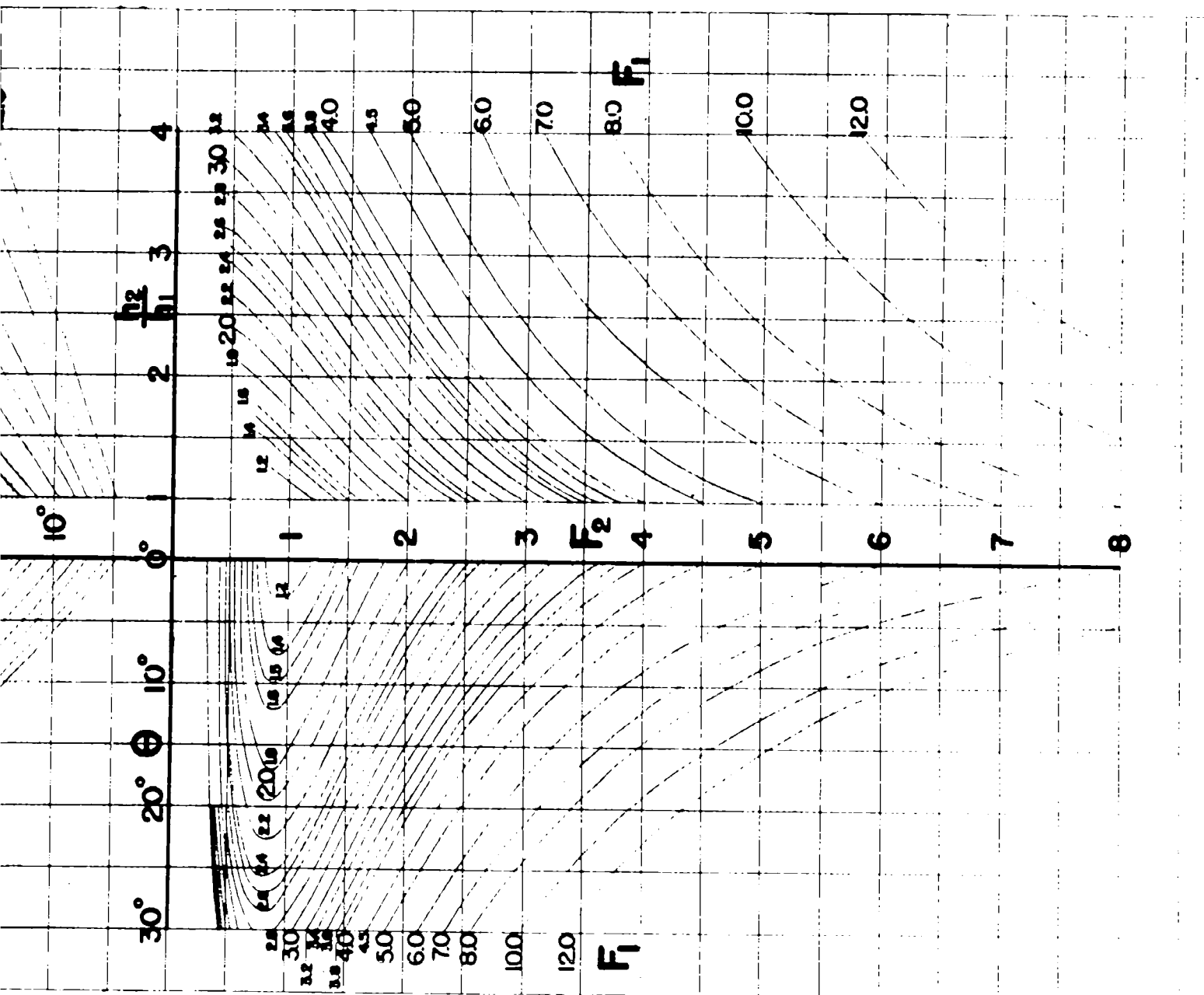
Fig. 4. Flow Parameters Across Oblique Shocks in Water

for Various Initial Froude Numbers

USAF-TR-5985

14 - 15

Part II



ters Across Oblique Shocks in Water

Initial Froude Numbers

vector $V_{n1} - V_{n2}$ by ΔV_n . Then by the law of sines

$$\frac{\Delta V_n}{V_i} = \frac{\sin \Delta \theta}{\sin(90^\circ - \beta + \Delta \theta)}$$

and, for infinitesimal changes in θ ,

$$(dV_n) = \frac{V(d\theta)}{\cos \beta} \quad (40)$$

Combining Eq. (39) and (40) and eliminating V_n by $V \sin \beta$,

$$(dh) = \frac{V^2}{g} \tan \beta (d\theta) \quad (41)$$

An additional relation is obtained from Eq. (34a) if h_2/h_1 approaches unity

$$\sin \beta = \frac{1}{F} = \frac{\sqrt{gh}}{V} \quad (42a)$$

Thus β here defines the characteristic or "Mach" lines of infinitesimal discontinuities. Equation (41) may be integrated by replacing V from the energy Eq. (38) by $V = \sqrt{2g(H-h)}$ and $\tan \beta$ from Eq. (42a)

$$\tan \beta = \frac{V_n}{V_i} = \frac{\sin \beta}{\sqrt{1 - \sin^2 \beta}} = \frac{\sqrt{gh}}{\sqrt{V^2 - gh}} = \frac{\sqrt{h}}{\sqrt{2H - 3h}} \quad (42b)$$

Equation (41) becomes finally,

$$\frac{dh}{d\theta} = \frac{2(H-h)\sqrt{h}}{\sqrt{2H-3h}} = \frac{\sqrt{2h/H}(1-h/H)H}{\sqrt{1-3/2 h/H}} \quad (43)$$

which was obtained by von Karman in 1935. Integration of Eq. (43) gives

$$\theta = \sqrt{3} \tan^{-1} \sqrt{\frac{h}{2H/3}} - \tan^{-1} \frac{1}{\sqrt{3}} \sqrt{\frac{h}{2H/3}} - \theta_1 \quad (44a)$$

θ_1 is the constant of integration defined by the initial boundary conditions that for $\theta = 0$, h equals the initial depth h_1 . Equation (44a) may also be written in an alternate form employing the Froude number

to express $\frac{h}{2H/3} = \frac{3}{2 + F^2}$. Substituting in Eq. (44a) results in

$$\theta = \sqrt{3} \tan^{-1} \frac{\sqrt{3}}{\sqrt{F^2 - 1}} - \tan^{-1} \frac{1}{\sqrt{F^2 - 1}} - \theta_1 \quad (44b)$$

inasmuch as $\sin \beta = \frac{1}{F}$ a third form is also obtainable. All three forms have been plotted in Fig. 5. Both Fig. 4 and Fig. 5 were developed for use in hydraulic problems by A. T. Ippen and a complete discussion of their use may be found in Ref. 16.

7. Oblique Compression Shocks

Following the same procedure as with the oblique hydraulic jump, the velocity V_{n1} is resolved into components V_1 and V_{t1} parallel to the shock front and the same geometrical relations, Eq. (29), (30) and (31) are obtained. The Mach numbers before and after the shock are defined,

$$M_1 = \frac{V_1}{\sqrt{\gamma \frac{p_1}{\rho_1}}} \quad (45)$$

$$M_2 = \frac{V_2}{\sqrt{\gamma \frac{p_2}{\rho_2}}} \quad (46)$$

Equation (15) becomes,

$$\frac{\rho_2}{\rho_1} = \frac{M_1^2 \sin^2 \beta (\gamma + 1)}{M_1^2 \sin^2 \beta (\gamma - 1) + 2} \quad (47a)$$

and the alternate form is

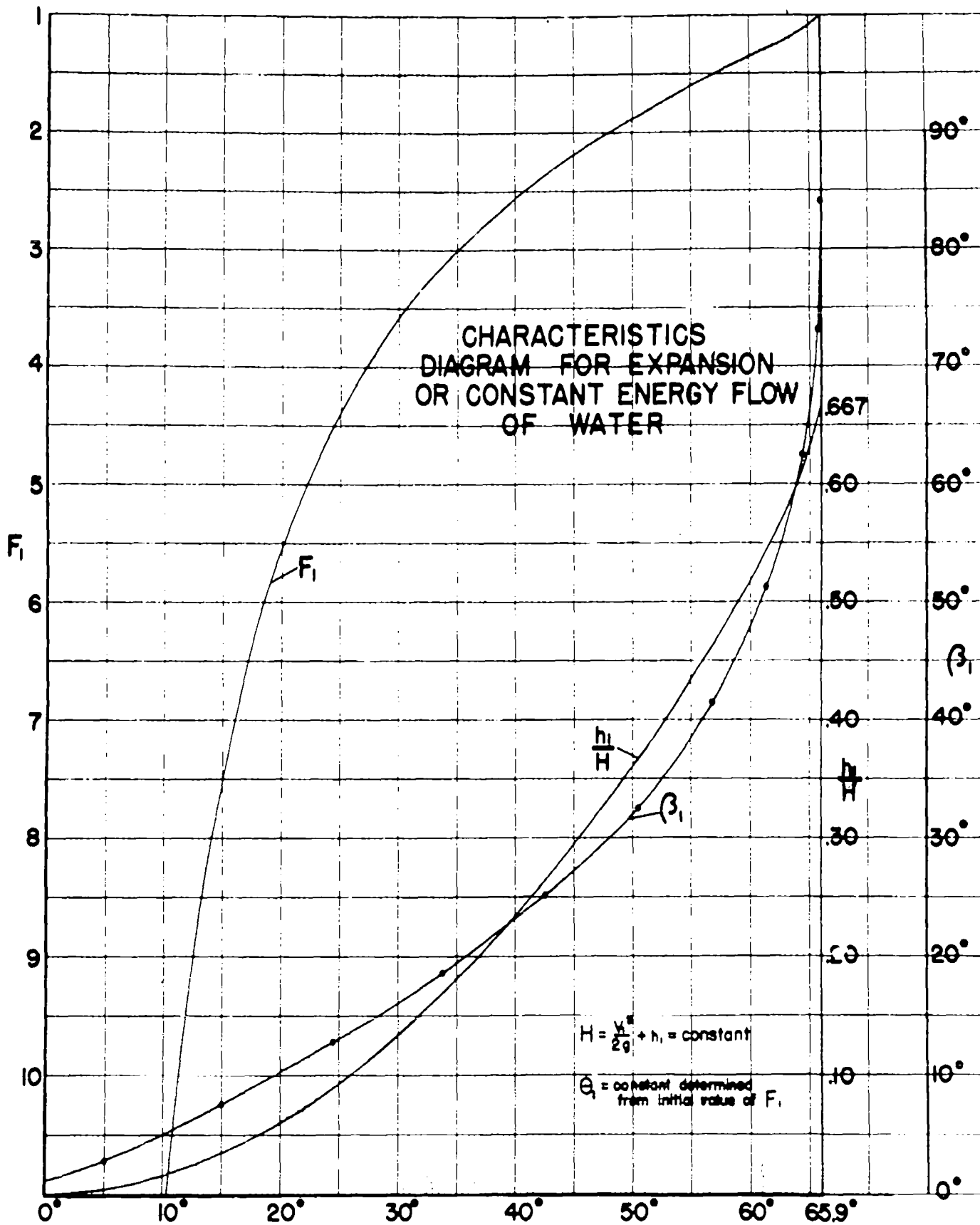
$$\sin \beta = \frac{1}{M_1} \sqrt{\frac{\rho_2}{\rho_1} \left(\frac{\frac{2}{\gamma-1}}{\frac{\gamma+1}{\gamma-1} - \frac{\rho_2}{\rho_1}} \right)} \quad (47b)$$

A combination of the geometric Eq. (29) and continuity Eq. (1g) gives a relation for the density ratio in terms of β and Θ ,

$$\frac{\rho_2}{\rho_1} = \frac{\tan \beta}{\tan(\beta - \Theta)} \quad (48)$$

It is noted that this equation is identical with that obtained for the depth ratio across an oblique jump (Eq. 35). Equations (47a) and (48) can be equated giving two useful relationships

$$\tan \Theta = \frac{-\cot \beta (1 - M_1^2 \sin^2 \beta)}{(1 - M_1^2 \sin^2 \beta) + \left(\frac{\gamma+1}{2}\right) M_1^2} \quad (49a)$$



USAF - TR - 5985
PART II

$\theta_1 + \theta_2$
FIG. 5
18

and

$$M_1 = \sqrt{\frac{1}{\sin^2(\beta - \frac{\gamma+1}{2}) (\frac{\sin \beta \cos \theta}{\cos(\beta - \theta)})}} \quad (49b)$$

Pressure and temperature ratios are obtained directly from Eqs. (16) and (17),

$$\frac{T_2}{T_1} = \frac{(M_1^2 \sin^2(\beta - \frac{\gamma-1}{2\gamma})) (M_1^2 \sin^2(\beta + \frac{2}{\gamma-1}))}{\frac{(\gamma+1)^2}{2\gamma(\gamma-1)} M_1^2 \sin^2 \beta} \quad (50)$$

$$\frac{p_2}{p_1} = \frac{(M_1^2 \sin^2(\beta - \frac{\gamma-1}{2\gamma}))}{\frac{\gamma+1}{2\gamma}} \quad (51)$$

The Rankine-Hugoniot pressure-density relation Eq. (19) and the temperature relation Eq. (18) are unchanged by the transformation and apply also to the oblique shock. The Mach number M_2 after the shock is obtained from Eq. (47b) with the aid of Eqs. (45) and (46) and the geometry

$$M_2 = \frac{1}{\sin(\beta - \theta)} \sqrt{\frac{(\frac{\gamma-1}{2})}{(\frac{\gamma+1}{2}) \frac{p_2}{p_1} - 1}} \quad (52a)$$

or in terms of M_1 ,

$$M_2 = \sqrt{\left(M_1^2 - \frac{2(1 - (\frac{p_2}{p_1})^2)}{\frac{p_2}{p_1}(\gamma+1) - (\gamma-1)}\right) \left(\frac{p_1}{p_2} \cdot \frac{\beta_2}{\beta_1}\right)} \quad (52b)$$

Tables and charts of the oblique shock relations for air are available in Refs. 17, 18, 19, 20 and 21.

8. Isentropic Flow

Portions of a flow field which accomplish changes without shocks such as expansion flow around corners must, of course, be handled by the method of characteristics. A cartesian plot of the characteristics diagram for air which is analogous to Fig. 5 for water is found in Ref. 18.

For convenience, the isentropic flow relationships are summarized here in terms of the density ratio. The equation of state yields,

$$\frac{P_2}{P_1} = \left(\frac{\rho_2}{\rho_1} \right)^\gamma \quad (53)$$

and from the perfect gas law,

$$\frac{T_2}{T_1} = \left(\frac{\rho_2}{\rho_1} \right)^{\gamma-1} \quad (54)$$

The value of the local Mach number is obtained from the energy equation

$$\frac{V_1^2}{2} + \frac{\gamma}{\gamma-1} \frac{P_1}{\rho_1} = \frac{V_2^2}{2} + \frac{\gamma}{\gamma-1} \frac{P_2}{\rho_2}$$

by use of Eq. (53)

$$\frac{M_1^2 + \frac{2}{\gamma-1}}{M_2^2 + \frac{2}{\gamma-1}} = \left(\frac{\rho_2}{\rho_1} \right)^{\gamma-1}$$

so that finally M_2 may be expressed in terms of the density ratio and the initial Mach number:

$$M_2 = \sqrt{\frac{M_1^2 + \frac{2}{\gamma-1}}{\left(\frac{\rho_2}{\rho_1} \right)^{\gamma-1}} - \frac{2}{\gamma-1}} \quad (55)$$

SECTION II

POSSIBLE MODIFICATIONS IN THE ANALOGY FOR QUANTITATIVE APPLICATION

1. Introduction

The ultimate aim of the hydraulic analogy method of investigation is to predict with reasonable accuracy the aerodynamic characteristics of a given shape or structure by means of results obtained in a water channel. The most direct way to approach this problem is to consider the agreement of various theoretical quantities obtained for water with the theoretical aerodynamic results thus establishing a basis for the application of the analogy in experimental work. In other words, certain simple shapes for which it is possible to calculate flow characteristics both for water and for air will be compared to point out the accuracy to be expected by the hydraulic analogy method. It is then the rôle of the experimental program to show how closely actual experiments agree with either theory. The following divisions show the accuracy of applying the direct analogy quantitatively and the improved agreement resulting from a few simple modifications.

2. Correlation of Water-Air Data by Direct Analogy

By direct analogy is meant the relationships between water and air quantities obtained by a comparison of the fundamental equations as given in section I. Table I lists the relationships between analogous quantities required by the direct analogy.

TABLE I

Summary of Gas-Water Flow Direct Analogy

GAS FLOW	WATER FLOW
Speed of propagation of sound wave $a = \sqrt{\gamma P/\rho}$	Speed of propagation of small gravity wave $c = \sqrt{gh}$
Mach number, $M = \frac{V}{\sqrt{\gamma P/\rho}}$	Froude number, $F = \frac{V}{\sqrt{gh}}$
Density ratio, ρ_2/ρ_1	Depth ratio, h_2/h_1
Pressure ratio, P_2/P_1	(Depth ratio) ² , $(h_2/h_1)^2$
Temperature ratio, T_2/T_1	Depth ratio, h_2/h_1

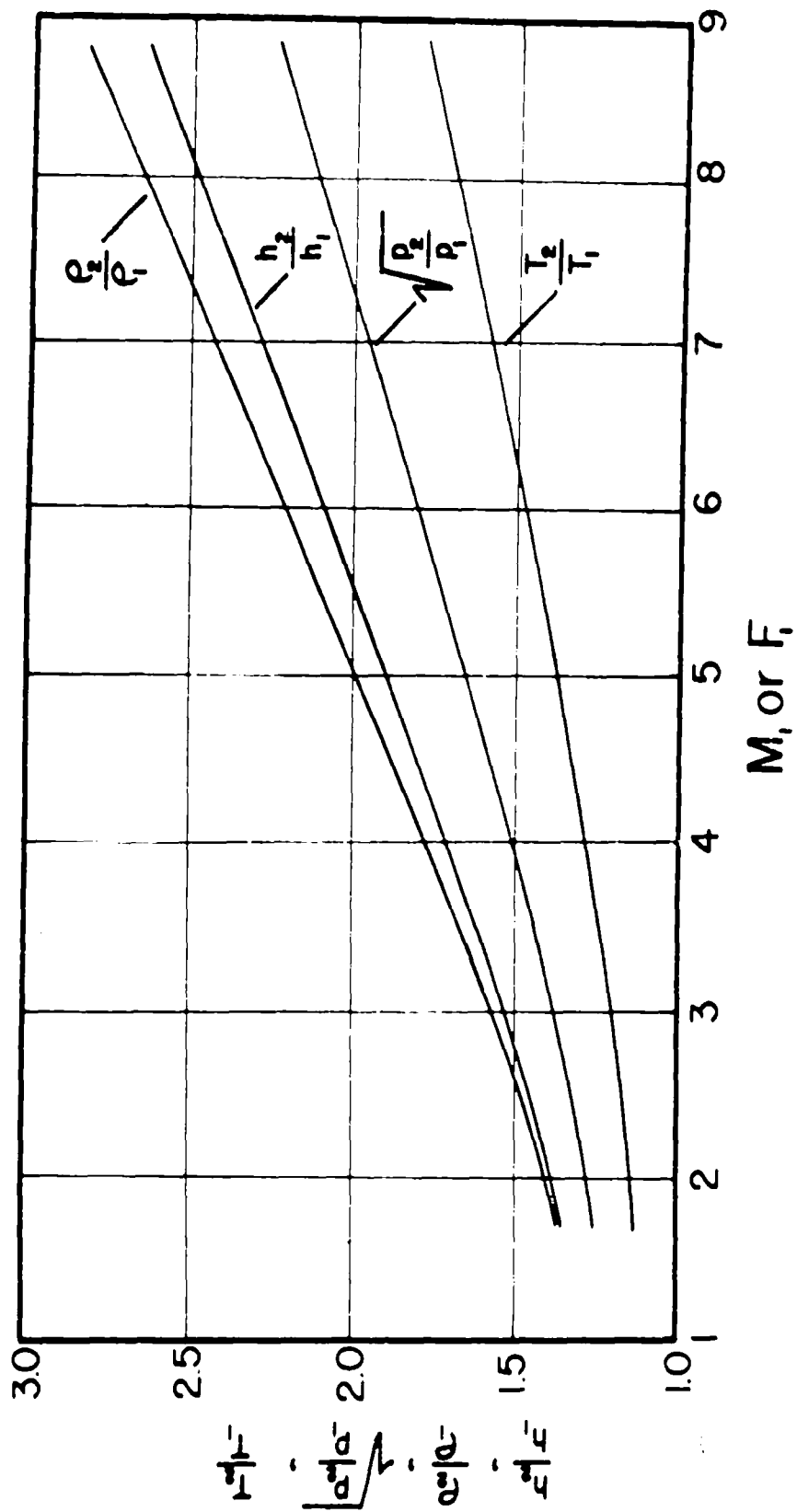
It has been pointed out previously that the water-air analogy for flows involving shocks is imperfect for two basic reasons. First, $\gamma = 1.4$ for air while the analogy requires $\gamma = 2$; second, the change in internal energy for gas is not equivalent to the change in internal energy for water. As an example, the change in flow produced by a 9° deflection at initial Mach numbers ranging from 1 to 9 will be investigated. Figure 6 shows the theoretical correlation between the aerodynamic ratios of density, pressure and temperature as calculated from aerodynamic theory and the analogous hydraulic depth ratio for $\Theta = 9^\circ$. It is seen that best agreement is obtained between the depth ratio and the density ratio. It has been the practice up to now to determine the desired aerodynamic quantities from hydraulic data according to the relationships given in Table I; thus, varying degrees of agreement are obtained depending on the quantities desired.

3. First Modification of the Direct Analogy

It is proposed that in order to improve the theoretical agreement of the analogy, a departure be made from the derived relationships summarized in Table I. If in a gas flow analysis the initial Mach number and the geometry of the shape are known, and if the pressure variation along the body is obtained from experiments, the corresponding densities, temperatures and local Mach numbers can be determined from the aerodynamic equations developed in section I. If an analogous test were performed with water, it does not seem desirable in view of the information given in Fig. 6 to correlate the measured depth ratios to the corresponding air quantities by strict adherence to the direct analogy. Instead, it is proposed to use the depth ratio only to determine the analogous density ratio and then to calculate with this density ratio the temperature, pressure and local Mach number values by means of the aerodynamic relations. This method seems to give good agreement for all practical values of the deflection angle Θ .

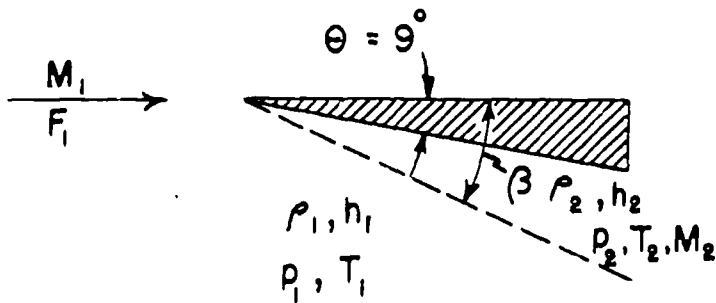
In summary, it may be stated that for actual gases for all practical purposes, the analogy holds only as far as density and water depth are concerned. The derivation of pressures and temperatures directly from the water depths is not feasible.

Table II shows the results of a comparison made for two Mach numbers and a deflection angle of 9° . In this example the pressure ratio for $M_1 = 2.50$ as obtained from the direct analogy differs from the theoretical air results by 22%, while the same quantity obtained from the first modification of the analogy differs by 2.3%. Temperature and local Mach number show even better improvement. It should be pointed out that when crossing a shock, the pressure, temperature and Mach number ratios must be calculated from the equations taking account of the change in entropy. (e.g. Eq. (18), (19) and (52b)). In crossing



THEORETICAL CORRELATION BETWEEN ANALOGOUS
WATER AND AIR CHARACTERISTICS FOR $M_1 = F_1$ AND $\theta = 9^\circ$

FIG 6



$$M_1 = 2.50$$

Initial Mach No. = 2.5 = Initial Froude No. $\theta = 9^\circ$						
Method of Analysis	Wave Angle β	h_2/h_1	ρ_2/ρ_1	p_2/p_1 Eq (19a)	T_2/T_1 Eq (18)	M_2/M_1 Eq (52b)
Aerodynamic Theory	$30^\circ 54'$	—	1.489	1.759	1.181	0.852
Direct Hydraulic Analogy	$32^\circ 30'$	1.465	1.465 (-1.6%)	2.146 (+22.0%)	1.465 (+24.0%)	0.753 (-11.6%)
First Modification Hyd. Analogy	$32^\circ 30'$	1.465	1.465 (-1.6%)	1.718 (-2.3%)	1.173 (-0.7%)	0.858 (+0.8%)

$$M_1 = 5.00$$

Initial Mach No. = 5.00 = Initial Froude No. $\theta = 9^\circ$						
Method of Analysis	Wave Angle β	h_2/h_1	ρ_2/ρ_1	p_2/p_1 Eq (19a)	T_2/T_1 Eq (18)	M_2/M_1 Eq (52b)
Aerodynamic Theory	$18^\circ 27'$	—	2.004	2.759	1.377	0.820
Direct Hydraulic Analogy	$19^\circ 30'$	1.911	1.911 (-4.6%)	3.662 (+32.3%)	1.911 (+38.4%)	0.692 (-15.7%)
First Modification Hyd. Analogy	$19^\circ 30'$	1.911	1.911 (-4.6%)	2.560 (-7.2%)	1.340 (-2.7%)	0.835 (+1.8%)

note: percentages are differences between the quantities obtained from the analogy and theoretical air results.

TABLE II

THEORETICAL CORRELATION OF AIR-WATER DATA
BY FIRST MODIFICATION OF THE ANALOGY.

an "expansion" wave or in other regions of isentropic flow, the equations developed in section I-8 are used; thus, for $\gamma = 1.40$,

$$\frac{p_2}{p_1} = \left(\frac{\rho_2}{\rho_1}\right)^{1.40} \quad (53)$$

$$\frac{T_2}{T_1} = \left(\frac{\rho_2}{\rho_1}\right)^{0.40} \quad (54)$$

and

$$M_2 = \sqrt{\frac{M_1^2 + 5}{\left(\frac{\rho_2}{\rho_1}\right)^{0.40}} - 5} \quad (55)$$

Therefore, it is seen that after having obtained the density ratio from the water depth ratio, all the other characteristics may be calculated from the aerodynamic relations which apply to the region in question.

4. Second Modification of the Direct Analogy

The progress toward a quantitative application of the analogy suggested a further modification which may be used for flows involving shocks. The first modification leaves the fundamental difference between the water depth ratio and the density ratio for equal initial Mach and Froude numbers unchanged, but relates the other aerodynamic characteristics to the density ratio rather than to the depth ratio. The second modification aims at a better numerical agreement for the depth ratios and density ratios. It then incorporates the first modification to obtain the other quantities, thereby improving at the same time their numerical values.

The equations relating h_2/h_1 and ρ_2/ρ_1 to the geometry of the flow across a shock are identical (see Eq. (35) and (48)). Thus,

$$\frac{\rho_2}{\rho_1} = \frac{\tan \beta}{\tan(\beta - \theta)} = \frac{h_2}{h_1}$$

The density and depth ratios can be expected to be of the same magnitude only when deflection angles and shock wave angles are identical for water and air. The necessary adjustment in the flow geometry is accomplished by changing the Froude number of the water flow. As an example, consider again the 9° wedge shown in Table II. When the initial Mach number equals the initial Froude number of 2.50 for deflection angle

$\theta = 9^\circ$, the shock angle for water is $\beta = 32^\circ 30'$, while for air $\beta = 30^\circ 54'$. The Froude number necessary to give a $\beta = 30^\circ 54'$ for water is $F_1 = 2.65$ as compared to $M_1 = 2.50$ for air. It is evident that if the water experiments are conducted with $F_1 = 2.65$, and if the results are interpreted as corresponding to air flow with $M_1 = 2.50$, the depth ratio will theoretically

equal the density ratio and thus all quantities determined from this density ratio will be identical with the aerodynamic analysis. In a similar manner, the $M_1 = 5.00$ example shown in Table II would require that the hydraulic test be made with $F_1 = 5.48$. For the case of successive shocks or curved shocks, it is of course impossible to obtain geometrically similar flow patterns; however, the initial Froude number may be adjusted in such a way as to give the best overall agreement of the flow geometry. It should again be pointed out that all comparisons as to the accuracy of the analogy made in this section are based on theoretical analyses both for the water and air flows. While they are not immediately of practical value, they do show how the analogy can eventually be improved for cases which must be analyzed experimentally. The question of such Froude number adjustments is further discussed in section IV-7, Correlation of Experimental Results with Aerodynamic Theory.

A curve showing the adjustment to the Froude number may be plotted against density ratio for all possible combination of Θ and β . The curve is obtained by rewriting Eq. (34b) and (47b) as follows:

$$F_1 \sin \beta_1 = \sqrt{\frac{h_2}{h_1} \cdot \frac{1}{2} \left(1 + \frac{h_2}{h_1}\right)} \quad (34b)$$

$$M_1 \sin \beta_1 = \sqrt{\frac{\rho_2}{\rho_1} \left(\frac{5}{6 - \rho_2/\rho_1}\right)} \quad (47b)$$

For similar geometry of flow, $h_2/h_1 = \rho_2/\rho_1$. If Eq. (34b) is divided by Eq. (47b):

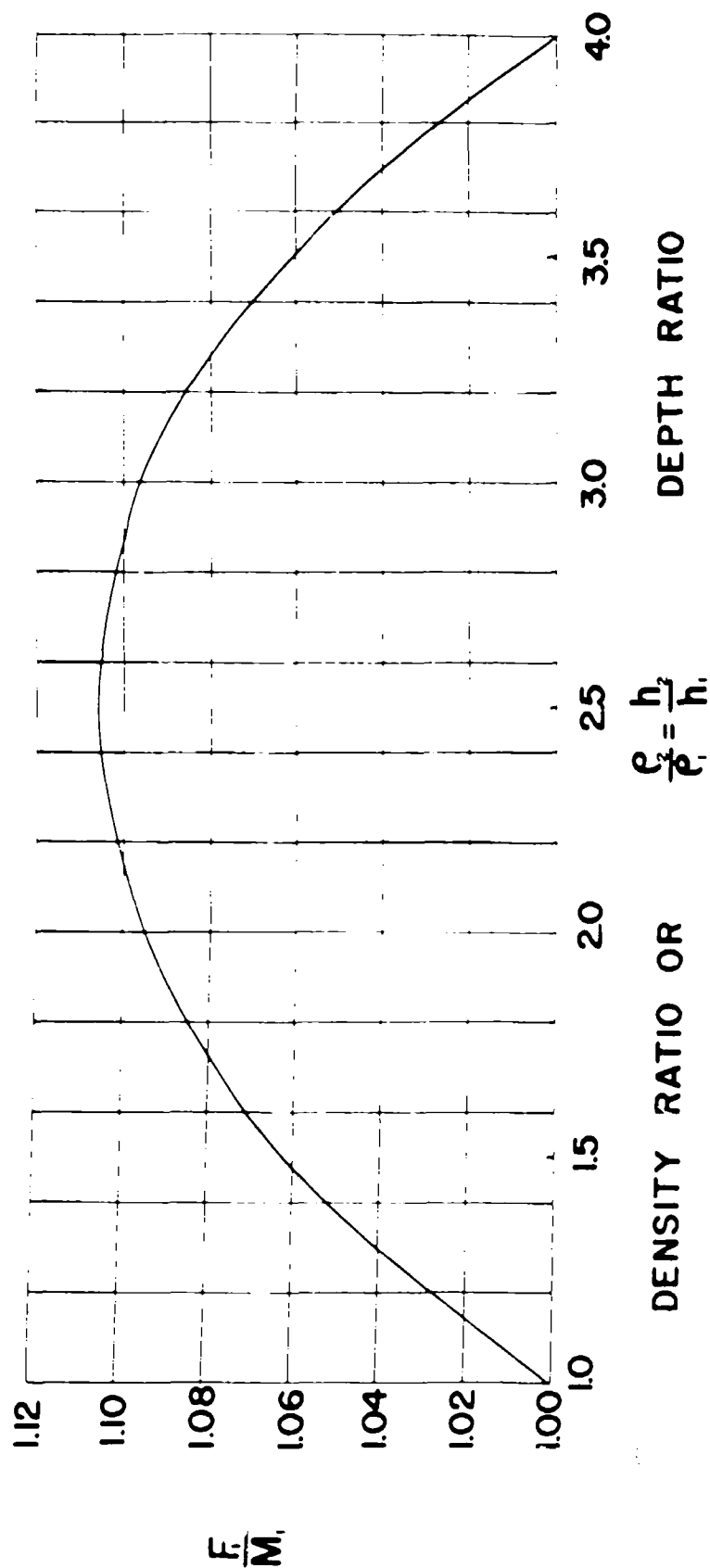
$$\frac{F_1}{M_1} = \sqrt{\frac{(1 + \rho_2/\rho_1)(6 - \rho_2/\rho_1)}{10}} \quad (56)$$

This relation is plotted in Fig. 7.

The curve exhibits several interesting features:

1. The difference between F_1 and M_1 for similar flow geometry reaches a maximum for $\rho_2/\rho_1 = 2.50$ with $F_1/M_1 = 1.107$. This property has the fortunate effect of making large errors in the adjustment to the Froude number impossible in cases in which complicated shock configurations occur. Thus in practice, all adjustments to F will fall between 1.00 and 1.107 for $\rho_2/\rho_1 = h_2/h_1 < 4$.

2. At $\rho_2/\rho_1 = 4$, the flows become geometrically similar for the same F and M ($F/M = 1$). Beyond $\rho_2/\rho_1 = 4$, the ratio F/M becomes



RATIO OF FROUDE NUMBER TO MACH
NUMBER FOR SIMILAR GEOMETRY OF FLOW

FIG 7

less than unity and the ratio approaches zero as $\rho_2/\rho_1 \rightarrow 6$. The failure of the equation at $\rho_2/\rho_1 = 6$ is due to a breakdown in the air flow theory. The temperature ratios across such high compression shocks become very large, and the assumption of a perfect gas is no longer valid. Flows in this range are designated as hypersonic. The hydraulic analogy as considered here is therefore not applicable. For ready comparison of initial Froude and Mach numbers for similar geometry of flow and for a single oblique shock, a set of curves is presented in Fig. 8. This figure has a plot of Eq. (38a) relating F_1/β and θ for water on the left, and a plot of Eq. (49a) on the right relating the same variables for air. Starting on the right side with a given M_1 and θ ,

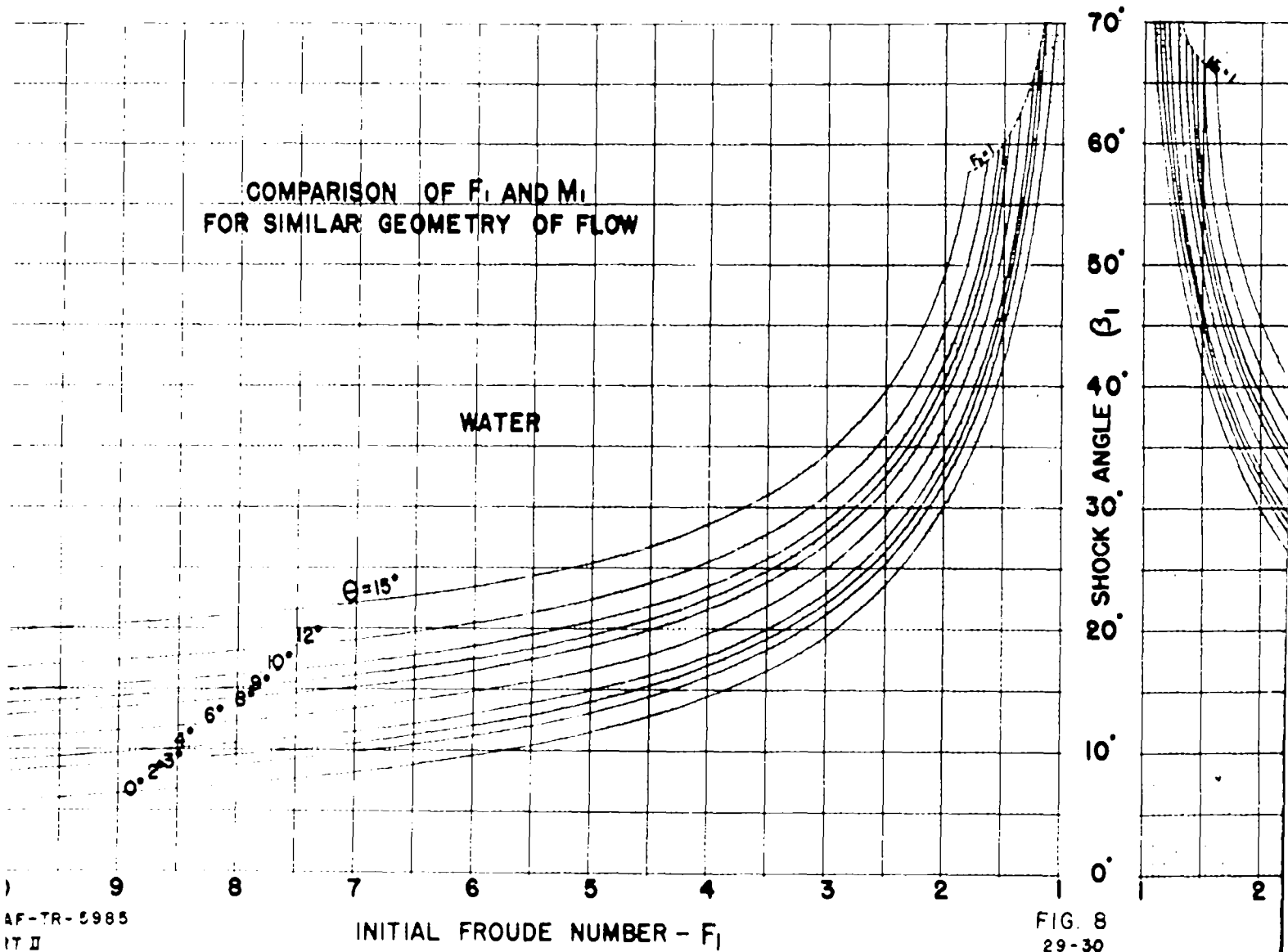
β is determined; crossing over to the left for the same θ the value of F_1 giving the same flow pattern is obtained. The same adjustment to the Froude number is obtained from the curve as from Fig. 7 if the density ratio corresponding to the given M_1 and θ were used in Fig. 7. In addition to use of this curve in adjustment of initial Froude or Mach number, the curves are convenient when analyzing water and air flows independently in conjunction with Fig. 4.

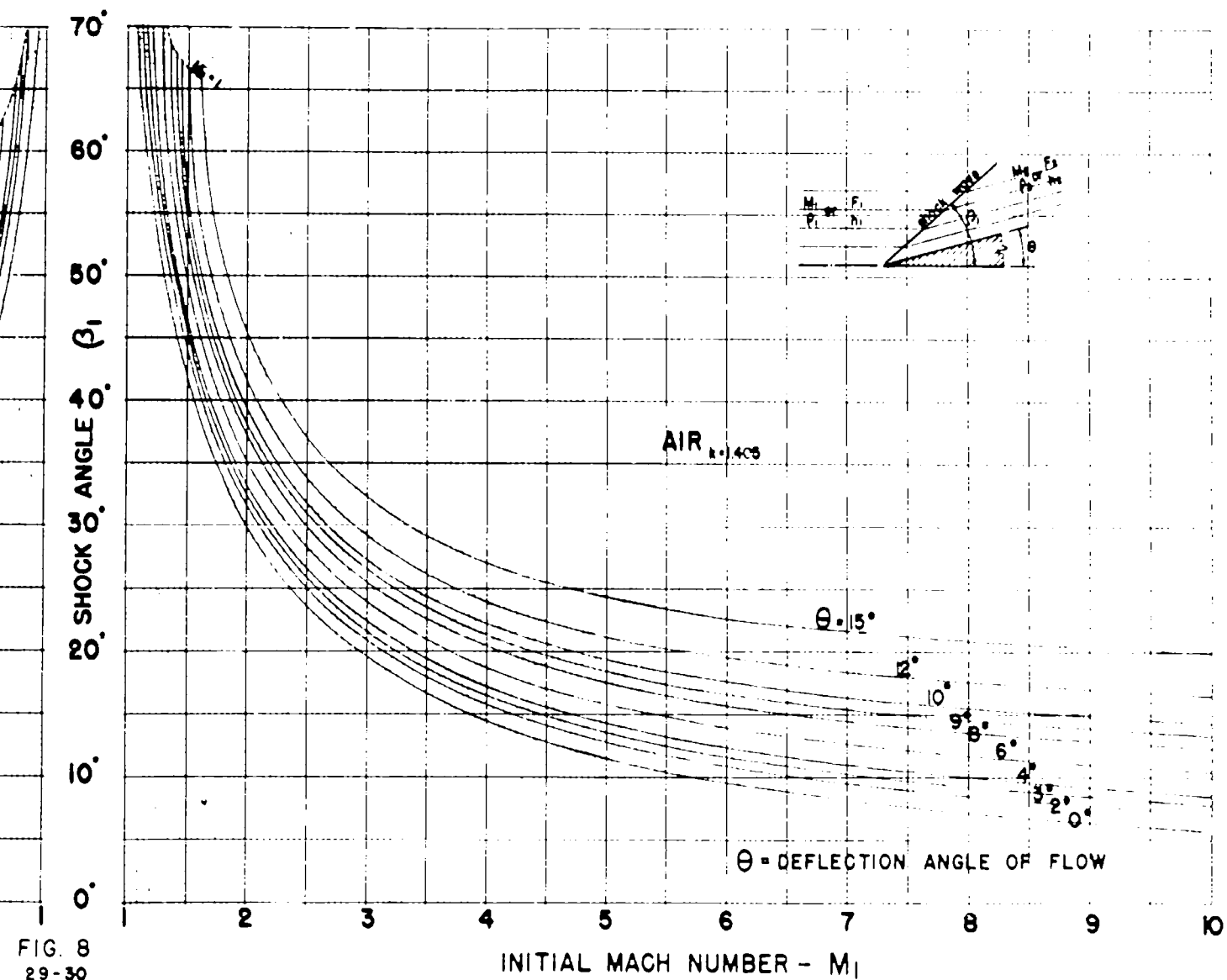
Two additional examples are presented to show the results of the second modification when applied to flows involving successive shocks and combinations of shocks and expansion waves. Figure 9 illustrates the case of successive shocks. In the analysis by the first modification, $F_1 = M_1$, the differences in pressure ratio compared to theoretical air is 3.9% for the first shock and 8.3% for the second successive shock. The Froude number is then adjusted according to the procedure of the second modification. In this case, it was decided to make the first shock angle in water equal to the corresponding angle in air; thus from Fig. 8, $F_1 = 3.22$, and the differences in pressure ratios are reduced to zero for the initial shock and to 3% for the second shock. The values of the local Mach numbers M_2 and M_3 are not equal to the local Froude numbers but are obtained from the density ratio by means of Eq. (52b). It is seen that the characteristics of successive shocks are improved by the initial adjustment even though similar flow patterns are not possible. Other methods of adjustment might have been used, such as: (1) approximating the boundary by a single straight line and basing the adjustment on this fictitious deflection angle or (2) assuming an average value for the depth change, and by use of Fig. 7, determining the necessary adjustment. Both of these methods can be used when dealing with curved boundaries.

Figure 10 illustrates the case in which combinations of shocks and expansion waves are present. In the second modification, the adjustment to the Froude number was made by obtaining similar flow geometry for the first shock on the bottom side of the diamond shaped airfoil. It is seen that in all regions, the correlation is improved; in most places, the error is halved. Thus, a shock followed by an expansion wave and two successive expansion waves all benefit from the original adjustment.

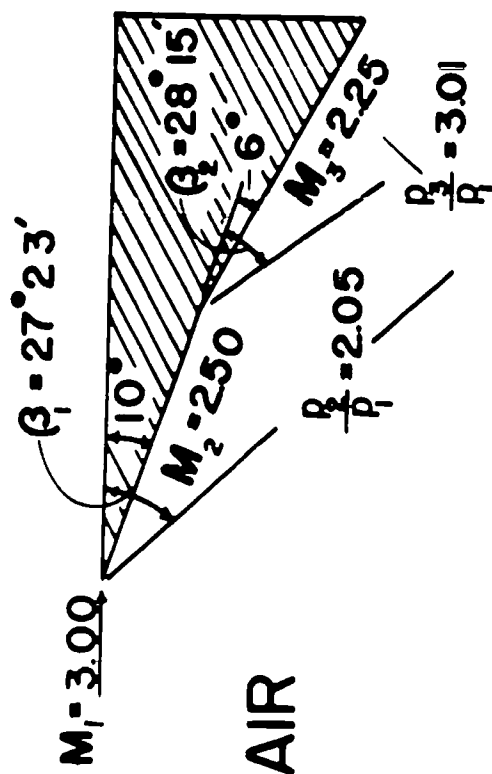
COMPARISON OF F_1 AND M_1
FOR SIMILAR GEOMETRY OF FLOW

WATER





note: pressure ratios obtained from
water analysis are calculated
from eq. (19a) where $\frac{h_2}{h_1} = \frac{p_2}{p_1}$
and $\gamma = 1.40$
local Mach Numbers are
calculated from eq. (52b)



THEORETICAL COMPARISON
OF MODIFIED ANALOGY
FOR SUCCESSIVE SHOCKS

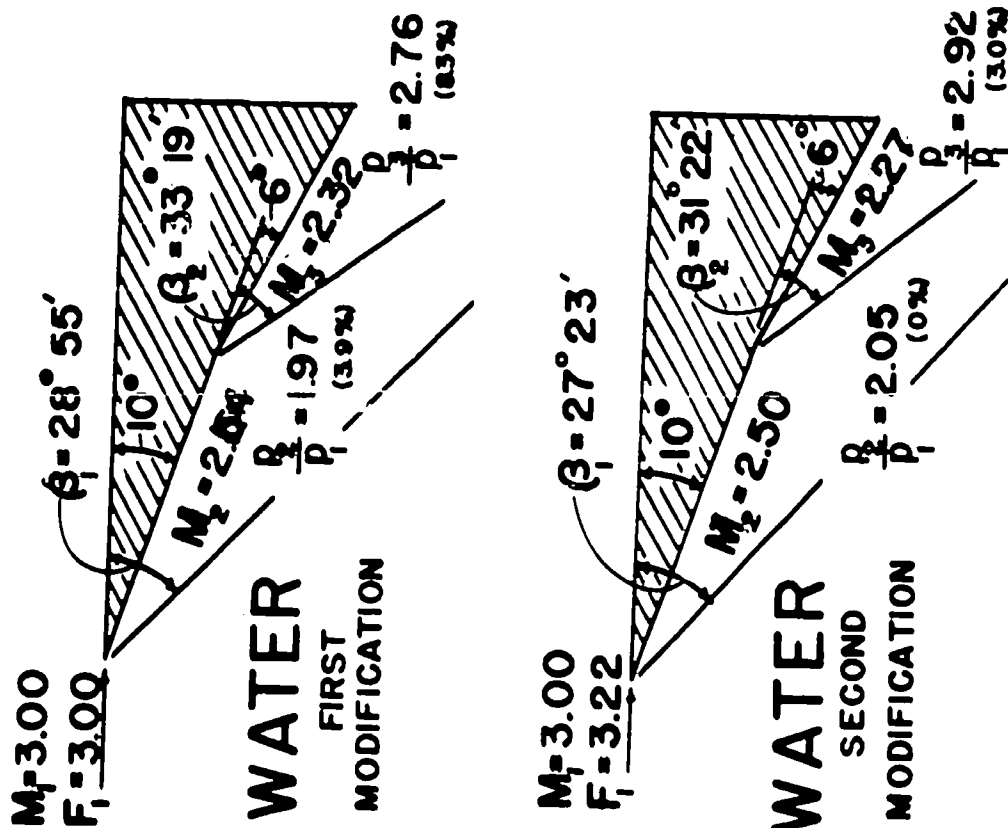
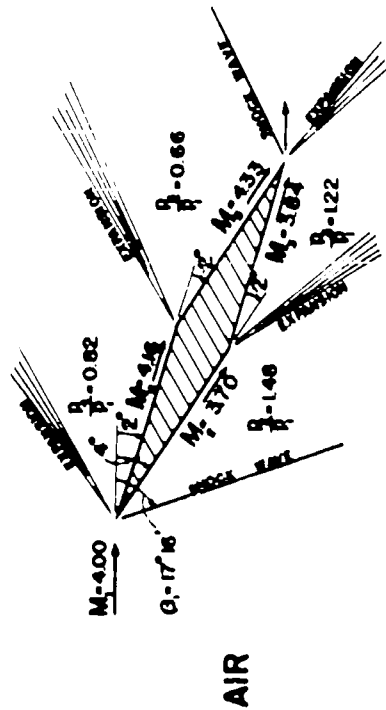


FIG. 9

note: AIRFOIL SECTION
ANALYSIS OBTAINED
FROM NACA-T.N. 1143



THEORETICAL COMPARISON OF MODIFIED ANALOGY FOR COMBINED SHOCK AND EXPANSION WAVES

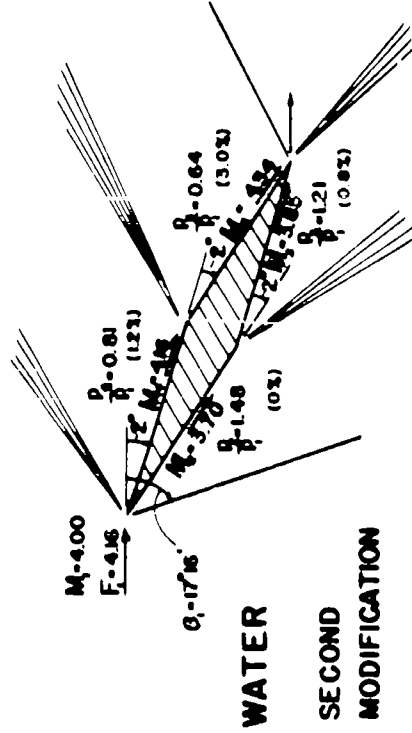
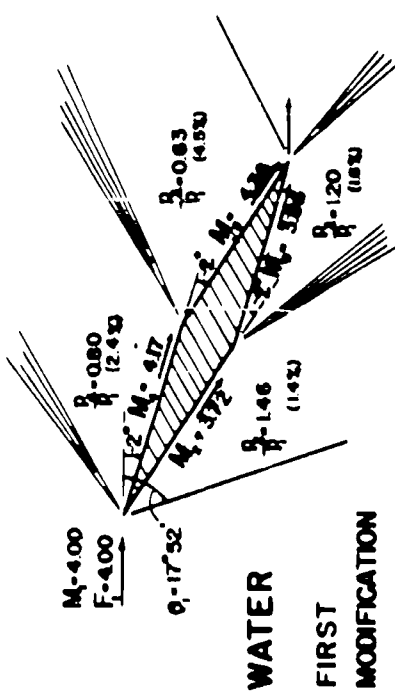


FIG. 10

The experimental results pertaining to the direct and modified analogy are presented in section IV-7. It is not within the scope of this research project to present experimental results on shapes such as the diamond airfoil. The purpose of the foregoing considerations is to point out the possibilities of improving the experimental and analytical methods as a means of obtaining better quantitative agreement between results obtained from a water channel and actual results in air. These methods seem especially promising for securing pressure distributions around various aerodynamic shapes.

SECTION III

EXPERIMENTAL PROGRAM AND PROCEDURE

All of the experimental investigations described herein were conducted in the supercritical flow channel in the Hydrodynamics Laboratory of the Massachusetts Institute of Technology. The design and construction and the methods of operation of the channel constitute Phase I of the research project and are dealt with in USAF Technical Report No. 5985, Part I.

The purpose of the experimental work which comprises phase II of the research project is to establish experimentally the characteristics of oblique shock waves and to compare these to the theoretical characteristics developed in section I of this report. Specifically, the following quantities have been determined: shock wave height, shock-wave angle, Froude number before and after the shock, all as a function of the deflection angle of the flow. Additional experiments have also been made to investigate the effects of velocity distribution and boundary layer development upon the basic wave characteristics. These experimental studies served to delineate the approximate range within which experimental results may be expected to conform to the theory, and outside of which inherent limitations imposed by basic assumptions lead to excessive deviations.

1. Experimental Series I

This series comprises the basic experimental runs B to K for the determination of depth ratios across shocks and of the shock-wave angles. Table III summarizes the experimental runs in this series. The initial Froude numbers F_1 range from a minimum of 2.00 to a maximum of 7.00 for initial depths of $h_1 = 0.90$ inches and $h_1 = 1.50$ inches. The deflection angles Θ were varied in increments of 3° up to a maximum which reached 21° in several cases.

The experimental procedure for a given run is described below. Having chosen nominal values for initial Froude number and initial depth, the channel settings were obtained from the channel calibration curves. (Figs. 8, 9 and 15, Phase I report) Further slope adjustments were then made to produce uniform flow throughout the length of the test section. A plan view of the test section is shown in Fig. 11 which gives also the location of the variable angle deflector vane and the orientation of the transverse and longitudinal scales.

The first step in the experimental run is the determination of the actual initial Froude number F_1 by means of measured velocity distributions which are obtained at station 15 with the deflector vane

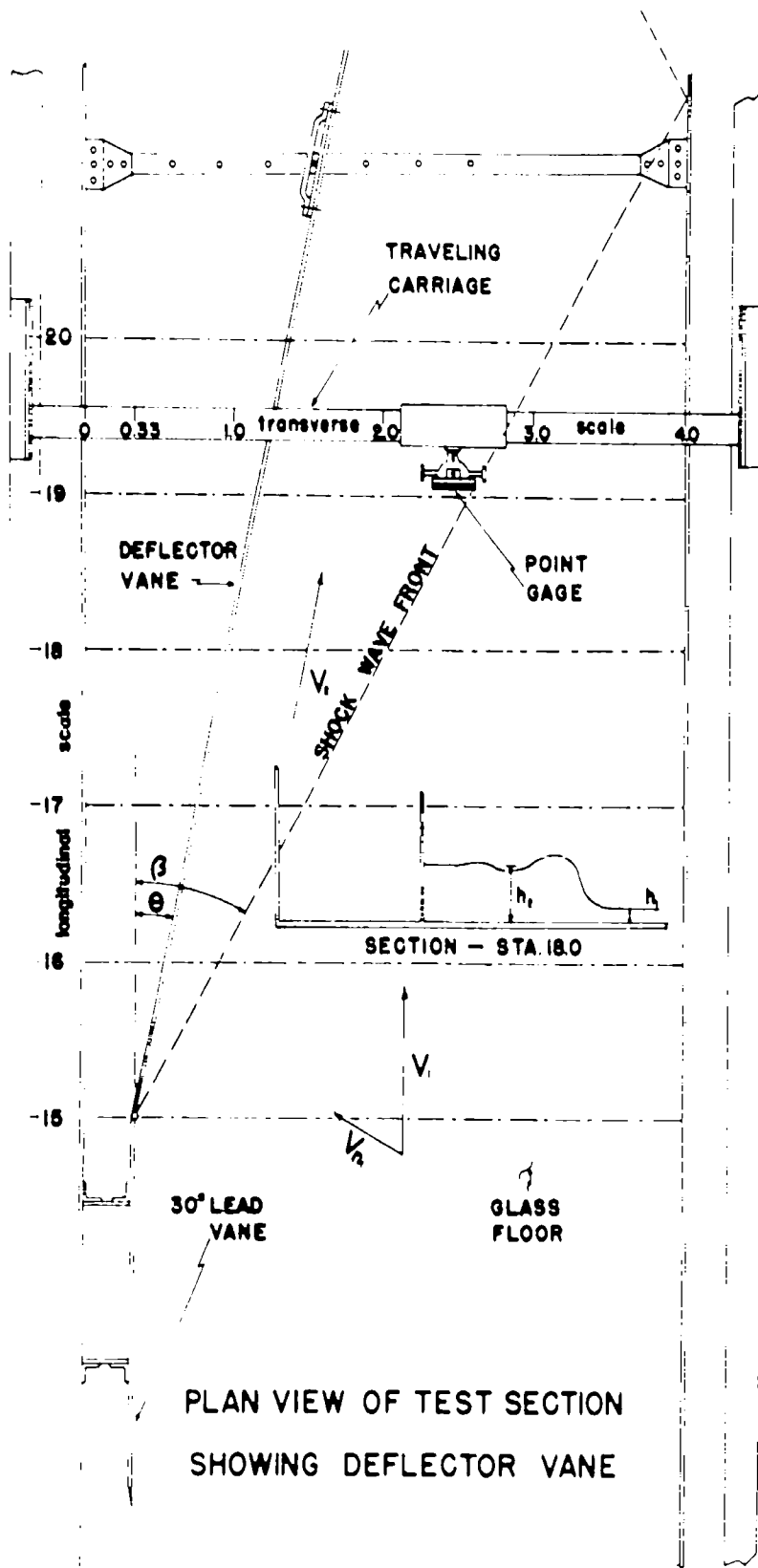
TABLE III

Experimental Series ISUMMARY OF EXPERIMENTAL RUNS FOR DETERMINATION OF SHOCK CHARACTERISTICS BY VARIATION OF F_1 & Θ_1

RUNS B to K

Initial Froude No.	Initial Depth $h_1 = 0.90''$ *	Initial Depth $h_1 = 1.50''$ *
2.00	RUN I $\Theta = 3^\circ, 6^\circ, 9^\circ, 12^\circ$	
2.08		RUN D $\Theta = 3^\circ, 6^\circ, 9^\circ, 12^\circ$
3.05		RUN B $\Theta = 3^\circ, 6^\circ, 9^\circ, 12^\circ, 15^\circ, 18^\circ$
3.20	RUN F $\Theta = 3^\circ, 6^\circ, 9^\circ, 12^\circ, 15^\circ, 18^\circ, 21^\circ$	
3.80		RUN C $\Theta = 3^\circ, 6^\circ, 9^\circ, 12^\circ, 15^\circ, 18^\circ, 21^\circ$
4.18	RUN J $\Theta = 3^\circ, 6^\circ, 9^\circ, 12^\circ, 15^\circ, 18^\circ$	RUN K $\Theta = 9^\circ, 15^\circ$
5.91	RUN G $\Theta = 3^\circ, 6^\circ, 9^\circ, 12^\circ, 15^\circ, 18^\circ$	
6.30		RUN H $\Theta = 3^\circ, 6^\circ, 9^\circ, 12^\circ$
7.00	RUN E $\Theta = 3^\circ, 6^\circ, 9^\circ, 12^\circ, 15^\circ, 18^\circ$	

* All above runs used 30" lead vane.



at $\Theta = 0^\circ$. Nine sections are chosen in the transverse direction between the lead vane and the right hand wall. A standard Pitot tube of the Prandtl type was employed which was attached to the point gage carriage. Before and after the Pitot tube measurements, a transverse depth profile was taken with a dial point gage at station 15.00 in intervals of 0.2 foot. Detailed descriptions and photographs of these instruments are found in Phase I report, section II.

The second step is the determination of the shock-wave depth profiles for successive settings of the deflector vane at intervals of 3° . Starting at longitudinal station 15.00, a depth profile is taken transversely across the test section in the undisturbed region in intervals of 0.2 ft. Thereafter, transverse depth profiles across the shock wave are taken at stations 16.00, 17.00, 18.00, 19.00 and 20.00. All of these depths are read at intervals of 0.05 ft. Following these measurements, a depth profile is obtained along the deflector vane itself. The discharge was measured by means of the 10" x 6" Venturi meter.

For the low Froude numbers, nominal $F_1 = 2$, the maximum angle is limited by a "choking" condition in which the reflection of the shock on the right hand wall strikes the deflector vane. When this occurs, a normal hydraulic jump is formed which moves to a position just upstream of the deflector vane. For certain cases, it was possible to delay this jump formation somewhat by the introduction of a jet of water along the right wall near the point at which the wave is reflected. At high Froude numbers, the maximum practical angle is limited by the overturning of the wave front which introduced considerable difficulties in defining its location. A complete classification of shock waves according to shape is given in the analysis section IV-6.

A series of photographs of the shock-waves obtained in runs J and F are presented in Fig. 12 and Fig. 13 respectively. Figure 12(a) shows the undular type of shock at $\Theta = 6^\circ$ which is associated with small angles; Figure 12(b) through 12(d) show the regular shock and 12(e) illustrates the overturning of the wave front or the "curl-over" obtained for $\Theta = 21^\circ$ at the initial Froude number = 4.18. Figure 13 shows a range of deflection angles for a lower initial Froude number of 3.20. In this case it is seen that the undular type is obtained for $\Theta = 9^\circ$ (Fig. 13(a)) while the jump becomes regular for $\Theta = 12^\circ$ and $\Theta = 15^\circ$, Figs. 13(b) and 13(c). At $\Theta = 20^\circ$ a maximum deflection angle is reached in this particular channel (Fig. 13(d)) and Fig. 13(e) illustrates the choking condition for larger angles.

2. Experimental Series II

This series comprises six runs which were made at the same initial Froude number specifically for the purpose of investigating viscous effects on the shock characteristics. In addition to the deflection angle, the



(a) $\theta = 9^\circ$

INITIAL FROUDE
NUMBER

$F_i = 4.18$

RUN J

INITIAL DEPTH

$h_i = 0.90''$

no lead vane



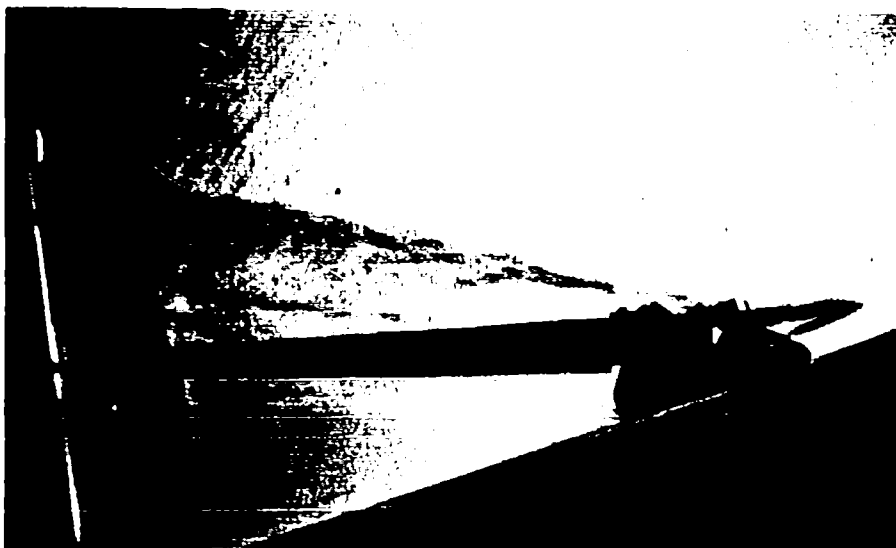
(b) $\theta = 12^\circ$

PHOTOGRAPHS OF SHOCK-WAVES LOOKING
DOWNSTREAM ALONG DEFLECTOR VANE

FIG. 12



(c) $\theta = 12^\circ$

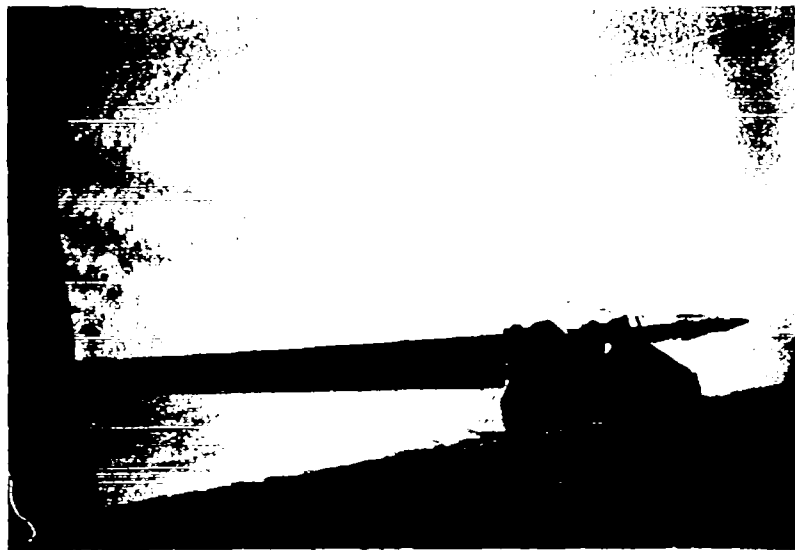


(d) $\theta = 15^\circ$



(e) $\theta = 18^\circ$

FIG. 12 (cont.)



(a) $\theta = 9^\circ$

INITIAL FROUDE
NUMBER

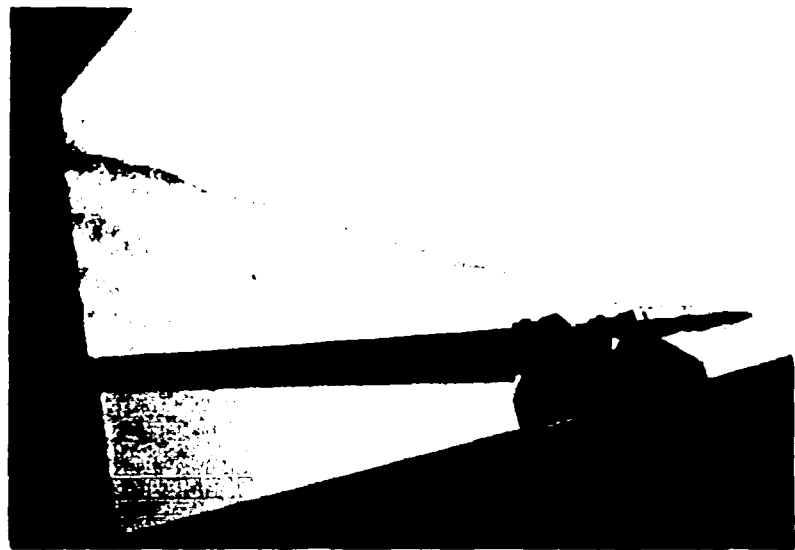
$F_i = 3.20$

RUN F

INITIAL DEPTH

$h_i = 0.90''$

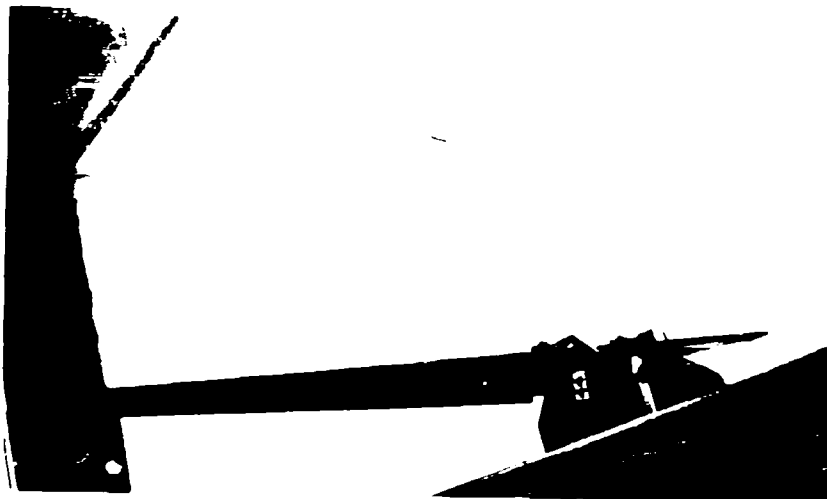
no lead vane



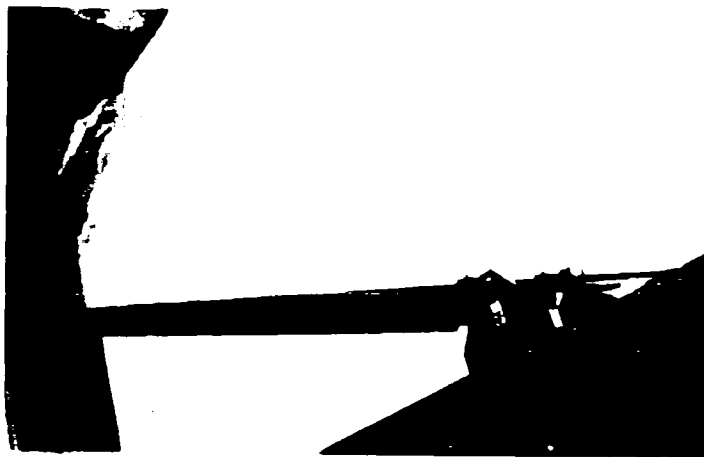
(b) $\theta = 12^\circ$

PHOTOGRAPHS OF SHOCK-WAVES LOOKING
DOWNSTREAM ALONG DEFLECTOR VANE

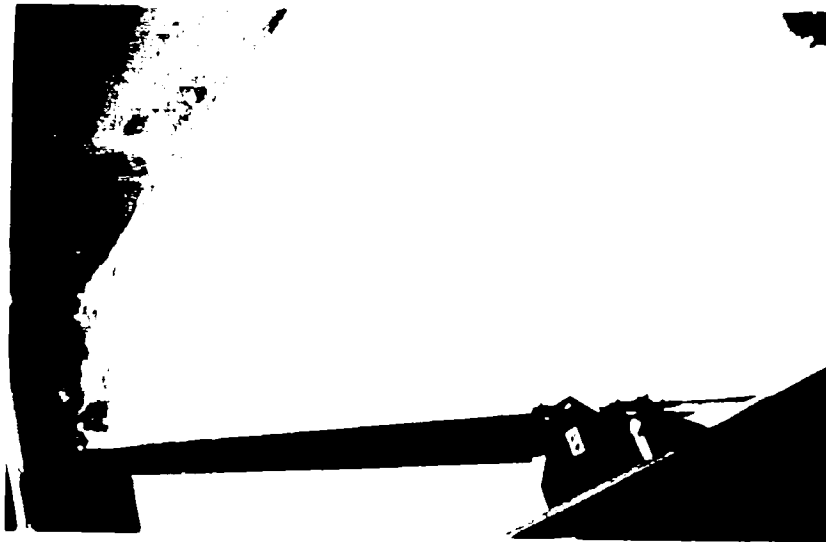
FIG. 13



(c) $\theta = 15^\circ$



(d) $\theta = 20^\circ$



(e) $\theta = 21^\circ$

MAXIMUM ANGLE
WITHOUT CHOKING

NORMAL JUMP
MOVING UPSTREAM

FIG. 13 (cont.)

variables in this series were: the initial depth h_1 and the length of the lead vane. Two sets of runs were made, each with three different initial depths. In the first set, a lead vane of 30" length preceded the deflector vane, and in the second set the lead vane was omitted. It was found unnecessary to add runs with intermediate lengths of lead vane. The runs are summarized in Table IV.

A great deal of care was necessary to obtain the same Froude number at various initial depths. Several preliminary velocity distributions were necessary in order to calculate F_1 and make the adjustments to reach the prescribed value of $F_1 = 4.18$. Experimentally, the procedure is otherwise exactly the same as for Series I.

3. Experimental Series III

This series of experiments is designed to show the effect of initial flow conditions on the depth profile along the deflector vane. The results of these experiments are intended to be chiefly useful in determining the size of models necessary to produce good experimental results. The variables investigated were length of lead vane, initial Froude number, initial depth and deflection angle. The experimental runs in this series are summarized in Table V.

The experimental procedure consists of setting up the required flow conditions determined by F_1 and h_1 ; the depth profile along the deflector vane was then measured with the point gage for lead vanes of length 30", 6" and zero for various deflection angles. The actual depths were measured at a distance of $3/16$ " away from the wall to avoid the slight effect of the meniscus. The depth profiles for the 30" lead vane were obtained from the runs of Series I. Thereafter, the same flow conditions were duplicated for the two sets of runs with 6" and zero lead vane.

4. Experimental Series IV

Two experimental runs were made to obtain data for the direct determination of the Froude number F_2 behind the shock-wave. Complete velocity distributions in back of the shock-wave were necessary for this purpose. These runs are designated 1B-V₂ and 1F-V₂. The Pitot tube was placed with its nose parallel to the deflector vane set at $\Theta = 90^\circ$ in both cases. At station 20.68 eight locations were chosen in a direction perpendicular to the deflector vane extending completely across the shock and into the undisturbed flow. At each location, a vertical velocity distribution was measured, and the corresponding depth profile was also determined across this same section.

TABLE IV

Experimental Series II

SUMMARY OF EXPERIMENTAL RUNS FOR DETERMINATION OF SHOCK CHARACTERISTICS
BY VARIATION OF h_1 AND LENGTH OF LEAD VANE.

$F_1 = 4.18$ Constant for All Runs

Runs J to O

30" lead vane			No lead vane		
$h_1 = 1.50"$	$h_1 = .90"$	$h_1 = .60"$	$h_1 = 1.50"$	$h_1 = .90"$	$h_1 = .60"$
RUN K $\Theta = 9^\circ, 15^\circ$	RUN J $\Theta = 3^\circ, 6^\circ, 9^\circ, 12^\circ, 15^\circ, 18^\circ$	RUN L $\Theta = 9^\circ, 15^\circ$	RUN N $\Theta = 9^\circ, 15^\circ$	RUN M $\Theta = 9^\circ, 15^\circ$	RUN O $\Theta = 9^\circ, 15^\circ$

TABLE V

Experimental Series III

SUMMARY OF EXPERIMENTAL RUNS FOR DETERMINATION OF DEPTH PROFILE ALONG
DEFLECTOR VANE.

Runs B to J, 1B to 1J and 2B to 2J

Initial Froude No.	30" lead vane		6" lead vane		No lead vane	
	$h_1 = .90"$	$h_1 = 1.50"$	$h_1 = .90"$	$h_1 = 1.50"$	$h_1 = .90"$	$h_1 = 1.50"$
2.00	I		1I		2I	
2.08		D		1D		2D
3.05		B		1B		2B
3.20	F		1F		2F	
3.80		C		1C		2C
4.18	J		1J		2J	
5.91	G		1G		2G	
6.30		H		1H		2H
7.00	E		1E		2E	

SECTION IV

ANALYSIS OF EXPERIMENTAL DATA

1. Method of Determining the Shock-Wave Characteristics from Experiments

In this section, the method is described by which experimental values are determined for -

- a. Initial Froude number - F_1
- b. Depth ratio across shock - h_2/h_1
- c. Shock wave angle - β
- d. Froude number behind shock - F_2

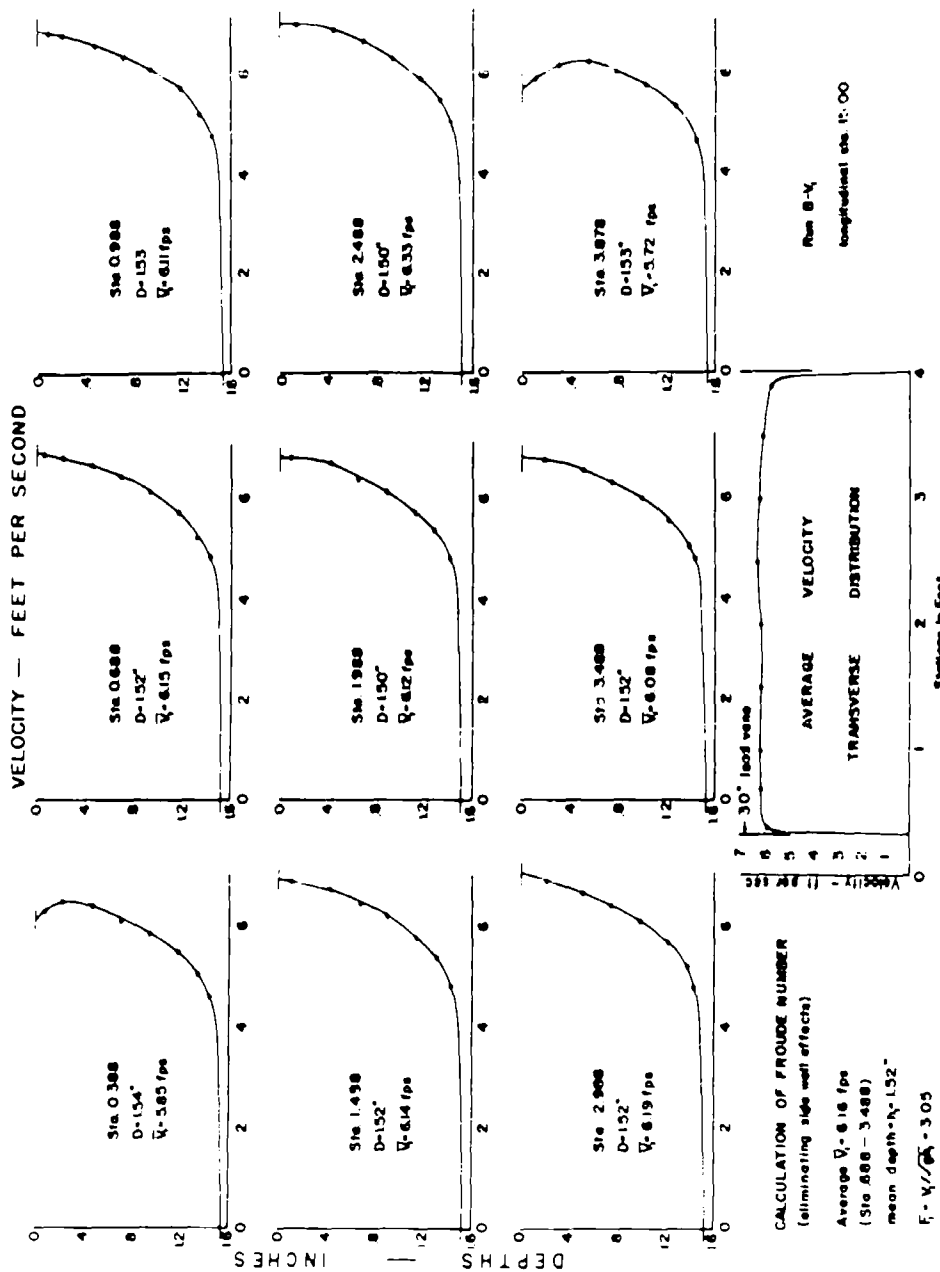
a. Determination of Initial Froude Number

The results of the velocity distribution measurements described in section III are plotted in Fig. 14 for Run B and in Fig. 15 for Run G. The average velocity for each vertical profile is determined by planimetry of the area under the velocity curve. The average velocities are then plotted to obtain the transverse distribution curve. Since the shock wave is surveyed in the center portion of the channel, the Froude number must be determined from the velocity distribution measured in that part of the channel. Effectively, this means that the boundary layers along the sides of the channel are excluded in determining the effective Froude number. This overall average of the velocities as determined in run B, for example Fig. (14), is designated as V_1 . The corresponding depths are then averaged for this same section into a mean value of h_1 . The initial Froude number F_1 for the run is then computed

from $F_1 = \frac{V_1}{\sqrt{gh_1}}$. This value is recorded in column 2 on the summary sheets of Table VI.

b. Determination of Depth Ratio Across Shock

For a given run, a plot is made in which a plan view of the channel bottom is represented to the same longitudinal and transverse scales. The wave profiles are then plotted at their respective longitudinal stations; the actual depths being plotted to a vertical scale independent of the longitudinal scale. The resulting plot gives a "perspective" view of the shock front while retaining all dimensions in true scale, the only restriction being that angles be measured in the plane of the channel floor. These plots have been made for the experimental series A through O comprising a total of 59 runs. The plots for each series A through J for



VELOCITY DISTRIBUTION FOR
DETERMINATION OF INITIAL FROUDE NUMBER

FIG. 14

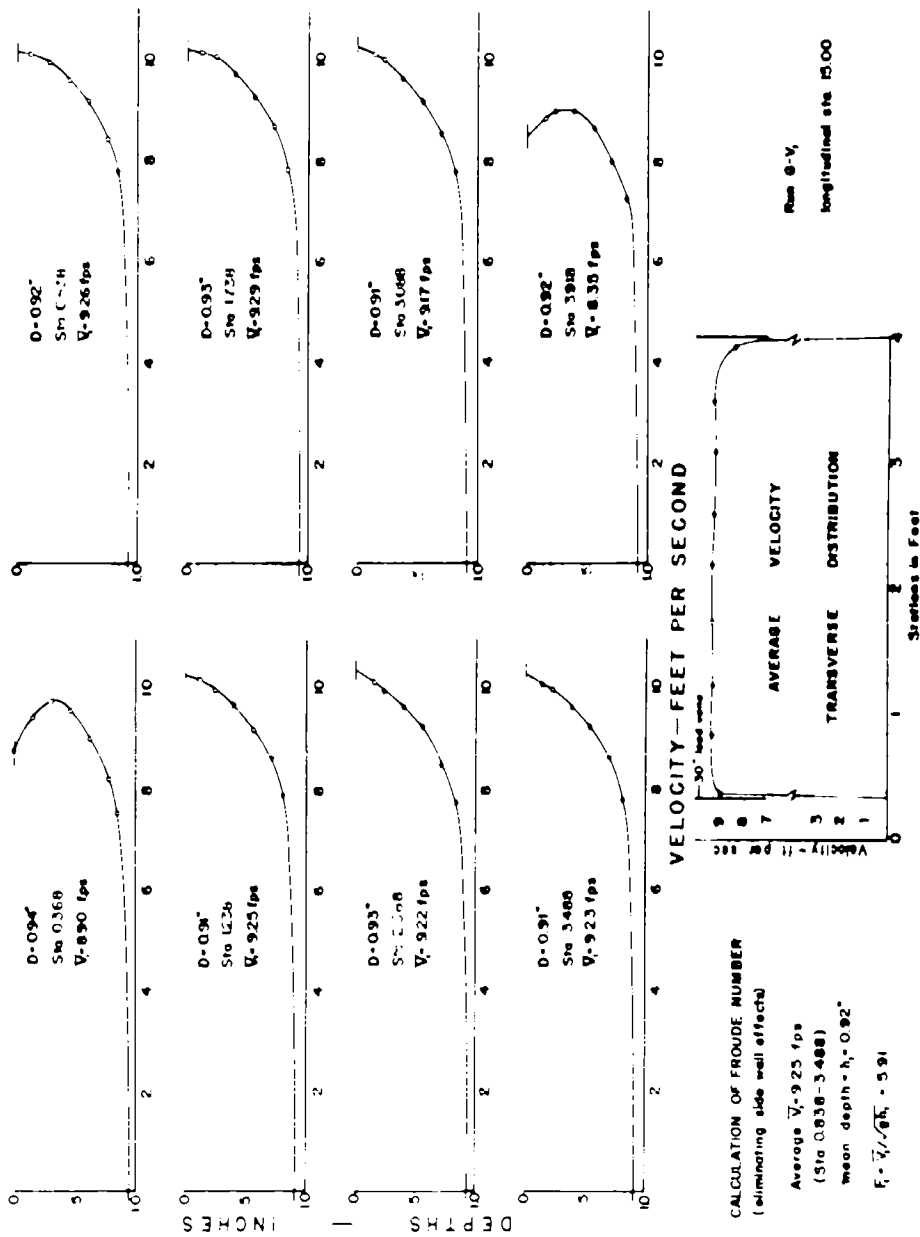


FIG. 15

$\Theta = 9^\circ$ only are reproduced in this report as Figs. 16(a) through 16(j). The depth h_1 , being the depth of the undisturbed portion of the flow, is readily determined since the wave profile levels off in front of the shock. The depth h_2 , i.e. the depth following the shock, is determined by a consideration of the type of shock produced by the flow conditions. While the classification of the shocks is treated in section IV-6; it may suffice to say here that in general the basic form of the shock wave may be either undular or regular. In the case of the undular form, the equilibrium depth is well defined. The small undulations behind the initial front gradually disappear leaving a region of constant depth as the deflector vane is approached. Furthermore, it is known (Ref. 22) and confirmed by the above experiments that the line of the equilibrium depth passes through the points of inflection of the undulations following the initial front. In the case of the regular shocks, the depth h_2 is less easily defined due to the increasingly intense surface disturbances near the shock front. The depths h_1 and h_2 are represented on the plots, Fig. 16(a-j), by horizontal dashed lines. It should be pointed out that the depth ratios are determined from those profiles where the shock front lies a considerable distance away from the deflector vane and where, therefore, the profile is no longer affected by the initial distortion of the shock wave. This distortion is due to the vertical accelerations set up by the sudden change in direction required of the flow approaching the front portion of the deflector vane. For each run, the region of distortion may be observed from a consideration of the depth profile along the deflector vane which is also included in Figs. 16(a-j). The final value of h_2/h_1 for each run is the average of the individual ratios for several transverse depth profiles. This value is again recorded on the summary sheets, Table VII, column 7.

c. Determination of Shock Wave Angle

The shock wave angle, β , is obtained by use of the horizontal lines denoting average value of h_1 and h_2 . Let Fig. 17 represent a typical wave profile. The effective location of the wave front has been consistently assumed herein as being determined by a vertical line drawn so that area $abo = a'b'o$. The intersection of this line with the channel floor is marked as point (q). Point (q) is determined for each profile lying outside of the region of initial distortion, and a straight line is drawn in plan through the points to determine the shock front.. While this method seems off hand somewhat arbitrary, it is a logically consistent system based on previous experimental experience in this laboratory (Ref. 8). This method has the advantage of not placing undue weight upon any one measured point on the wave front; in addition, the position of the vertical line can be rapidly determined by breaking up the areas into small triangles and parallelograms. The consistency of the method is shown by the fact that in most cases a straight line passes through the points determined in the above manner. The value of β exp. thus obtained is recorded on the summary

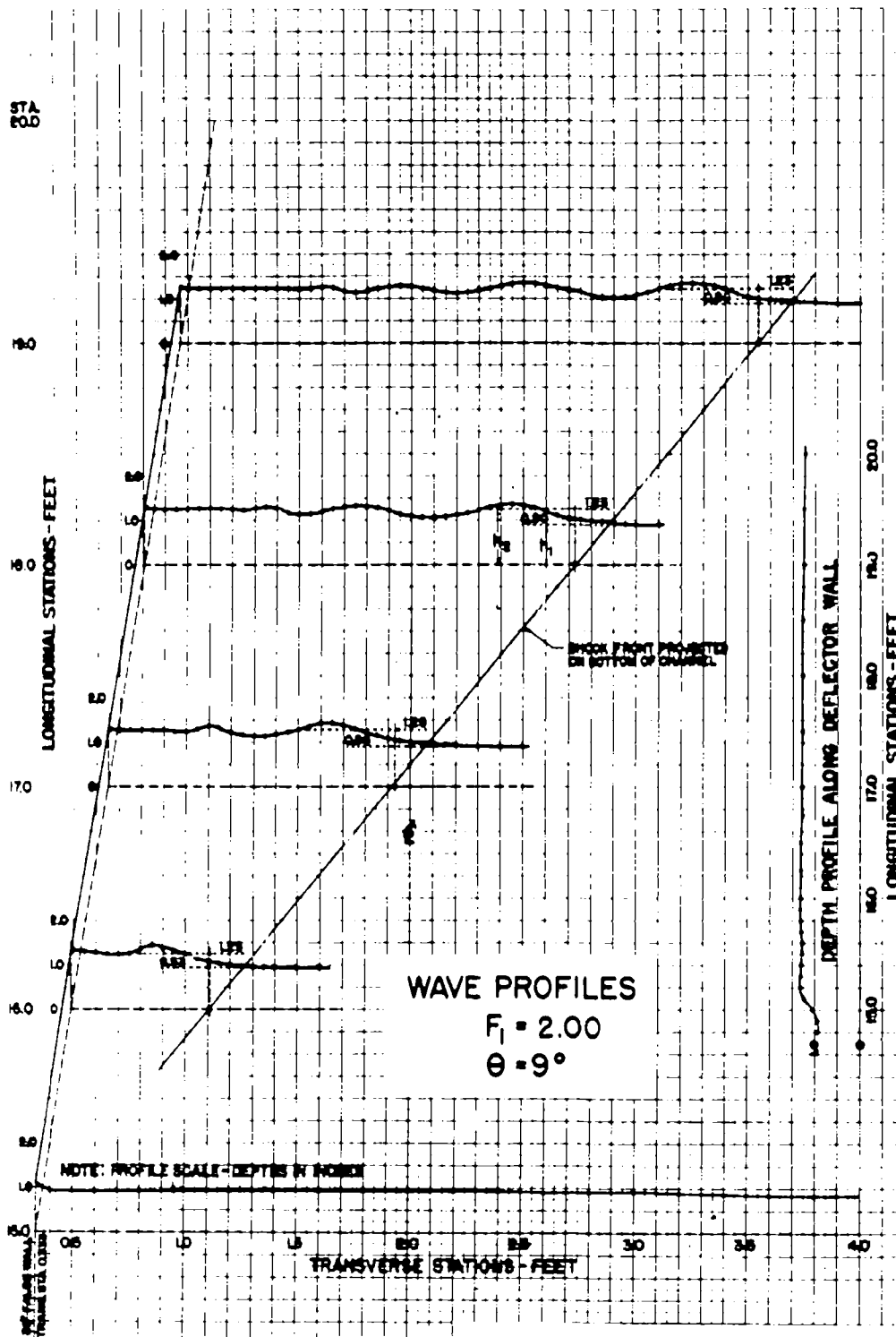


FIG. 16a

MASSACHUSETTS INSTITUTE OF TECHNOLOGY
 HYDRODYNAMICS LABORATORY
 DEPARTMENT OF CIVIL AND SANITARY ENGINEERING
 HYDRAULIC ANALOGY TO SUPERSONIC
 FLOW OF GASES

U.S.A.F. RESEARCH PROJECT
 SHEET 1-3

DIC 3-6547

MAY 1949

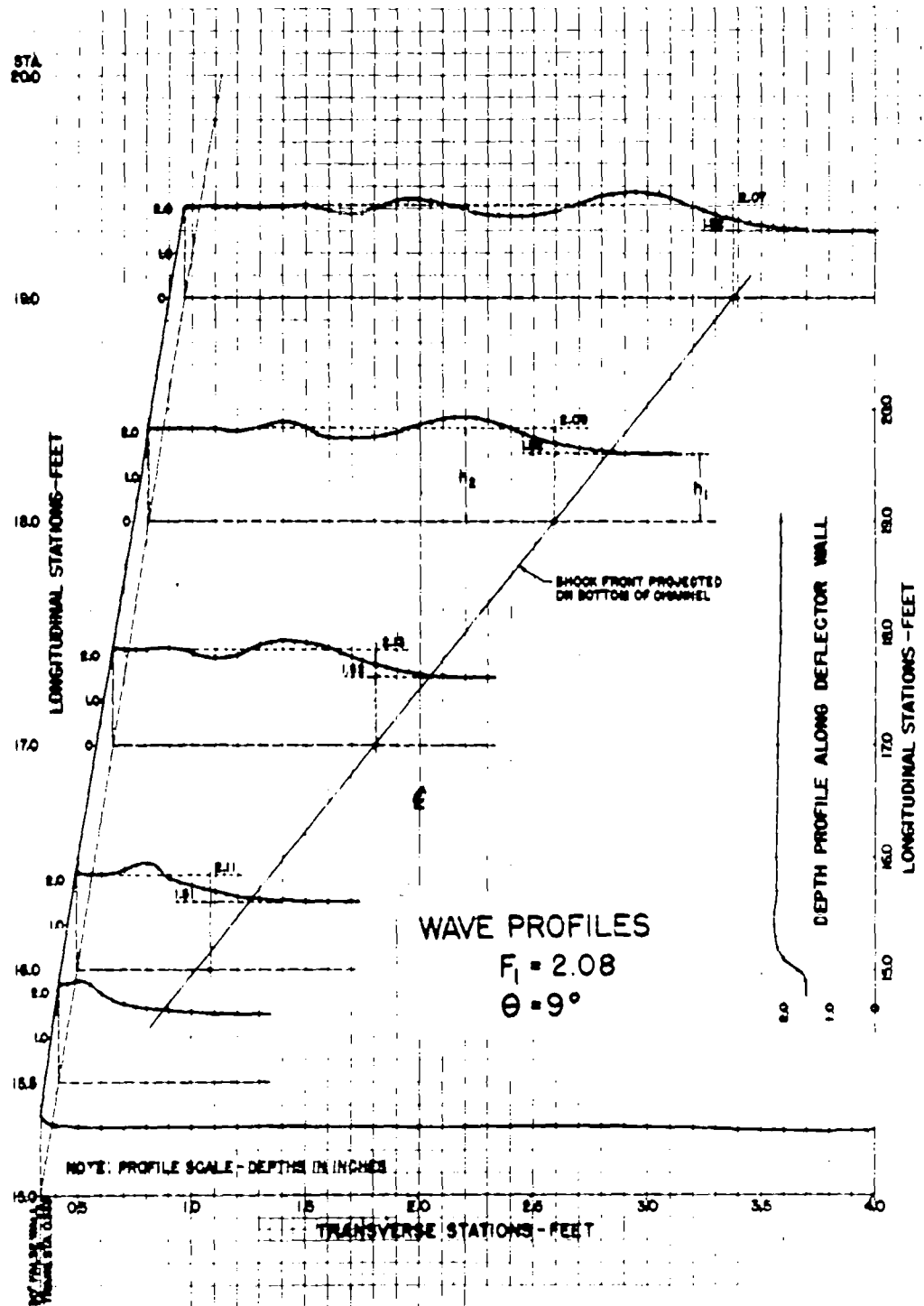


FIG. 16b

MASSACHUSETTS INSTITUTE OF TECHNOLOGY
 HYDRODYNAMICS LABORATORY
 DEPARTMENT OF CIVIL AND SANITARY ENGINEERING
 HYDRAULIC ANALOGY TO SUPERSONIC
 FLOW OF GASES

U.S.A.F. RESEARCH PROJECT
 SHEET D-3 DIC 3-6547 MAY 1949

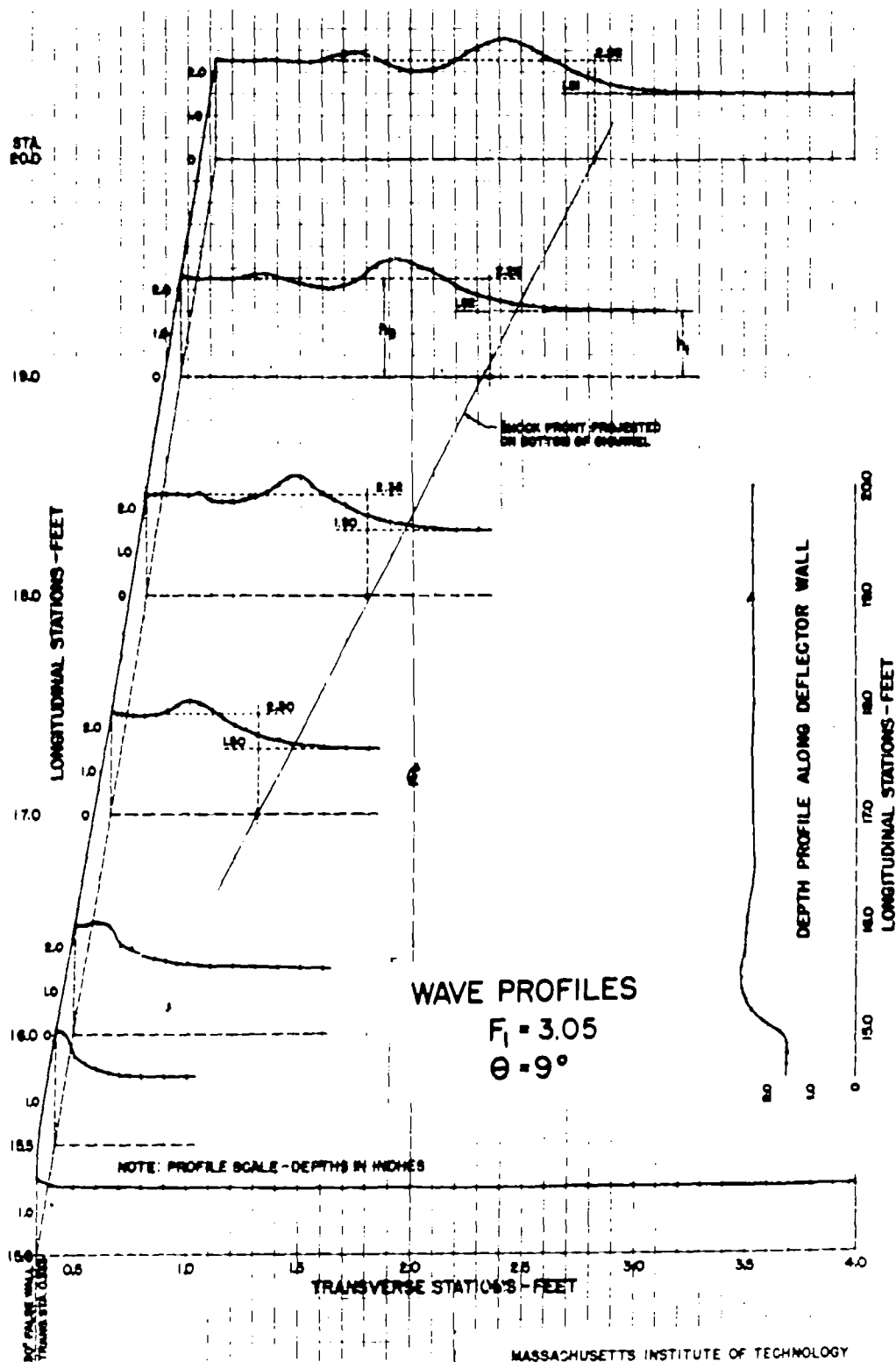


FIG. 16c

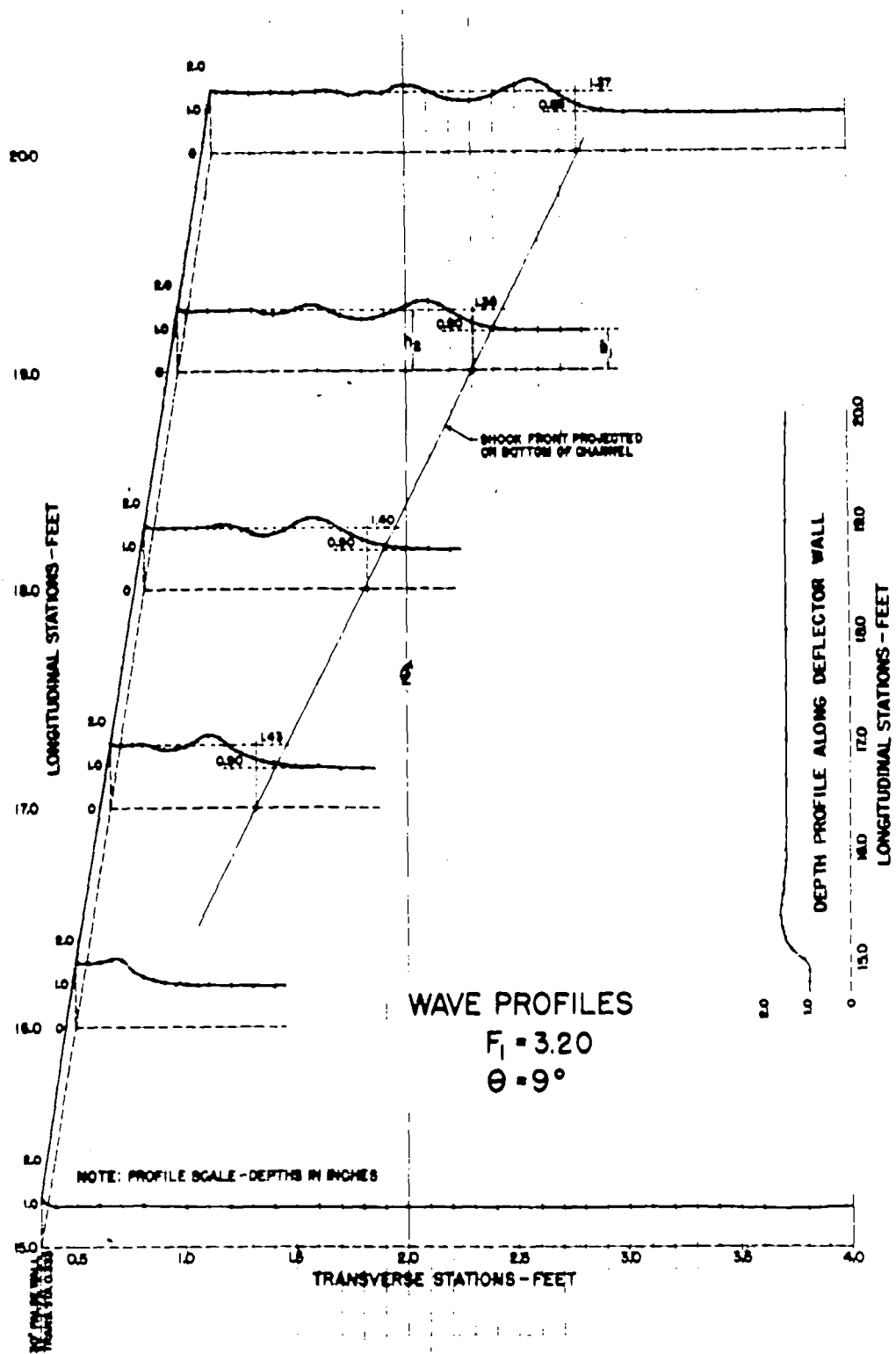


FIG. 16 d

MASSACHUSETTS INSTITUTE OF TECHNOLOGY
HYDRODYNAMICS LABORATORY
DEPARTMENT OF CIVIL AND SANITARY ENGINEERING
HYDRAULIC ANALOGY TO SUPERSONIC
FLOW OF GASES

U.S.A.F. RESEARCH PROJECT
SHEET F-3 DIC 3-6547 MAY 1949

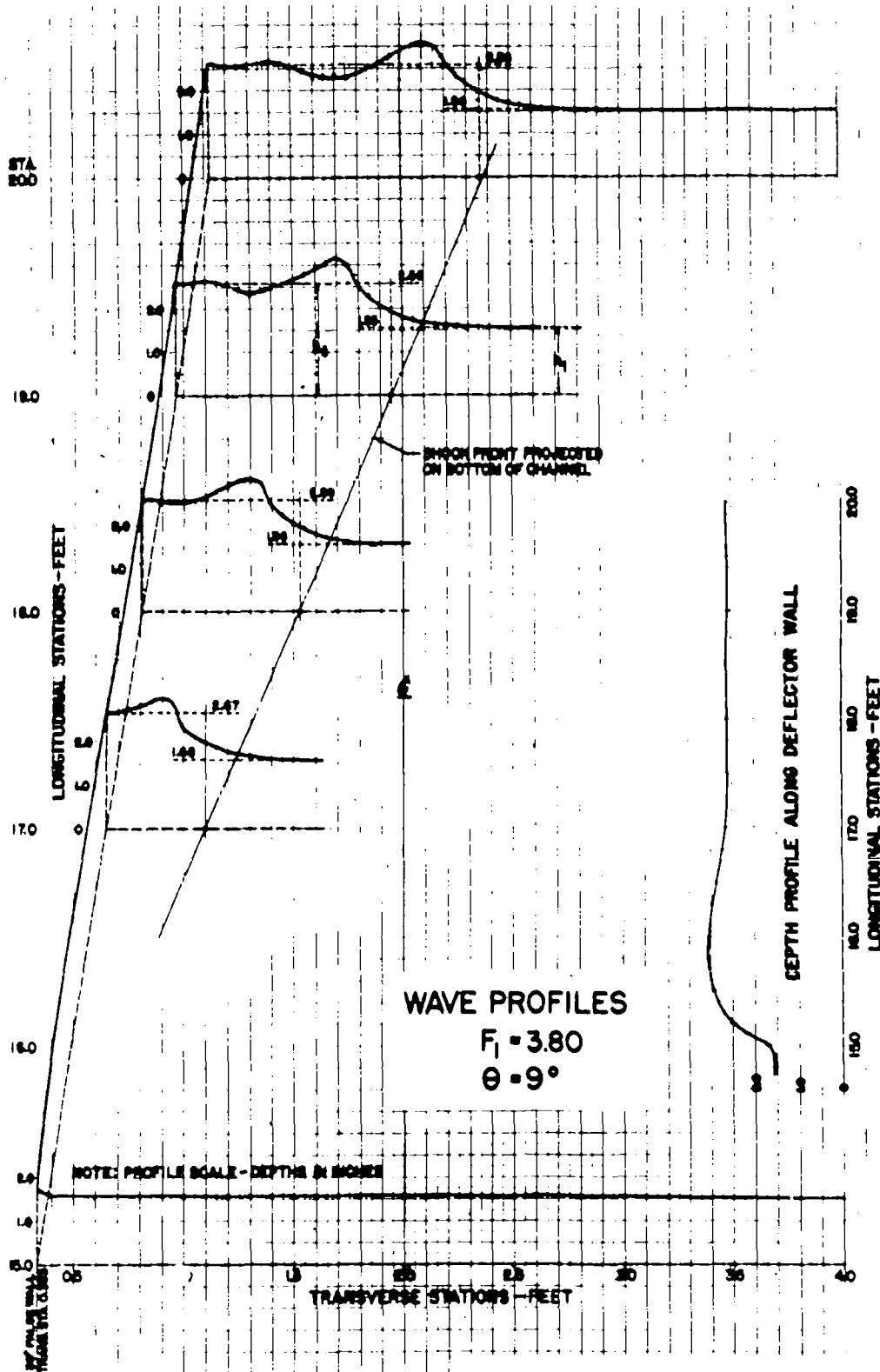


FIG. 16e

MASSACHUSETTS INSTITUTE OF TECHNOLOGY
 HYDRODYNAMICS LABORATORY
 DEPARTMENT OF CIVIL AND SANITARY ENGINEERING
 HYDRAULIC ANALOGY TO SUPERSONIC
 FLOW OF GASES

U.S.A.F. RESEARCH PROJECT
 SHEET C-3 D1C 3-6547 MAY 1949

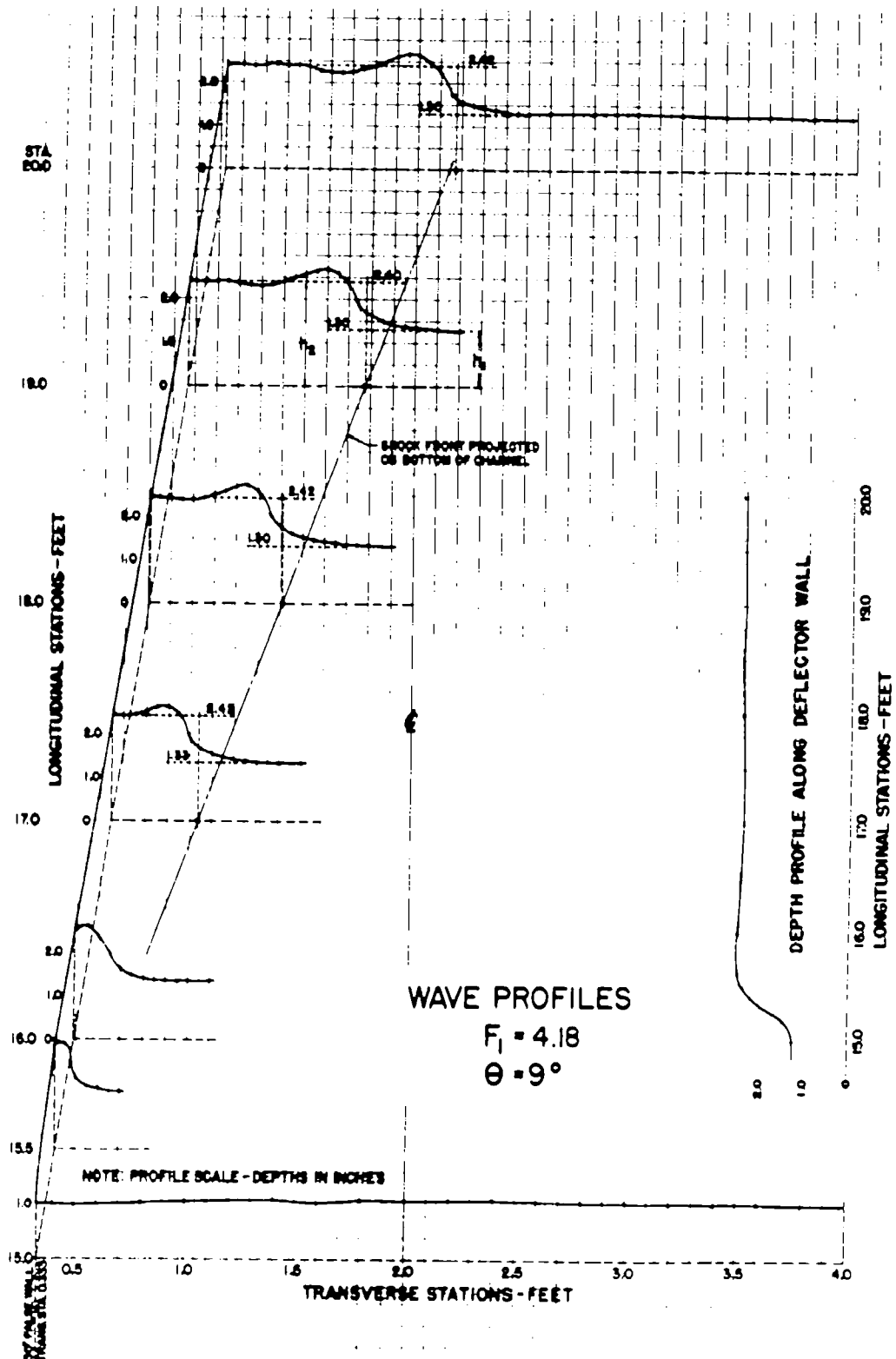


FIG. 16f

MASSACHUSETTS INSTITUTE OF TECHNOLOGY
HYDRODYNAMICS LABORATORY
DEPARTMENT OF CIVIL AND SANITARY ENGINEERING
HYDRAULIC ANALOGY TO SUPERSONIC
FLOW OF GASES

U.S.A.F. RESEARCH PROJECT
SHEET A-3 DIC 3-6547

MAY 1949

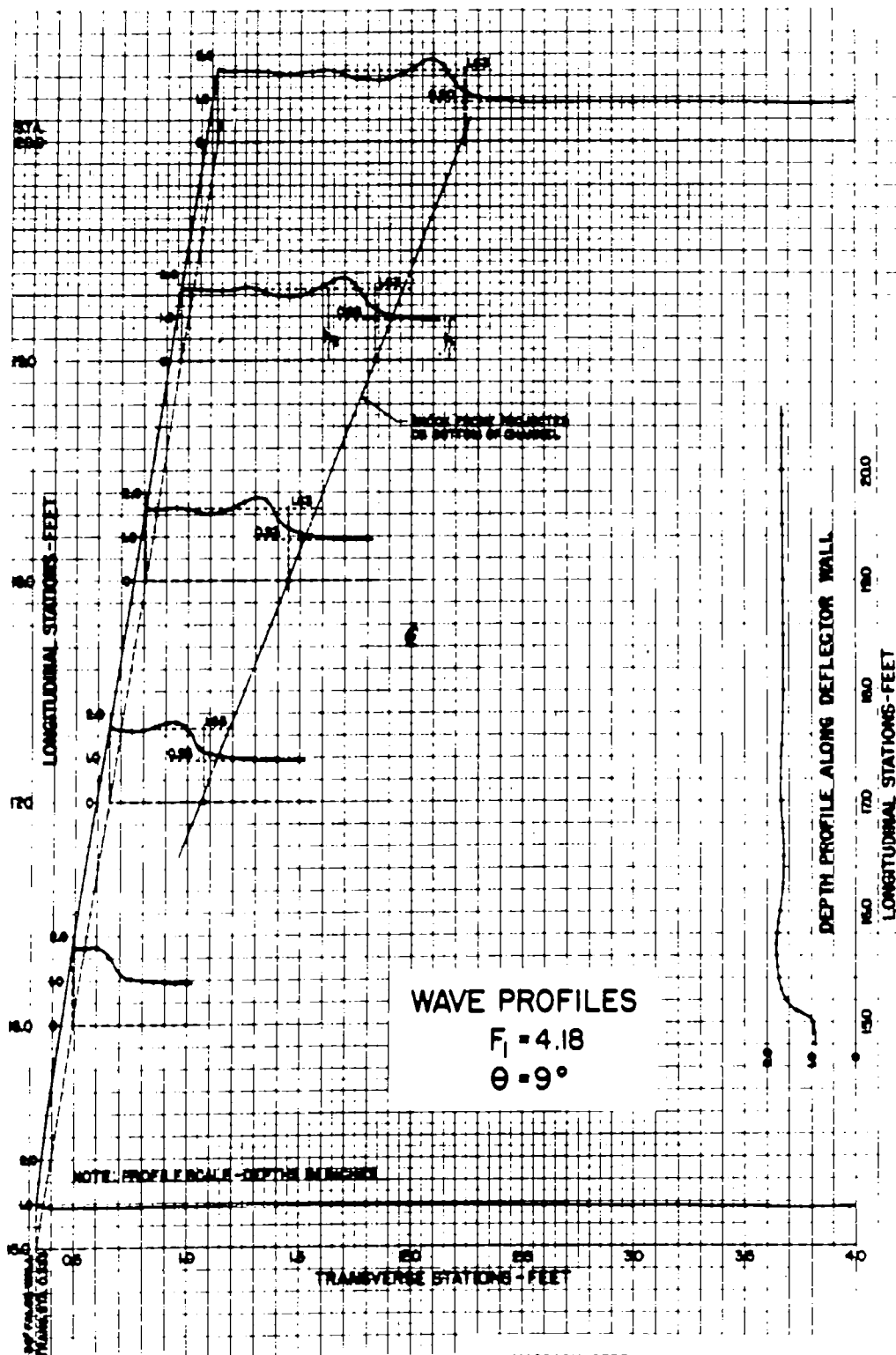


FIG. 16 g

MASSACHUSETTS INSTITUTE OF TECHNOLOGY
 HYDRODYNAMICS LABORATORY
 DEPARTMENT OF CIVIL AND SANITARY ENGINEERING
 HYDRAULIC ANALOGY TO SUPERSONIC
 FLOW OF GASES

U.S.A.F. RESEARCH PROJECT
 SHEET J-3 D10 3-6547 MAY 1949

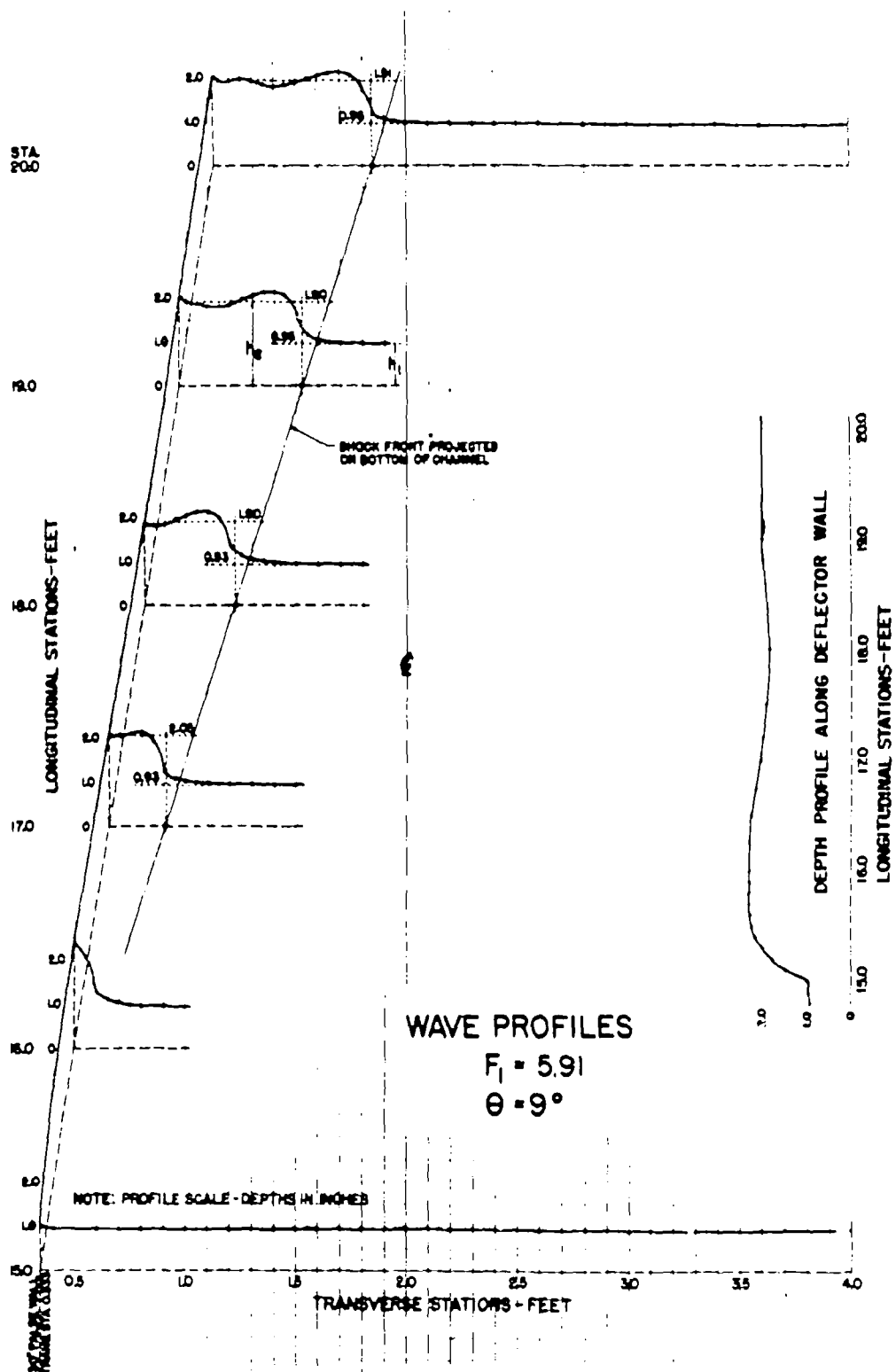


FIG. 16h

MASSACHUSETTS INSTITUTE OF TECHNOLOGY
HYDRODYNAMICS LABORATORY
DEPARTMENT OF CIVIL AND SANITARY ENGINEERING
HYDRAULIC ANALOGY TO SUPERSONIC
FLOW OF GASES

U.S.A.F. RESEARCH PROJECT
SHEET G-3 DIC 3-6547 MAY 1949

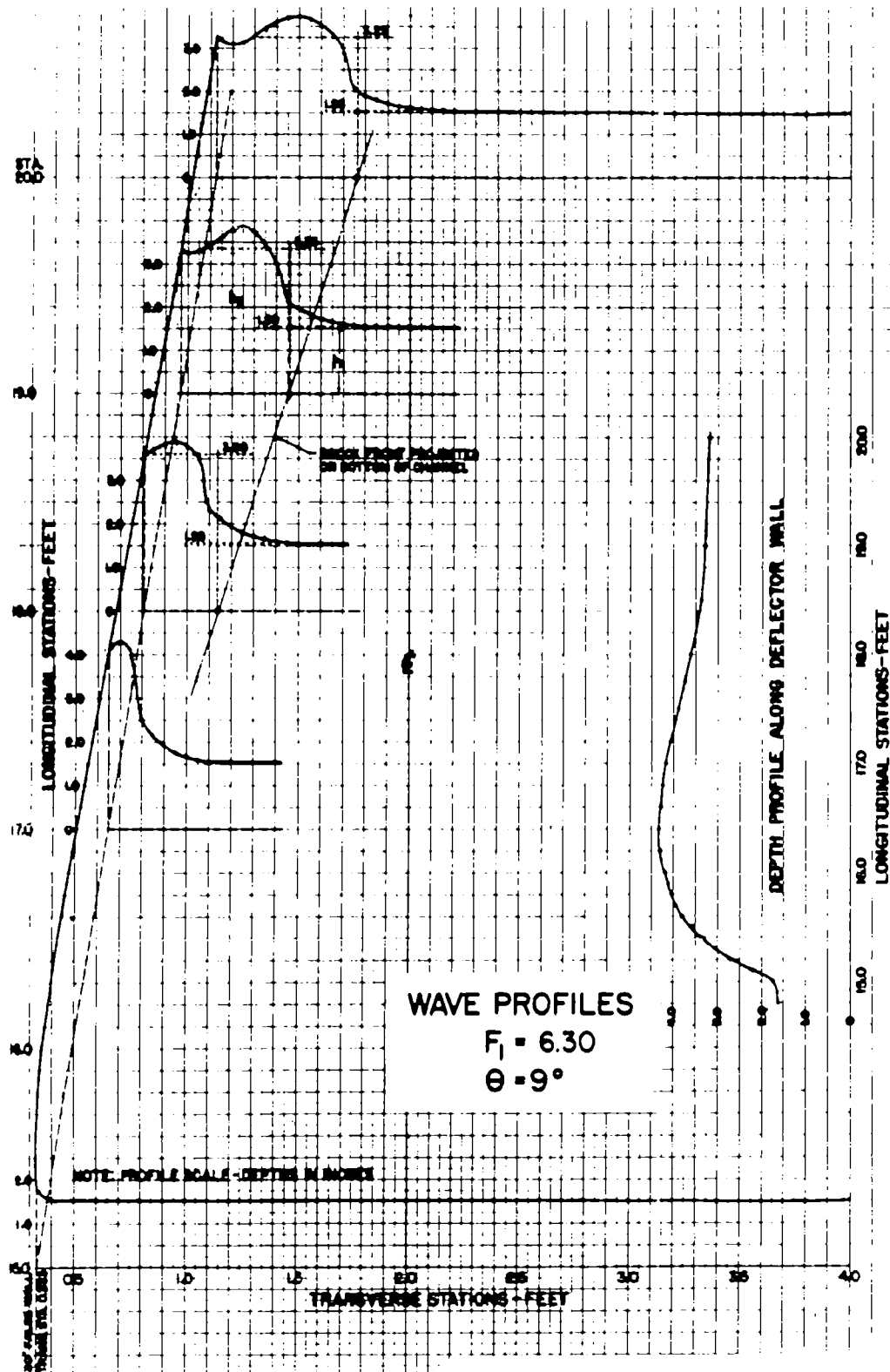


FIG. 16i

MASSACHUSETTS INSTITUTE OF TECHNOLOGY
 HYDRODYNAMICS LABORATORY
 DEPARTMENT OF CIVIL AND SANITARY ENGINEERING
 HYDRAULIC ANALOGY TO SUPERSONIC
 FLOW OF GASES

U.S.A.F. RESEARCH PROJECT
 SHEET M-3 DIC 3-6547 MAY 1949

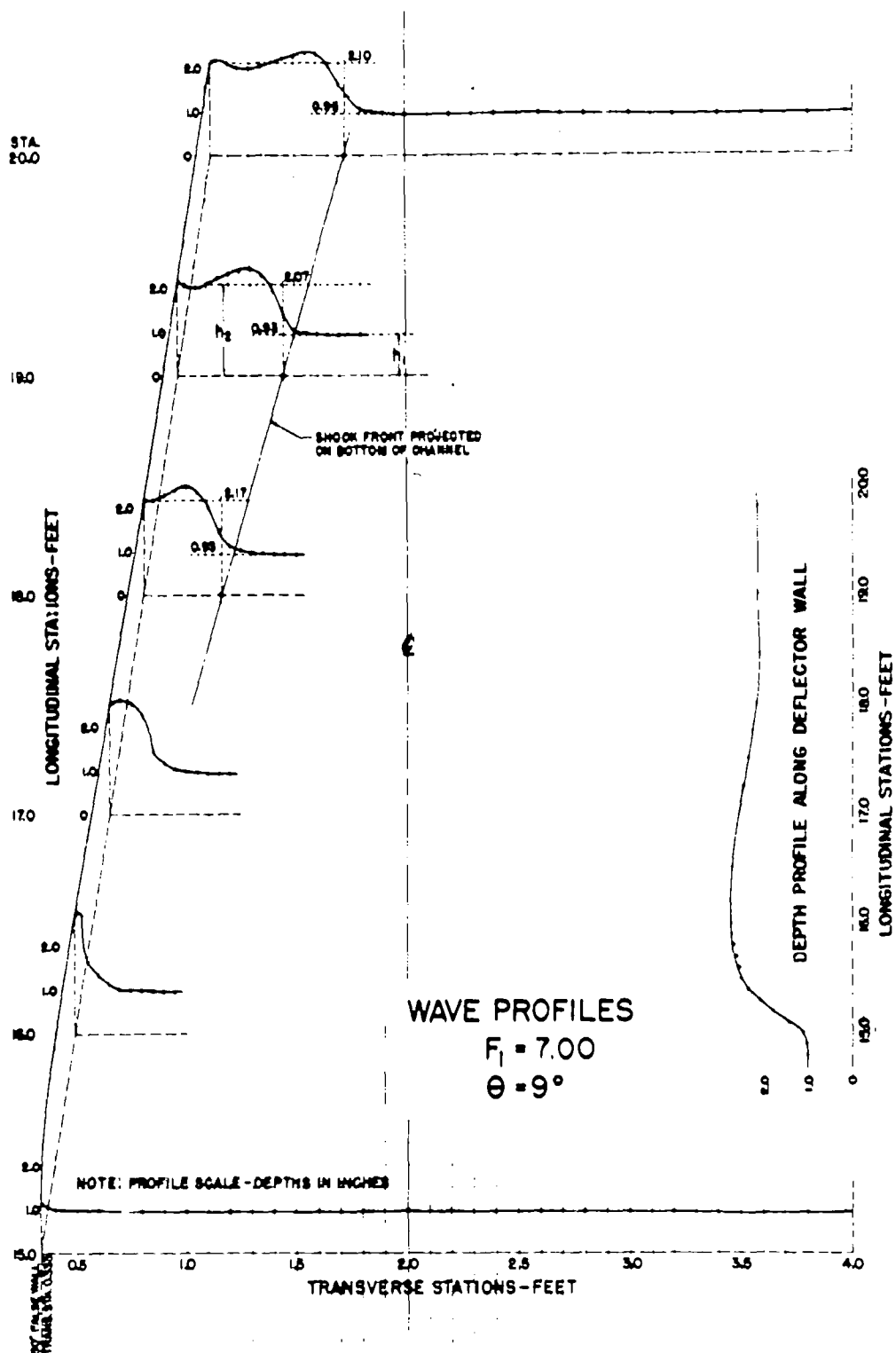


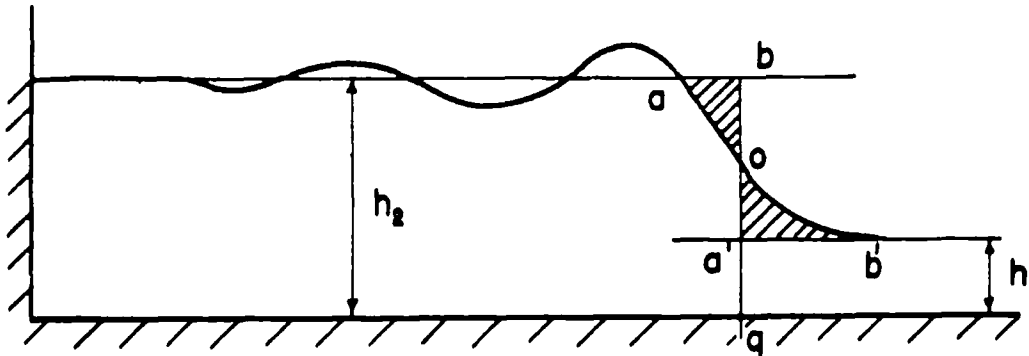
FIG. 16 j

MASSACHUSETTS INSTITUTE OF TECHNOLOGY
HYDRODYNAMICS LABORATORY
DEPARTMENT OF CIVIL AND SANITARY ENGINEERING
HYDRAULIC ANALOGY TO SUPERSONIC
FLOW OF GASES

U.S.A.F. RESEARCH PROJECT
SHEET E-3 DIC 3-6547 MAY 1949

sheets, Table VI, in column 4.

AREA $abo = a'b'o$



Section through Shock Wave Showing
Method of Determining Shock Front

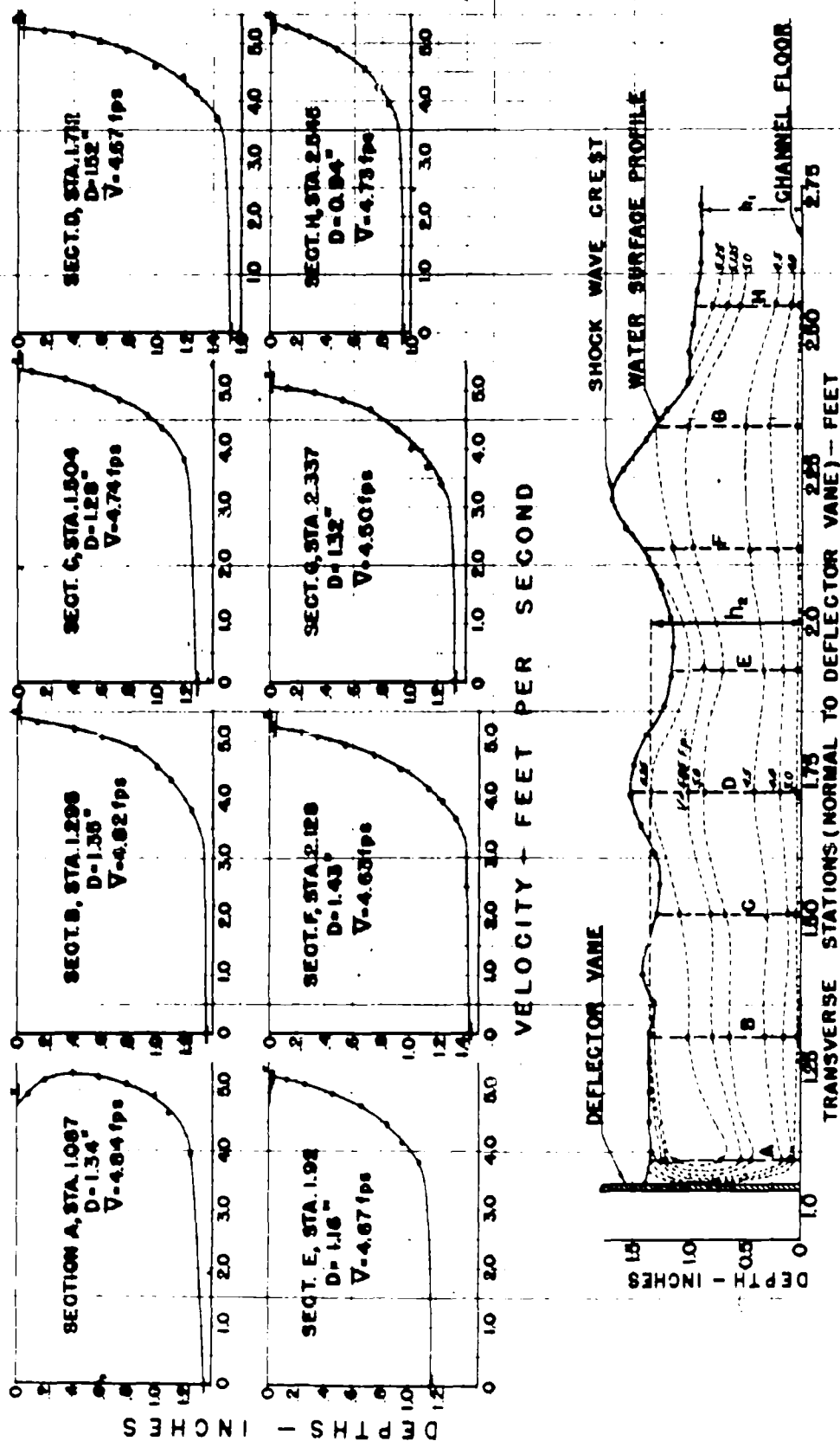
Fig. 17

d. Determination of Froude Number behind Shock

The Froude number in back of the shock is calculated from the initial Froude number and the experimental depth ratio by means of Eq. (37b).

$$F_2 = \sqrt{\frac{h_1}{h_2} \left[F_1^2 - \frac{1}{2} \frac{h_1}{h_2} \left(\frac{h_2}{h_1} - 1 \right) \left(\frac{h_2}{h_1} + 1 \right)^2 \right]} \quad (37-b)$$

This value of F_2 (since it is determined from experimental values of F_1 , h_1 and h_2) is recorded in the summary sheets, Table VII, column 10, as F_2 exp. In order to check the accuracy of this indirect method, the special experimental runs designated as Series IV were made. The data for both runs were plotted as illustrated in Fig. 18 for run 1F - V2. The vertical velocity distributions corresponding to the locations in the section of the shock-wave perpendicular to the deflector vane are plotted in the top half of the figure. The cross section in the lower half shows the actual velocity contours for this transverse section. The values of \bar{V}_2 obtained from each vertical section A through G were averaged to obtain the value of V_2 used to calculate F_2 . The equilibrium depth h_2 is shown by the horizontal dashed line. Table VI gives a comparison of the values of F_2 obtained by this method with values obtained by use of F_1 and of experimental values of h_2/h_1 .



RUN IF-V2

VELOCITY PROFILES AND CONTOURS BEHIND SHOCK
FRONT FOR $\theta = 9^\circ$; INITIAL FROUDE NO. $F_1 = 3.20$, $h_1 = 0.90$ ".
AVERAGE $V_2 = 4.69$ (sect. A to G), $h_2 = 1.35$ ". $F_2 = V_2/\sqrt{gh_2} = 2.47$

FIG. 18

TABLE VI
COMPARISON OF METHODS FOR DETERMINATION OF F_2

Method of Analysis	RUN IF-V ₂		RUN IB-V ₂	
	F_1	Calculation of F_2	F_1	Calculation of F_2
Velocity Dist. Behind Shock	3.20	$V_2 = 4.69 \text{ fps}, h_2 = 1.35"$ $F_2 = 2.47$	3.05	$V_2 = 5.95 \text{ fps}, h_2 = 2.34"$ $F_2 = 2.37$
Eq. (37b) using F_1 and h_2/h_1 (exp)	3.20	h_2/h_1 (exp) = 1.50 $F_2 = 2.47$	3.05	h_2/h_1 (exp) = 1.51 $F_2 = 2.34$

Table VI indicates that a reliable value for F_2 may be obtained using Eq. (37) as was done consistently in this report.

2. Correlation of Oblique Jump Characteristics with Hydraulic Theory

This section presents the principal experimental and theoretical correlations of this investigation. The experimentally determined shock wave characteristics of each experimental Series B through O are given in Tables VII (a-j) together with the corresponding theoretical characteristics and the percentage differences between experiment and theory. The method of obtaining the experimental characteristics was described in the preceding section 1. A brief description of the calculated quantities follows. Column 3 lists a Froude number based on the deflection angle and the experimental shock-wave angle (Eq. 36b); it is not a theoretical quantity and is presented for comparative purposes only. In all calculations, the initial Froude number, (obtained from Pitot tube traverses) which is constant for a given run, is used, and the computation of this value is shown at the bottom in the correlation Tables VII. Column 5 records the theoretical wave angle β as determined from Eq. (36). (See Fig. 8 left-hand side) Column 6 gives the percent difference between calculated and experimental values. The theoretical depth ratio is given in column 8 as obtained from Eq. (35) using the theoretical shock-wave angle and Θ . Column 9 again gives the percentage difference for experimental and calculated values for the depth ratio. The values of F_2

Run	(1) Wall Angle	(2) Froude No.	(3) Froude No.	(4) Wave Angle	(5) Wave Angle	(6) Wave Angle	(7) Depth Ratio	(8) Depth Ratio	(9) Depth Ratio	(10) Froude No.	(11) Froude No.	(12) Froude No.
	Θ	F_1	F_1	β_1	β_1	β_1	h_2/h_1	h_2/h_1	h_2/h_1	F_2	F_2	F_2
		*Exp.	based on Θ and β exp.	Exp.	Calo.	% Diff. Calc. vs. Exp.	Exp.	Calo.	% Diff. Calc. vs. Exp.	Exp.	Calo.	% Diff. Calc. vs. Exp.
B-1	3°	3.05	3.18	20.90°	21.80°	-4.1%	1.15	1.17	-1.7%	2.80	2.76	+1.4%
B-2	6°	3.05	3.14	24.05°	24.60°	-2.2%	1.31	1.36	-3.7%	2.57	2.50	+2.8%
B-3	9°	3.05	3.17	27.00°	27.55°	-2.0%	1.52	1.56	-2.6%	2.32	2.28	+1.8%
B-4	12°	3.05	3.22	29.45°	30.65°	-3.9%	1.70	1.76	-3.4%	2.14	2.09	+2.4%
B-5	15°	3.05	3.15	33.25°	33.95°	-2.1%	1.93	1.96	-1.5%	1.94	1.91	+1.6%
B-6	18°	3.05	3.17	36.60°	37.45°	-2.0%	2.11	2.17	-2.8%	1.79	1.74	+2.9%
<p>* Calculation of Initial Froude Number based on average Pitot tube velocity in test section, eliminating side-wall effect.</p> <p>$F_1 = \bar{V}_1 / \sqrt{g h_1} = 3.05$</p>												
<p>Average Value-</p>												
<p>Sta.</p>												
<p>Ave. V_1 (fps.)</p>												
<p>Depth (in.)</p>												
<p>1.52 1.53 1.52 1.50 1.50 1.52 1.52 1.52-h₁</p>												
<p>6.15 6.11 6.14 6.12 6.33 6.19 6.08 6.16</p>												
<p>0.688 0.988 1.488 1.988 2.488 2.988 3.488</p>												
<p>EXPERIMENTAL SERIES B WITH 30" LEAD VANE FROUDE NUMBER $F_1 = 3.05$ NOMINAL DEPTH $h_1 = 1.50"$</p>												

HYDRAULIC CORRELATIONS SUMMARIZED

TABLE VII-a

Run	(1) Wall Angle	(2) Froude No.	(3) Froude No.	(4) Wave Angle	(5) Wave Angle	(6) Wave Angle	(7) Depth Ratio	(8) Depth Ratio	(9) Depth Ratio	(10) Froude No.	(11) Froude No.	(12) Froude No.
	Θ	F_1	F_1	β_1	β_1	β_1	h_2/h_1	h_2/h_1	h_2/h_1	F_2	F_2	F_2
		Exp.	based on Θ and β exp.	Exp.	Calo.	% Diff. Calo. vs. Exp.	Exp.	Calo.	% Diff. Calo. vs. Exp.	Exp.	Calo.	% Diff. Calo. vs. Exp.
C-1	3°	3.80	3.91	17.40°	17.80°	-2.2%	1.2	1.22	-1.6%	3.42	3.38	+1.2%
C-2	6°	3.80	3.93	19.85°	20.40°	-2.7%	1.43	1.45	-1.4%	3.08	3.24	-4.9%
C-3	9°	3.80	3.86	23.10°	23.30°	-0.9%	1.66	1.69	-1.8%	2.80	2.78	+0.7%
C-4	12°	3.80	3.79	26.45°	26.35°	+0.4%	1.89	1.94	-2.6%	2.57	2.52	+1.98%
C-5	15°	3.80	3.78	29.55°	29.50°	+0.1%	2.13	2.19	-2.8%	2.35	2.31	+2.2%
C-6	18°	3.80	3.82	32.65°	32.70°	-0.1%	2.38	2.45	-2.9%	2.16	2.12	+1.9%
C-7	21°	3.80	3.81	36.0°	36.10°	-0.1%	2.66	2.70	-1.5%	1.96	1.94	+1.03%
* Calculation of Initial Froude Number based on average Pitot tube velocity in test section, eliminating side-wall effect. $F_1 = \frac{V}{\sqrt{gh_1}} = \frac{7.75}{5.67 \times 0.36} = 3.80$												
							Stn.	Ave. V_1 (fps.)	Depth (in.)	EXPERIMENTAL SERIES C WITH 30" LEAD VANE FROUDE NUMBER $F_1 = 3.80$ NOMINAL DEPTH $h_1 = 1.50"$		
							0.416	7.80	1.56			
							0.834	7.70	1.58			
							1.253	7.61	1.57			
							1.713	7.87	1.56			
							2.713	7.90	1.57			
							2.633	7.85	1.56			
							3.093	7.61	1.54			
							3.507	7.68	1.52			
							Average Value-	7.75	1.56			

HYDRAULIC CORRELATIONS SUMMARIZED

TABLE VII-b

USAF 17 5985

63

Run	(1) Wall Angle	(2) Froude No. F_1	(3) Froude No. F_1	(4) Wave Angle β_1	(5) Wave Angle β_1	(6) Wave Angle β_1	(7) Depth Ratio h_2/h_1	(8) Depth Ratio h_2/h_1	(9) Depth Ratio h_2/h_1	(10) Froude No. F_2	(11) Froude No. F_2	(12) Froude No. F_2
	Θ	F_1	F_1	β_1	β_1	β_1	h_2/h_1	h_2/h_1	h_2/h_1	F_2	F_2	F_2
		*Exp.	based on Θ and β_1 exp.	Exp.	Calc.	% Diff. Calc. vs. Exp.	Exp.	Calc.	% Diff. Calc. vs. Exp.	Exp.	Calc.	% Diff. Calc. vs. Exp.
D-1	3°	2.08	2.09	31.70°	31.90°	-0.6%	1.13	1.13	0	1.90	1.89	+0.5%
D-2	6°	2.08	2.16	33.85°	35.10°	-3.6%	1.26	1.26	0	1.74	1.74	0
D-3	9°	2.08	2.12	38.20°	38.75°	-1.4%	1.39	1.40	-0.7%	1.59	1.58	+0.6%
D-4	12°	2.08	2.14	41.55°	42.75°	-2.8%	1.55	1.55	0	1.43	1.43	0

* Calculation of Initial Froude
Number based on average Pitot
tube velocity in test section,
eliminating side-wall effect.

$$F_1 = \frac{\bar{V}}{\sqrt{gh_1}} = \frac{4.15}{\sqrt{5.67 \times 0.352}} = 2.08$$

Average Value-	4.15	1.49
----------------	------	------

EXPERIMENTAL SERIES D
WITH 30" LEAD VANES
FROUDE NUMBER $F_1 = 2.08$
NOMINAL DEPTH $h_1 = 1.50"$

HYDRAULIC CORRELATIONS SUMMARIZED
TABLE VII-c

SAFETY 5985

Run	(1) Wall Angle	(2) Froude No.	(3) Froude No.	(4) Wave Angle	(5) Wave Angle	(6) Wave Angle	(7) Depth Ratio	(8) Depth Ratio	(9) Depth Ratio	(10) Froude No.	(11) Froude No.	(12) Froude No.
	Θ	F_1	F_1	β_1	β_1	β_1	h_2/h_1	h_2/h_1	h_2/h_1	F_2	F_2	F_2
		*Exp.	based on Θ and β exp.	Exp.	Calc.	% Diff. Calo. vs. Exp.	Exp.	Calo.	% Diff. Calo. vs. Exp.	Exp.	Calc.	% Diff. Calo. vs. Exp.
E-1	3°	7.00	7.25	10.30°	10.55°	-2.4%	1.44	1.41	+2.1%	5.78	5.87	-1.5%
E-2	6°	7.00	7.40	12.90°	13.40°	-3.7%	1.87	1.83	+2.2%	5.02	5.04	-0.4%
E-3	9°	7.00	7.40	15.70°	16.20°	-3.1%	2.26	2.30	-1.7%	4.52	4.46	+1.3%
E-4	12°	7.00	7.65	18.45°	19.10°	-3.4%	2.67	2.78	-4.0%	4.10	4.0	+2.5%
E-5	15°	7.00	9.15	20.30°	22.10°	-8.1%	3.32	3.26	+1.8%	3.58	3.62	-1.1%
E-6	18	7.00	9.00	23.55	25.20	-6.9%	4.00	3.72	+7.5%	3.15	3.29	-4.2%
* Calculation of Initial Froude Number based on average Pitot tube velocity in test section, eliminating side-wall effect. $F_1 = \frac{\bar{V}}{\sqrt{gh_1}} = \frac{11.09}{\sqrt{5.67 \times 0.278}} = 7.00$							Ave. V_1 (fps.)	Depth (in.)	EXPERIMENTAL SERIES E WITH 30" LEAD VANE FROUDE NUMBER $F_1 = 7.00$ NOMINAL DEPTH $h_1 = 0.90"$			
							0.833	0.94				
							1.257	0.94				
							1.712	0.92				
							2.172	0.93				
Average Value--							11.09	0.93				

HYDRAULIC CORRELATIONS SUMMARIZED

TABLE VII-d

Run	(1) Wall Angle	(2) Froude No.	(3) Froude No.	(4) Wave Angle	(5) Wave Angle	(6) Wave Angle	(7) Depth Ratio	(8) Depth Ratio	(9) Depth Ratio	(10) Froude No.	(11) Froude No.	(12) Froude No.
	Θ	F_1	F_1	β_1	β_1	β_1	h_2/h_1	h_2/h_1	h_2/h_1	F_2	F_2	F_2
		*Exp.	based on Θ and β exp.	Exp.	Calc.	% Diff. Calc. vs. Exp.	Exp.	Calc.	% Diff. Calc. vs. Exp.	Exp.	Calc.	% Diff. Calc. vs. Exp.
F-1	3°	3.20	3.06	21.75°	20.80°	+4.6%	1.18	1.18	0	2.89	2.9	-0.3%
F-2	6°	3.20	3.23	23.45°	23.60°	-0.6%	1.37	1.38	-0.7%	2.63	2.62	+0.4%
F-3	9°	3.20	3.26	26.20°	26.50°	-1.1%	1.56	1.58	-1.3%	2.41	2.4	+0.4%
F-4	12°	3.20	3.30	28.95°	29.60°	-2.2%	1.78	1.79	-0.5%	2.19	2.18	+0.46%
F-5	15°	3.20	3.28	32.35°	32.85°	-1.5%	2.00	2.00	0	2.00	2.00	0
F-6	18°	3.20	3.29	35.55°	36.25°	-1.9%	2.24	2.22	+0.9%	1.81	1.82	-0.55%
F-7	21°	3.20	3.32	39.00°	39.87°	-2.2%	2.45	2.44	+0.4%	1.66	1.72	-3.5%

*Calculation of Initial Froude
Number based on average Pitot
tube velocity in test section,
eliminating side-wall effect.

$$F_1 = \frac{V}{\sqrt{gh_1}} = \frac{4.93}{5.67 \times 0.272} = 3.20$$

Average Value -

Sta.	Ave. V_1 (fps.)	Depth (in.)
0.833	4.87	0.93
1.233	4.89	0.90
1.733	4.97	0.89
2.183	4.95	0.88
2.583	4.95	0.88
3.083	4.91	0.89
3.483	4.92	0.88
Average Value -	4.93	0.89

EXPERIMENTAL SERIES F
WITH 30" LEAD VANE
FROUDE NUMBER $F_1 = 3.20$
NOMINAL DEPTH $h_1 = 0.90"$

HYDRAULIC CORRELATIONS SUMMARIZED
TABLE VII-e

Run	(1) Wall Angle	(2) Froude No.	(3) Froude No.	(4) Wave Angle	(5) Wave Angle	(6) Wave Angle	(7) Depth Ratio	(8) Depth Ratio	(9) Depth Ratio	(10) Froude No.	(11) Froude No.	(12) Froude No.
	Θ	F_1	F_1	β_1	β_1	β_1	h_2/h_1	h_2/h_1	h_2/h_1	F_2	F_2	F_2
		*Exp.	based on Θ and β_{exp}	Exp.	Calo.	% Diff. Calo. vs. Exp.	Exp.	Calo.	% Diff. Calo. vs. Exp.	Exp.	Calo.	% Diff. Calo. vs. Exp.
G-1	3°	5.91	5.85	12.35°	12.20°	+1.2%	1.26	1.34	-6.0%	5.23	5.05	+3.5%
G-2	6°	5.91	6.21	14.50°	14.95°	-3.0%	1.61	1.70	-5.3%	4.57	4.4	+3.9%
G-3	9°	5.91	6.15	17.40°	17.60°	-1.1%	2.02	2.10	-3.8%	3.98	3.97	+0.25%
G-4	12°	5.91	6.15	20.25°	20.58°	-1.6%	2.41	2.49	-3.2%	3.62	3.65	-0.8%
G-5	15°	5.91	6.15	23.15°	23.55°	-1.7%	2.94	2.90	+1.4%	3.18	3.24	-1.9%
G-6	18°	5.91	6.75	25.60°	26.70°	-4.1%	3.33	3.29	+1.2%	2.92	2.94	-0.7%
<p>* Calculation of Initial Froude Number based on average Pitot tube velocity in test section, eliminating side-wall effect.</p> $F_1 = \frac{\bar{V}}{\sqrt{gh_1}} = \frac{3.25}{5.67 \times 0.278} = 5.91$												
<p>Average Value-</p>												
<p>Sta. Ave. V_1 (fps.) Depth (in.)</p>												
<p>0.838 9.26 0.92</p>												
<p>1.238 9.25 0.91</p>												
<p>1.738 9.29 0.93</p>												
<p>2.188 9.29 0.92</p>												
<p>2.588 9.22 0.93</p>												
<p>3.088 9.17 0.91</p>												
<p>3.488 9.23 0.91</p>												
<p>EXPERIMENTAL SERIES G WITH 30" LEAD VANE PROUDE NUMBER $F_1 = 5.91$ NOMINAL DEPTH $h_1 = 0.90"$</p>												

HYDRAULIC CORRELATIONS SUMMARIZED

TABLE VII-f

Run	(1) Wall Angle	(2) Froude No.	(3) Froude No.	(4) Wave Angle	(5) Wave Angle	(6) Wave Angle	(7) Depth Ratio	(8) Depth Ratio	(9) Depth Ratio	(10) Froude No.	(11) Froude No.	(12) Froude No.
	Θ	F_1	F_1	β_1	β_1	β_1	h_2/h_1	h_2/h_1	h_2/h_1	F_2	F_2	F_2
		*Exp.	based on Θ and β exp.	Exp.	Calc.	% Diff. Calc. vs. Exp.	Exp.	Calc.	% Diff. Calc. vs. Exp.	Exp.	Calc.	% Diff. Calc. vs. Exp.
E-1	3°	6.30	6.35	11.55°	11.60°	-0.4%	1.35	1.36	-0.7%	5.46	5.34	+2.3%
H-2	6°	6.30	6.50	14.15°	14.27°	-0.8%	1.74	1.75	-0.6%	4.68	4.66	+0.4%
H-3	9°	6.30	6.25	17.25°	17.10°	+0.9%	2.14	2.16	-0.9%	4.16	4.14	+0.5%
H-4	12°	6.30	6.55	19.65°	20.0°	-1.7%	2.58	2.59	-0.4%	3.72	3.72	0

* Calculation of Initial Froude Number based on average Pitot tube velocity in test section, eliminating side-wall effect.

$$F_1 = \frac{\bar{V}}{\sqrt{gh_1}} = \frac{12.75}{5.67 \times 0.357} = 6.30$$

Ave. V_1 (fps.)	Depth (in.)
0.368	1.54
0.858	1.53
1.358	1.52
1.858	1.52
2.258	1.54
2.758	1.54
3.258	1.53
3.758	1.50
Average Value-	1.52

EXPERIMENTAL SERIES H
WITH 30" LEAD VANE
FROUDE NUMBER $F_1 = 6.30$
NOMINAL DEPTH $h_1 = 1.50"$

HYDRAULIC CORRELATIONS SUMMARIZED

TABLE VII-E

(1)	(2)	(3)	(4)	(5)	(6)	(7)	(8)	(9)	(10)	(11)	(12)
Wall Angle	Froude No.	Froude No.	Wave Angle	Wave Angle	Wave Angle	Depth Ratio	Depth Ratio	Depth Ratio	Froude No.	Froude No.	Froude No.
Θ	F_1	F_1	β_1	β_1	β_1	h_2/h_1	h_2/h_1	h_2/h_1	F_2	F_2	F_2
	*Exp.	based on Θ and $\beta_{exp.}$	Exp.	Calo.	% Diff. Calo. vs. Exp.	Exp.	Calo.	% Diff. Calo. vs. Exp.	Exp.	Calo.	% Diff. Calo. vs. Exp.
I-1	2.00	1.99	33.40°	33.15°	+0.8%	1.12	1.12	0	1.83	1.84	-0.5%
I-2	2.00	2.07	35.25°	36.60°	-3.7%	1.25	1.26	-0.8%	1.67	1.66	+0.6%
I-3	2.00	2.07	39.05°	40.30°	-3.1%	1.39	1.40	-0.7%	1.52	1.51	+0.7%
I-4	2.00	2.07	42.95°	44.60°	-3.7%	1.52	1.54	-1.3%	1.35	1.36	+0.7%

* Calculation of Initial Froude Number based on average Pitot tube velocity in test section, eliminating side-wall effect.

$$F_1 = \frac{\bar{V}}{\sqrt{gh_1}} = \frac{3.13}{5.67 \times 0.276} = 2.00$$

Sta.	Ave. V_1 (fps.)	Depth (in.)
0.788	3.15	0.92
1.288	3.12	0.90
1.788	3.14	0.92
2.188	3.10	0.92
2.688	3.15	0.90
3.188	3.11	0.90
Average Value-	3.13	0.91

EXPERIMENTAL SERIES I
WITH 30" LEAD VANE
FROUDE NUMBER $F_1 = 2.00$
NOMINAL DEPTH $h_1 = 0.90"$

HYDRAULIC CORRELATIONS SUMMARIZED
TABLE VII-h

(1)	(2)	(3)	(4)	(5)	(6)	(7)	(8)	(9)	(10)	(11)	(12)
Wall Angle	Froude No.	Froude No.	Wave Angle	Wave Angle	Wave Angle	Depth Ratio	Depth Ratio	Depth Ratio	Froude No.	Froude No.	Froude No.
Θ	F_1	F_1	β_1	β_1	β_1	h_2/h_1	h_2/h_1	h_2/h_1	F_2	F_2	F_2
	*Exp.	based on Θ and $\beta_{exp.}$	Exp.	Calc.	% Diff. Calc. vs. Exp.	Exp.	Calc.	% Diff. Calc. vs. Exp.	Exp.	Calc.	% Diff. Calc. vs. Exp.
J-1	4.18	4.60	15.05°	16.30°	-7.7%	1.24	1.24	0	3.70	3.71	-0.3%
J-2	4.18	4.30	18.50°	18.90°	-2.1%	1.48	1.49	-0.7%	3.33	3.35	-0.6%
J-3	4.18	4.30	21.45°	21.80°	-1.6%	1.76	1.76	0	3.00	3.01	-0.3%
J-4	4.18	4.35	24.25°	24.80°	-2.2%	2.06	2.03	+1.5%	2.70	2.74	-1.5%
J-5	4.18	4.25	27.60°	27.85°	-0.9%	2.36	2.32	+1.7%	2.46	2.55	-3.5%
J-6	4.18	4.25	30.85°	31.10°	-0.8%	2.62	2.59	+1.2%	2.26	2.28	-0.9%
M-3	4.18	4.30	21.45°	21.80°	-1.6%	1.73	1.76	-1.7%	3.03	3.01	0.7%
M-5	4.18	4.23	27.65°	27.85°	-0.7%	2.29	2.32	-0.9%	2.51	2.51	0
* Calculation of Initial Froude Number based on average Pitot tube velocity in test section, eliminating side-wall effect. $F_1 = \frac{\bar{V}}{\sqrt{gh_1}} = \frac{6.56}{5.67 \times 0.277} = 4.18$			Average Value-		Sta.	Ave. V_1 (fps.)	Depth (in.)	Note: Series J - 30" LEAD VANE Series M - NO LEAD VANE EXPERIMENTAL SERIES J and M LEAD VANE - (See Note) FROUDE NUMBER $F_1 = 4.18$ NOMINAL DEPTH $h_1 = 0.90"$			
					0.788	6.57	0.91				
					1.288	6.53	0.93				
					1.788	6.54	0.93				
					2.188	6.59	0.93				
					2.688	6.56	0.92				
					3.188	6.59	0.90				

HYDRAULIC CORRELATIONS SUMMARIZED
TABLE VII-1

Run	(1)	(2)	(3)	(4)	(5)	(6)	(7)	(8)	(9)	(10)	(11)	(12)
	Wall Angle	Froude No.	Froude No.	Wave Angle	Wave Angle	Wave Angle	Depth Ratio	Depth Ratio	Depth Ratio	Froude No.	Froude No.	Froude No.
	Θ	F_1	F_1	(β_1)	(β_1)	(β_1)	h_2/h_1	h_2/h_1	h_2/h_1	F_2	F_2	F_2
		*Exp.	based on Θ and (β_{exp})	Exp.	Calc.	% Diff. Calc. vs. Exp.	Exp.	Calc.	% Diff. Calc. vs. Exp.	Exp.	Calc.	% Diff. Calc. vs. Exp.
K-3	9°	4.18	4.35	21.25°	21.80°	-2.5%	1.74	1.78	-1.1%	3.02	3.02	0
K-5	15°	4.18	4.42	27.00°	27.85°	-3.1%	2.24	2.32	-2.6	2.55	2.49	+2.4%
N-3	9°	4.18	4.43	21.00°	21.80°	-3.8%	1.72	1.76	-2.3%	3.04	3.02	+0.7%
N-5	15°	4.18	4.01	28.60°	27.85°	+2.6%	2.25	2.32	-3.0%	2.54	2.49	+2.0%
* Calculation of Initial Froude Number based on average Pitot tube velocity in test section, eliminating side-wall effect, $F_1 = \frac{\bar{V}}{\sqrt{gh_1}} = \frac{8.60}{5.67 \times 0.363} = 4.18$ Average Value-						Sta.	Ave. V_1 (fps.)	Depth (in.)	Note: Series K - 30° LEAD VANE Series N - NO LEAD VANE			
						0.425	8.70	1.57				
						1.140	8.75	1.60				
						1.850	8.59	1.62				
						2.560	8.62	1.59				
						3.260	8.37	1.53				
						Average Value-	8.60	1.59				
EXPERIMENTAL SERIES K and N LEAD VANE - (See Note) FROUDE NUMBER $F_1 = 4.18$ NOMINAL DEPTH $h_1 = 1.60"$												

HYDRAULIC CORRELATIONS SUMMARIZED
TABLE VII-J

Run	(1)	(2)	(3)	(4)	(5)	(6)	(7)	(8)	(9)	(10)	(11)	(12)
	Wall Angle	Froude No.	Froude No.	Wave Angle	Wave Angle	Wave Angle	Depth Ratio	Depth Ratio	Depth Ratio	Froude No.	Froude No.	Froude No.
	Θ	F_1	F_1	(β_1)	(β_1)	(β_1)	h_2/h_1	h_2/h_1	h_2/h_1	F_2	F_2	F_2
		*Exp.	based on Θ and (β_{exp})	Exp.	Calc.	% Diff. Calc. vs. Exp.	Exp.	Calc.	% Diff. Calc. vs. Exp.	Exp.	Calc.	% Diff. Calc. vs. Exp.
L-3	9°	4.20	4.74	20.10°	21.70°	-2.8%	1.78	1.77	-1.1%	3.03	3.03	0
L-5	15°	4.20	4.73	26.10°	27.80°	-6.1%	2.33	2.32	+0.4%	2.49	2.51	-0.8%
O-3	9°	4.20	4.73	20.15°	21.70°	-7.1%	1.74	1.77	-1.7%	3.04	3.03	+0.3%
O-5	15°	4.20	4.74	26.05°	27.80°	-6.3%	2.30	2.32	-0.9%	2.52	2.51	+0.4%
* Calculation of Initial Froude Number based on average Pitot tube velocity in test section, eliminating side-wall effect.						Sta.	Ave. V_1 (fps.)	Depth (in.)	Note: Series L - 30° LEAD VANE Series O - NO LEAD VANE			
						1.14	5.38	0.60				
Average Value-						1.85	5.34	0.61				
						2.56	5.34	0.60				
						3.26	5.29	0.58				
						5.34	0.60	<div>EXPERIMENTAL SERIES L and O</div> <div>LEAD VANE - (See Note)</div> <div>FROUDE NUMBER $F_1 = 4.20$</div> <div>NOMINAL DEPTH $h_1 = 0.60"$</div>				
$F_1 = \frac{\bar{V}}{\sqrt{gh_1}} = \frac{5.34}{5.67 \times 0.224} = 4.20$												

HYDRAULIC CORRELATIONS SUMMARIZED
TABLE VII-K

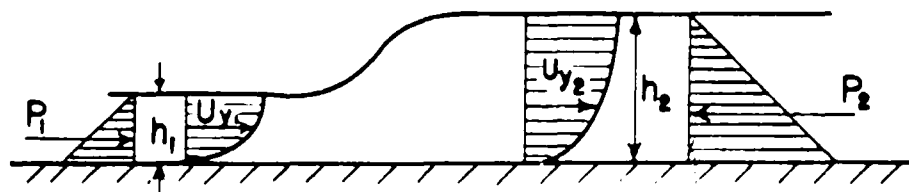
from Eq. (37b) using the theoretical depth ratio (Column 8) is found in column 11 with the percentage difference in column 12. The correlations are also given in graphical form. Figure 19 shows the agreement between shock wave angle and deflection angle for the experimental Froude numbers. To avoid crowding, the curves are separated according to their nominal initial depth of .90" and 1.50". The correlation does not seem to be greatly affected by the value of the initial depth; however, this factor is discussed in greater detail in the following section IV-3. The average agreement between theory and experiment for the shock-wave angle is of the order of magnitude of two percent which is within the experimental accuracy of the tests. The largest errors appear in the minimum and maximum deflection angles. In the small deflection angles, the errors are partly caused by the difficulty of determining the shock front accurately due to the very small depth changes involved. In the maximum deflection angles, an extremely turbulent shock front makes measurements in this region difficult. Small random scattering is probably due to errors in duplication of initial Froude numbers during the course of several days necessary to make a complete run. Figure 20 shows the agreement between the depth ratio h_2/h_1 across the shock for the same values of deflection angle and initial experimental Froude numbers. The average agreement is of the order of magnitude of 1% and shows larger differences, in general, only for high initial Froude numbers and large deflection angles. These differences may be attributed to comparatively large vertical accelerations present in this region. Again, no appreciable effect of initial depth can be noticed from the two sets of curves.

Figure 21 shows the agreement between the Froude number F_2 , behind the shock for the various deflection angles and initial Froude numbers. The correlation is approximately the same as that obtained for the depth ratio.

3. Effect of Initial Depth and Velocity Distribution on the Shock Characteristics

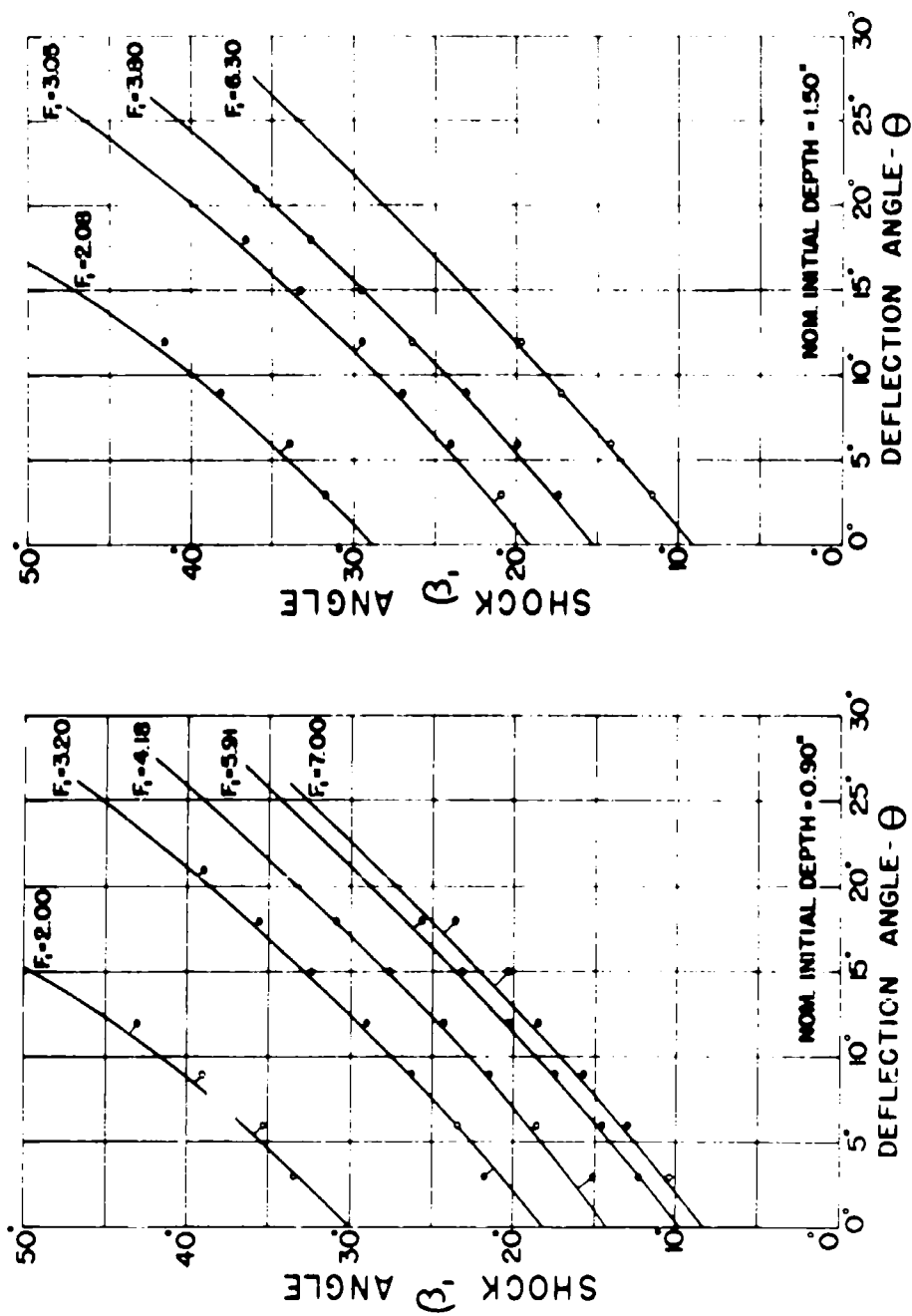
One of the assumptions inherent in the shock analysis presented in section I is that the velocity V is uniform throughout any vertical section of the flow. Inasmuch as the vertical velocity distribution is not uniform, the effect of this necessary deviation from the basic assumptions must be investigated. The momentum equation is written for the normal jump illustrated in Fig. 22. The unbalance in hydrostatic pressure forces is equated to the rate of change of momentum through the jump, thus

$$P_2 - P_1 = \rho \left[\int_0^{h_1} U_{y1}^2 dy - \int_0^{h_2} U_{y2}^2 dy \right] \quad (57)$$



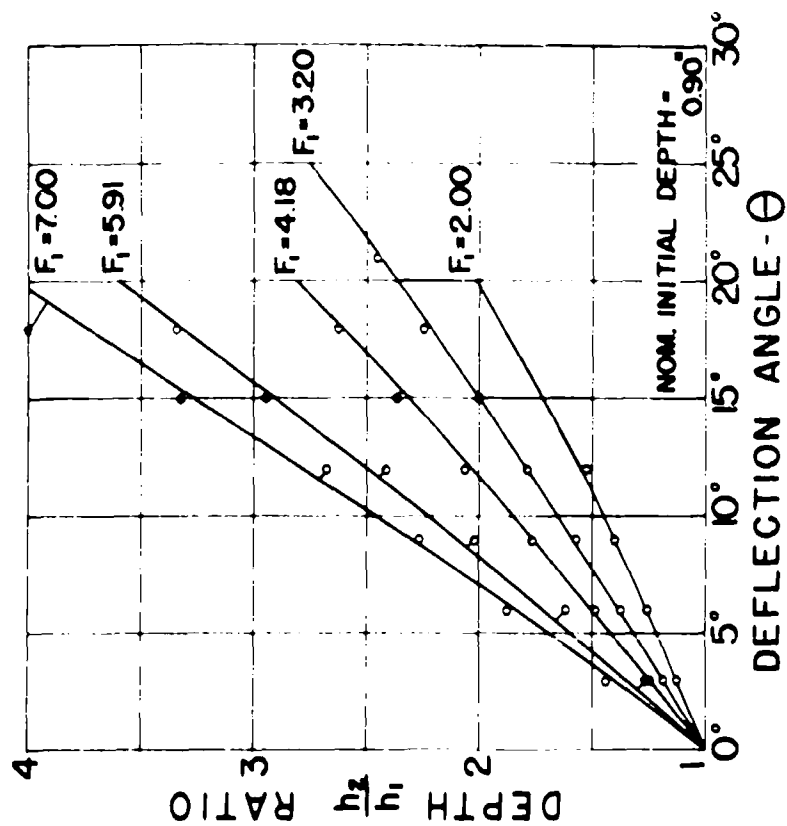
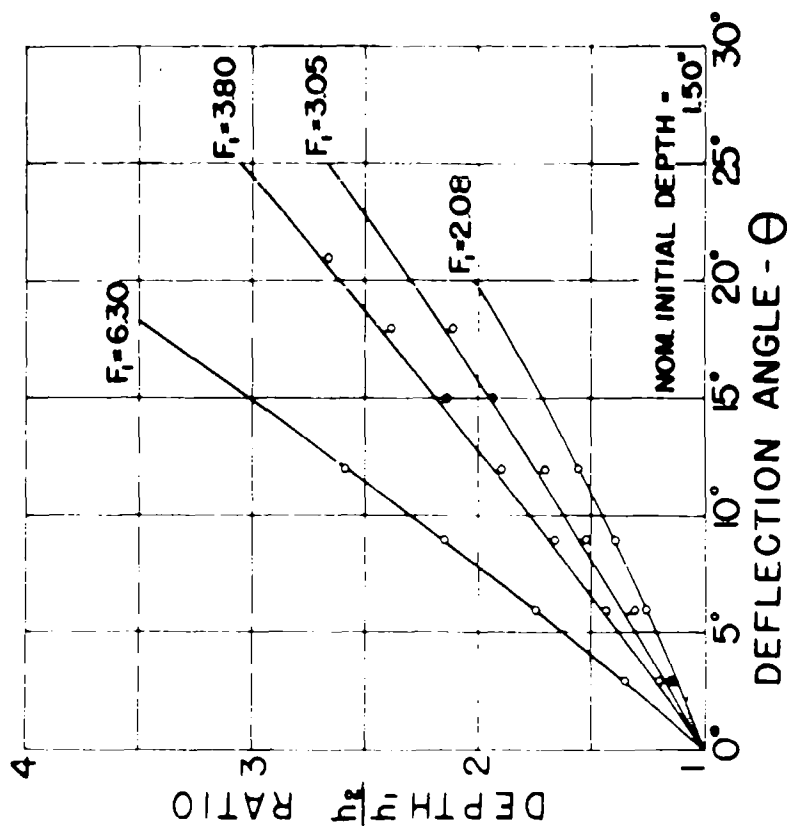
Velocity Distribution in Normal Jump

Fig. 22



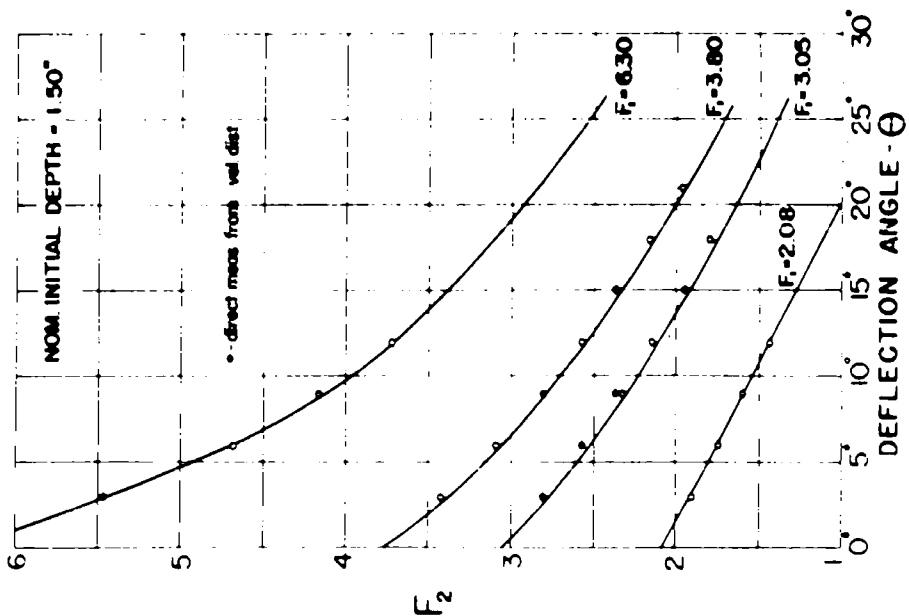
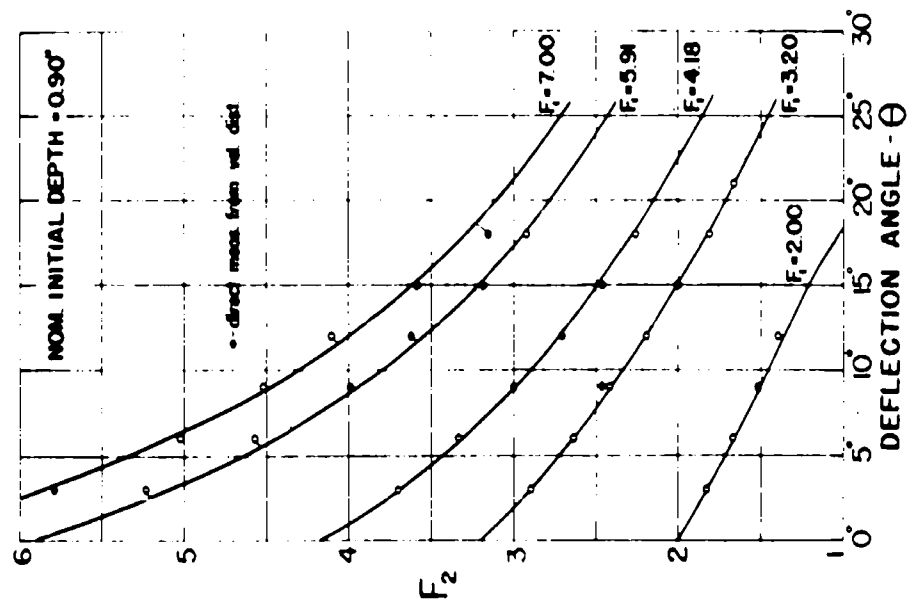
-HYDRAULIC CORRELATION -
COMPARISON OF EXPERIMENTAL AND THEORETICAL
VALUES FOR OBLIQUE SHOCK-WAVE ANGLES IN WATER

FIG. 19



- HYDRAULIC CORRELATION -
COMPARISON OF EXPERIMENTAL AND THEORETICAL
DEPTH RATIO ACROSS AN OBLIQUE SHOCK IN WATER

FIG. 20



- HYDRAULIC CORRELATION -
 COMPARISON OF EXPERIMENTAL AND THEORETICAL VALUES
 FOR FROUDE NUMBER BEHIND AN OBLIQUE SHOCK IN WATER
 FIG. 21

By definition, η is the ratio of the mean of the squares of U_y to the square of the mean U_y which is designated as \bar{U} . Thus,

$$\eta = \frac{\int_0^h U_y^2 dy}{\bar{U}^2 h} \quad (58)$$

this ratio η is a pure number and is known as the momentum correction factor. Rewriting Eq. (57) in terms of η and \bar{U} , and expressing the pressure forces in terms of the depth, there is obtained,

$$g \frac{(h_2^2 - h_1^2)}{2} = [\eta_1 \bar{U}_1^2 h_1 - \eta_2 \bar{U}_2^2 h_2] \quad (59)$$

By use of the continuity equation,

$$h_1 \bar{U}_1 = h_2 \bar{U}_2$$

\bar{U}_2 is eliminated and Eq. (59) can be solved for \bar{U}_1 which can be written as V_{n1} to conform to the previous notation; therefore,

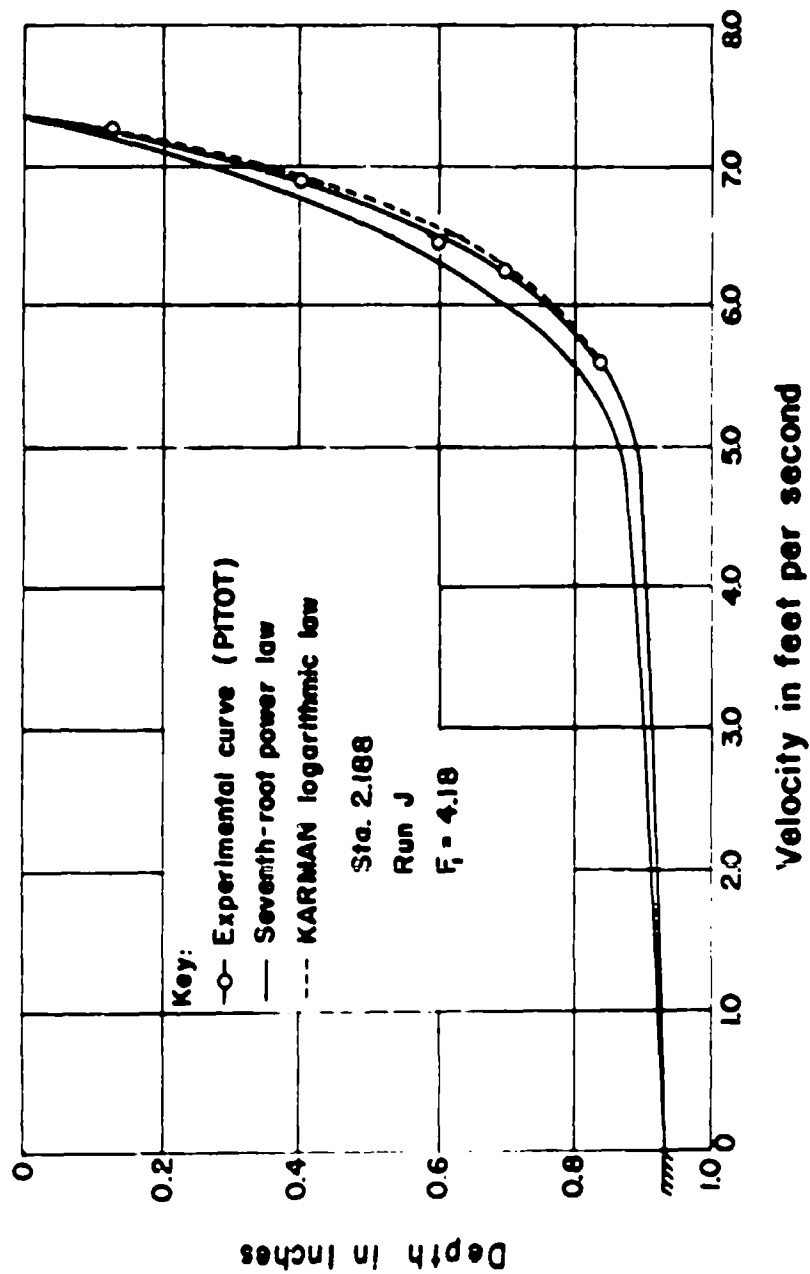
$$V_{n1} = V_1 \sin \beta = \sqrt{gh_1} \sqrt{\frac{h_2}{h_1} \cdot \frac{1}{2} \left[\left(\frac{h_2}{h_1} \right)^2 - 1 \right] \left(\frac{1}{\frac{h_2}{h_1} \eta_1 - \eta_2} \right)}$$

or,

$$\sin \beta = \frac{1}{F_1} \sqrt{\frac{h_2}{h_1} \cdot \frac{1}{2} \left[\left(\frac{h_2}{h_1} \right)^2 - 1 \right] \left(\frac{1}{\frac{h_2}{h_1} \eta_1 - \eta_2} \right)} \quad (60)$$

Equation (60) becomes identical with Eq. (34a) when $\eta_1 = \eta_2 = 1$ which is the value of η for uniform velocity distribution. In order to evaluate η , it is convenient to have an analytical expression for the velocity distribution curve.

It was observed that the turbulent boundary layer thickness was equal to the depth of flow within four to six feet after the stream emerged from the nozzle. Accordingly, an attempt was made to fit boundary layer velocity distributions to the experimentally obtained curves. It was found that the von Karman logarithmic distribution law agreed with the observed points very closely. The Karman equation is applied to open channels following the method discussed in Ref. 24. A typical velocity distribution curve is compared with the Karman equation in Fig. 23. It is seen that the seventh-root law does not agree as well. In addition, several dimensionless plots of velocity curves both in front of and in



**COMPARISON OF EXPERIMENTAL VELOCITY
DISTRIBUTION WITH BOUNDARY LAYER EQUATIONS**

FIG. 23

back of the shock were superimposed and found to have very similar shapes. A typical plot of this type is illustrated in Fig. 24. Therefore, for the purposes of this discussion η_1 may be assumed equal to η_2 . The integration indicated in Eq. (58) may be performed using the Karman relation,

$$U_y = \bar{U} + 2.50\sqrt{ghS} (1 + \ln y/h) \quad (61)$$

where \bar{U} is the average velocity for the vertical section, h is the depth and S the slope for uniform flow. y is measured from the bottom boundary. The result is:

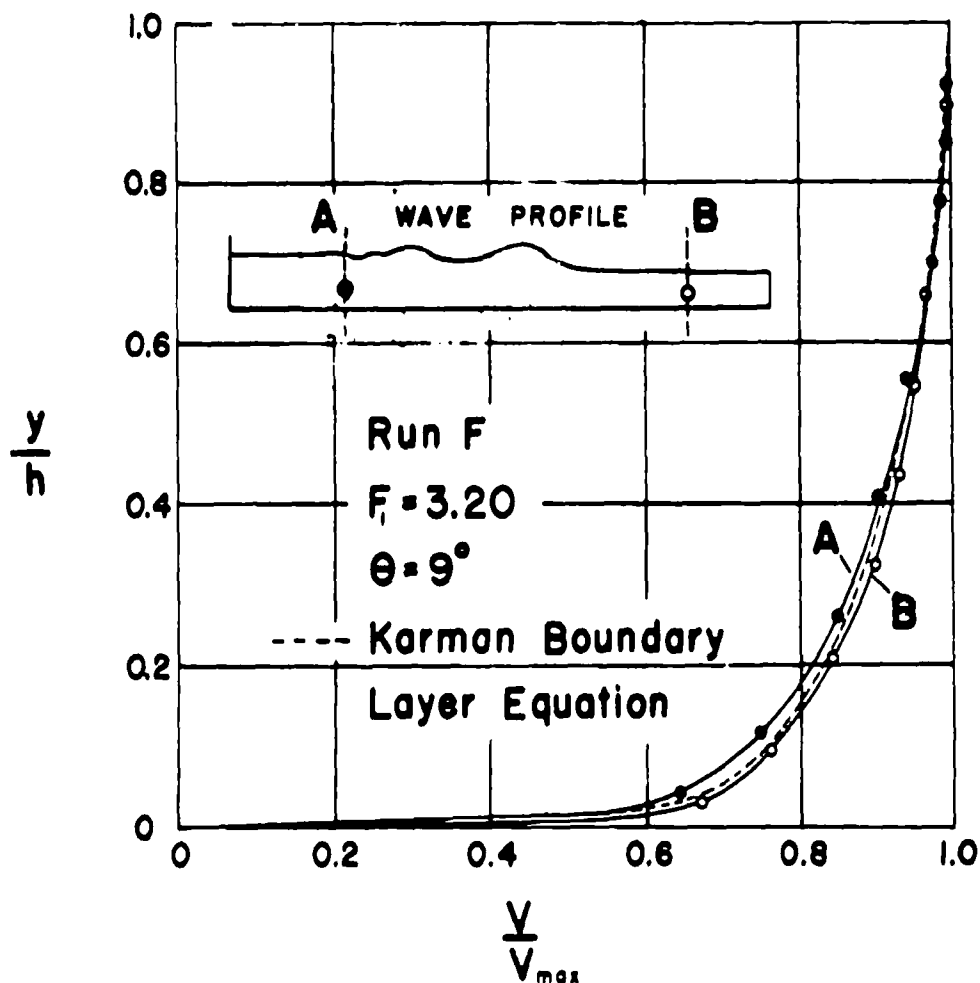
$$\eta = 1 + \frac{(ghS)}{\bar{U}^2} = 1 + \frac{6.25 S}{F^2} \quad (62)$$

Under the assumption that $\eta_1 = \eta_2$ Eq. (60) may be written,

$$\sin \beta = \frac{1}{(F_1)(\sqrt{\eta})} \sqrt{\frac{1}{2} \cdot \frac{h_2}{h_1} \left(1 + \frac{h_2}{h_1}\right)} \quad (63)$$

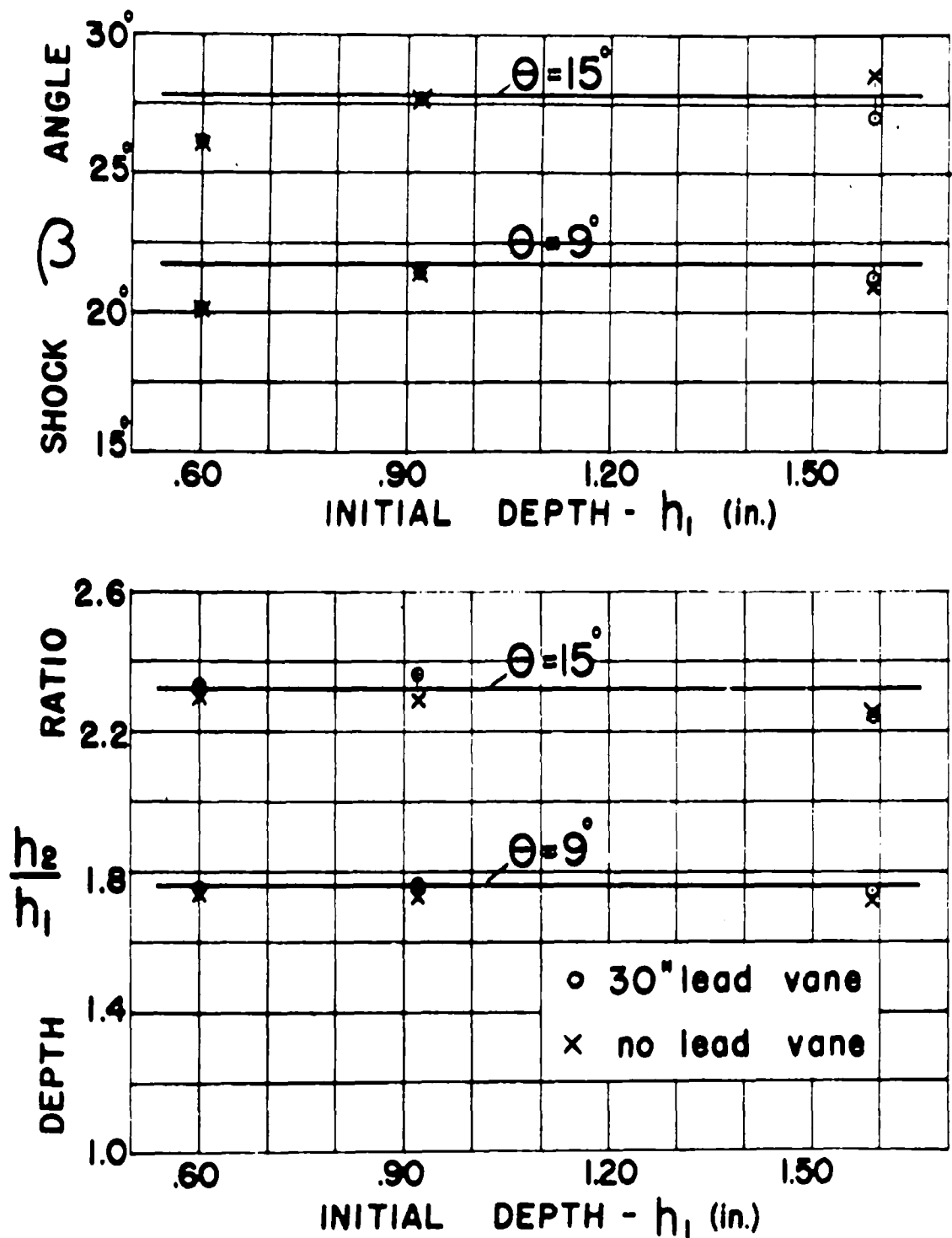
which is again identical with Eq. (34a) with the exception of the factor $\sqrt{\eta}$. The product $(F_1\sqrt{\eta})$ is actually the real value of the effective Froude number taking the velocity distribution into account. The numerical values of η range from a maximum of 1.015 at $F_1 = 2.00$ to a minimum of 1.007 at $F_1 = 6.30$ so that $\sqrt{\eta}$ has a maximum value of 3/4 of 1%. The foregoing development is substantiated by the fact that the increase in Froude number obtained by the product $F_1\sqrt{\eta}$ is in the direction which brings the experimental and calculated values into closer agreement. It is concluded that in view of the small magnitude of the correction, the effect of velocity distribution may be considered negligible.

Some experimental observations on the effect of initial depth follow. Figure 25 illustrates the effect on β and h_2/h_1 of varying the initial depth and deflection angle while keeping the initial Froude number constant. It is observed that good agreement for β is obtained at both $h_1 = .90"$ and $h_1 = 1.50"$; the larger difference at $h_1 = 0.60"$ may be due to the fact that experimental errors are of increased percentage magnitude when dealing with small depths. Figure 26 shows dimensionless plots of the wave profiles obtained at these three initial depths for a constant Froude number of 4.18 and a deflection angle of 9° . While the position of the undulations are changed, it is seen that the equilibrium depths are essentially the same. The initial distortion along the deflector vane is also only slightly affected. The $30"$ lead vane was used for all three runs.



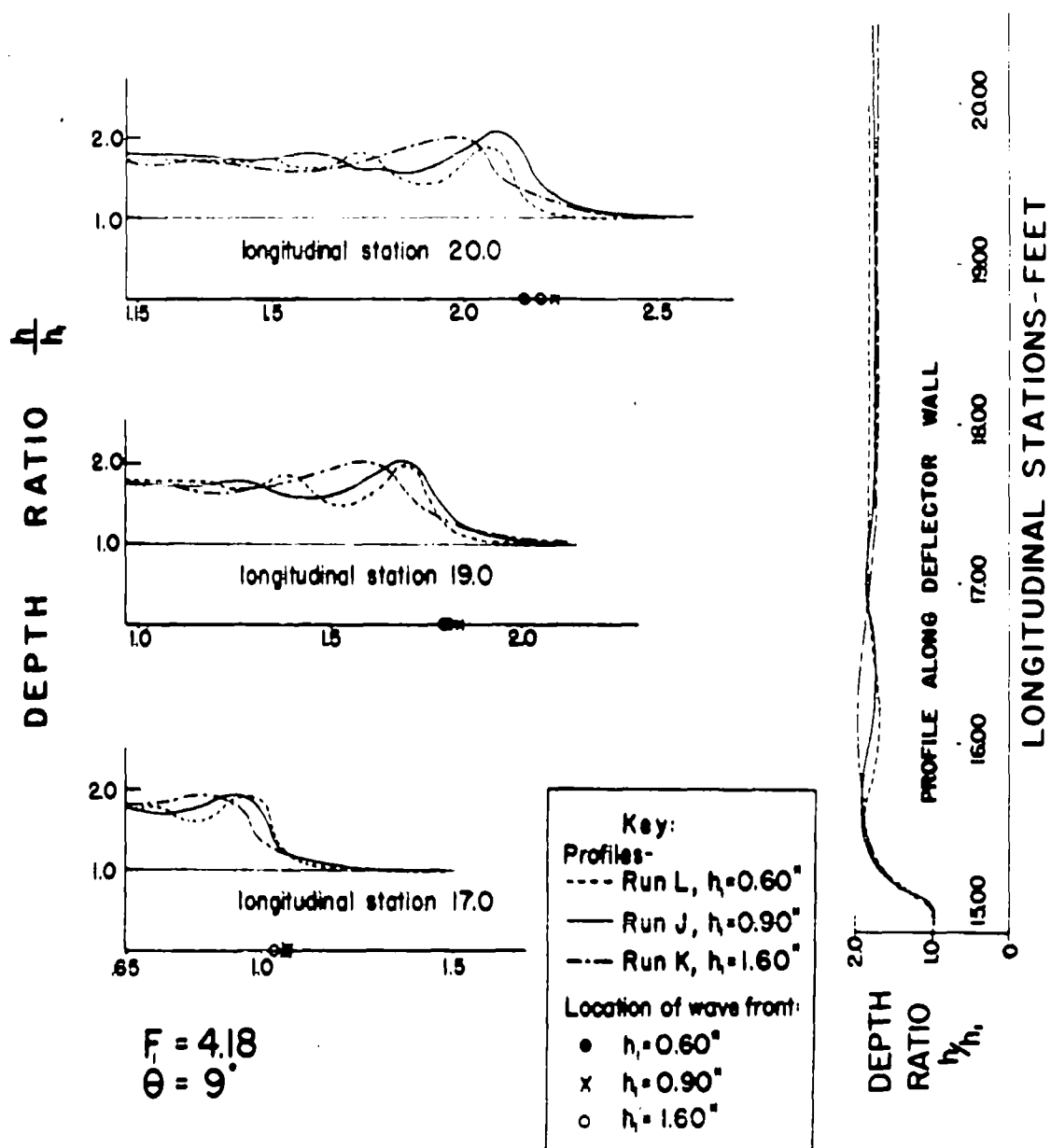
COMPARISON OF VELOCITY DISTRIBUTIONS
BEFORE AND AFTER SHOCK FRONT

FIG. 24



EFFECT OF INITIAL DEPTH ON
SHOCK CHARACTERISTICS - $F_1 = 4.18$

FIG. 25



EFFECT OF INITIAL DEPTH VARIATION ON
SHOCK CHARACTERISTICS FOR CONSTANT
FROUDE NUMBER AND DEFLECTION ANGLE

FIG. 26

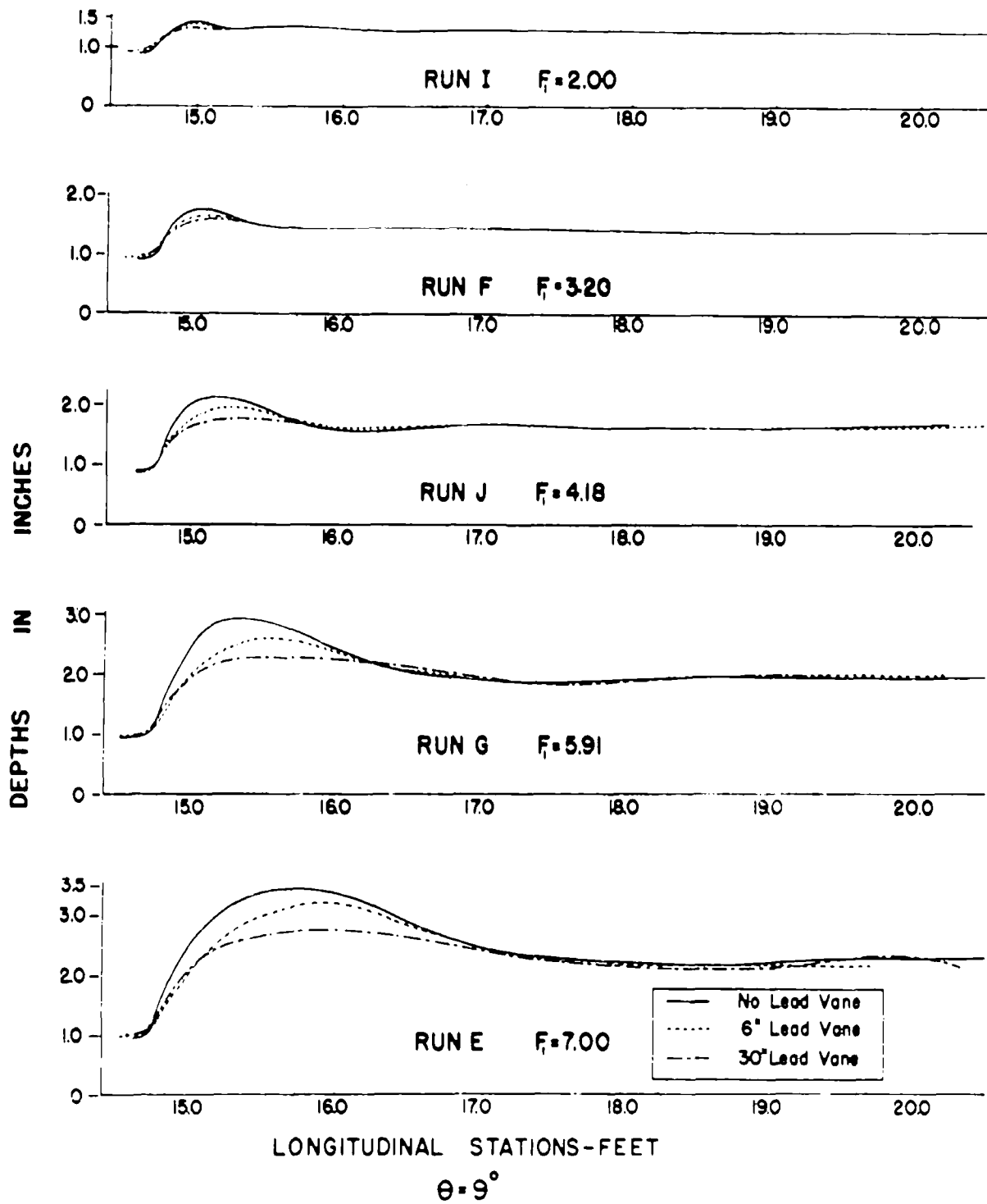
4. Effect of Initial Side-Wall Boundary Layer

Figure 11 shows the deflector vane in relation to the test section with the 30" lead vane in place. The deflector vane hinge was placed four inches away from the left channel wall in order to secure control of the initial wall boundary layer by varying the length of a lead vane set parallel to the channel walls. Figures 14 and 15 show that at a distance of 4 inches from the original channel wall, the average velocity of the section has been reached; therefore, with no lead vane, it is possible to secure a shock with no initial wall boundary layer present. Then by attaching lead vanes of various lengths, parallel to the channel wall, various thicknesses of the wall boundary layer may be built up ahead of the deflector vane. It is evident that the existence of a wall boundary layer will reduce the local value of the Froude number in direct proportion to the change in velocity in the boundary layer. Consequently, local vertical accelerations are also reduced, and the depth along the deflector vane assumes its equilibrium value more quickly.

The effect is illustrated by the following three figures. Figure 27 shows the effect of the side-wall boundary layer upon the depth profile along the deflector vane for a range of Froude numbers from $F_1 = 2.00$ to 7.00 with $\Theta = 9^\circ$ and of initial depth $h_1 = 0.90"$. It is seen that while the initial rise is very great for the case with no lead vane compared to the 30" lead vane, the equilibrium depth is not affected. Since only the region of equilibrium depth was used to determine the depth ratio h_2/h_1 , it is expected that the wall boundary layer would have very little effect upon this value. This conclusion is confirmed by Fig. 25, which shows only slight differences in depth ratio by measurements with no lead vane and 30" lead vane. Figure 28 shows results similar to Fig. 27 for approximately the same range of Froude numbers at an initial depth of $1.50"$. Figure 29 illustrates the result of varying the deflection angle from 3° to 18° for a constant Froude number. The above figures are valuable as an aid in determining the size of model necessary to obtain results which are not influenced by the initial distortion of the basic wave form. In other words, the size of the model must be great enough to obtain measurements in the region of equilibrium depth. This fact alone illustrates the need for working on a rather large scale when quantitative results are to be expected from the hydraulic analogy.

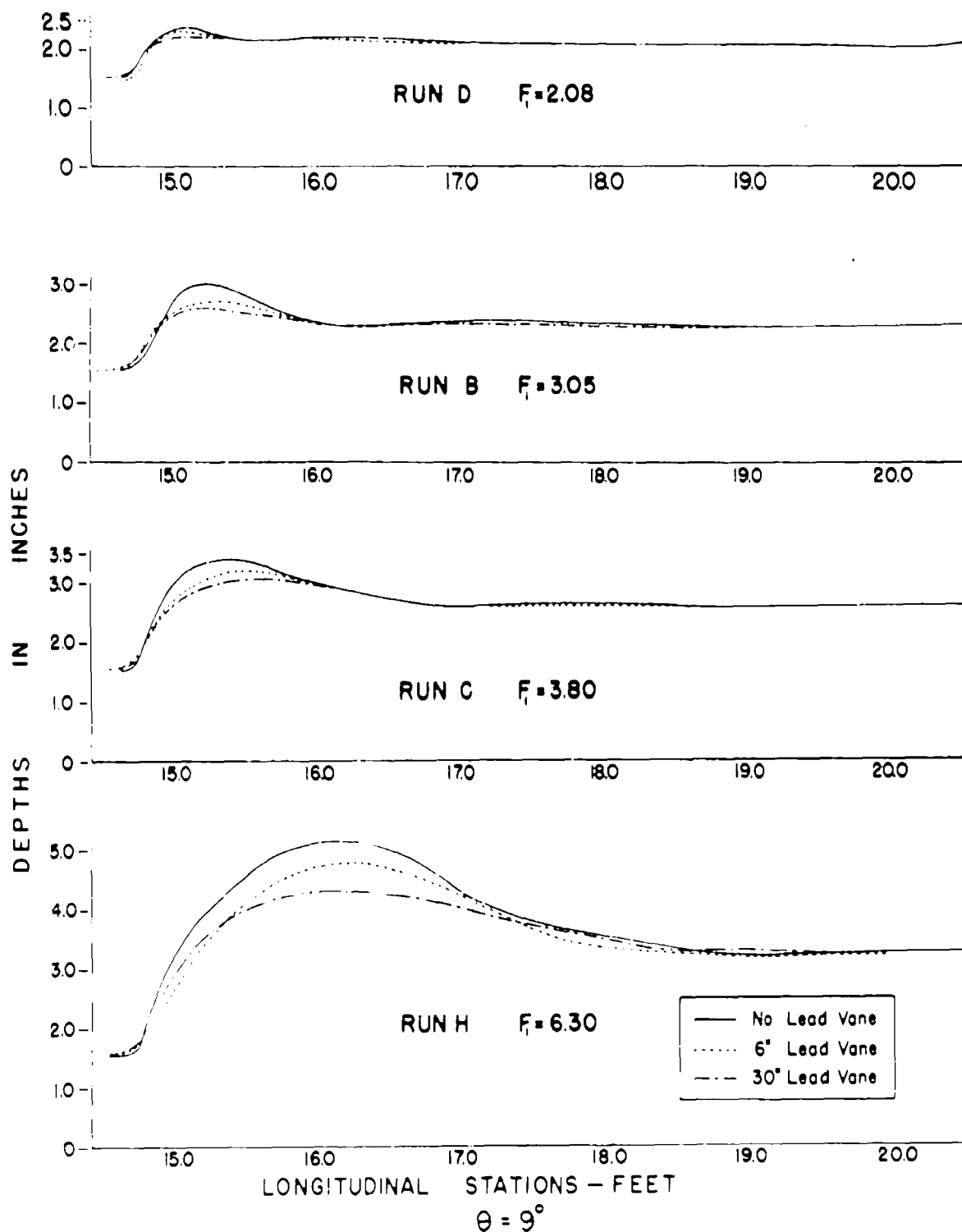
Figure 25 also shows that the shock angle β is only slightly influenced by the length of lead vane with the exception that due to the larger initial curvature of the shock, the front tends to be displaced very slightly parallel to itself.

It is concluded that in any problem in which it is possible to use a lead vane parallel to the initial flow direction, its use will permit smaller models or larger areas over which reliable measurements may be taken.



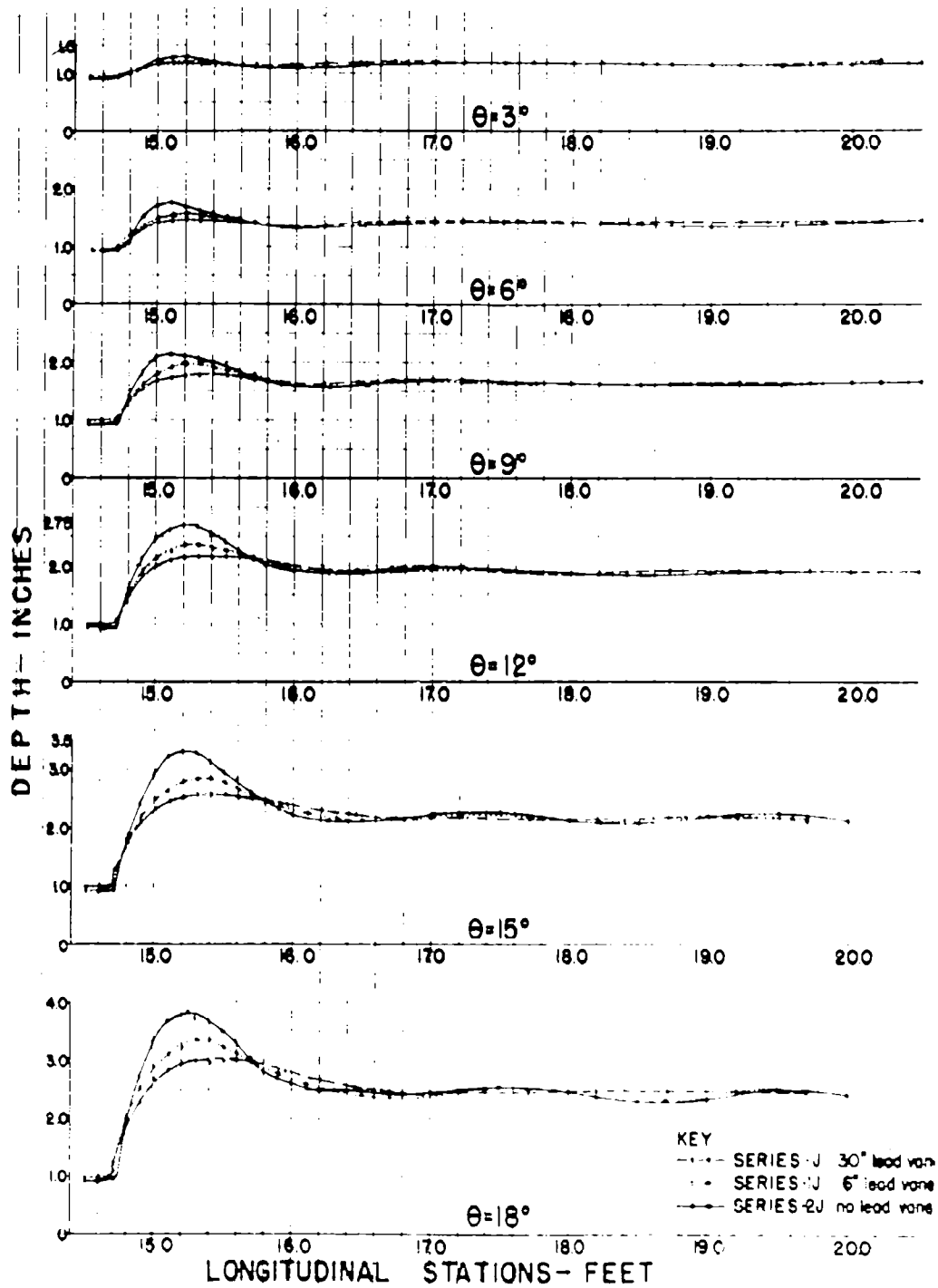
EFFECT OF LENGTH OF LEAD VANE ON DEPTH PROFILES,
 ALONG DEFLECTOR WALL, AT INITIAL DEPTH $h_1 = 0.90'$

FIG. 27



EFFECT OF LENGTH OF LEAD VANE ON DEPTH PROFILES,
ALONG DEFLECTOR WALL, AT INITIAL DEPTH $h_1 = 1.50''$

FIG. 28



COMPARISON OF WALL PROFILES FOR
VARIOUS LENGTHS OF LEAD VANE
 $F_1 = 4.18$, $h_1 = 0.90''$

FIG. 29

5. Effect of Surface Tension

The effect of surface tension on the basic shock wave characteristics has been a source of concern in much of the previous experimental work dealing with the hydraulic analogy. It is believed that these effects become negligible when the tests are conducted on a relatively large scale such as used in the experiments described in this report. A few calculations serve to show the order of magnitude of the capillary forces compared to the dominant gravitational forces. It is evident that surface tension has been assumed negligible in the theoretical development and that in addition, since capillarity has no counterpart in gas flow, these forces should be negligible for the analogy to hold as developed.

The change in pressure due to surface tension across a free liquid surface having a finite radius of curvature is given by -

$p = \frac{\sigma}{r}$ where σ is the surface tension of the liquid, and r the radius of curvature of the free surface. The condition that surface tension forces are negligible compared to gravitational forces requires

that $\frac{\sigma}{r_0} \ll (\rho gh)$, where (ρgh) is the hydrostatic pressure. Several

typical wave profiles were plotted to the same horizontal and vertical scales, and the minimum radius of curvature was determined graphically. For example, the smallest radius of curvature for Run C-3, Station 20.0 is $r = 0.12$ ft. which occurs at the crest of the shock where $h = .258$ ft., then $\frac{\sigma}{r} = 0.041 \text{ \#/ft}^2$ and $\rho gh = 16.1 \text{ \#/ft}^2$. Thus, the magnitude

of the capillary pressure compared to the hydrostatic pressure is approximately three-tenths of one percent. This example is typical, and it is concluded that capillary forces can safely be assumed negligible in experimental work on this scale and with the magnitude of velocities encountered.

6. Discussion of Shock-Wave Shape

The vertical accelerations along the shock front due to the required change in depth give rise to a series of undulations in back of the shock which dampen rapidly to an equilibrium depth along the deflector vane. However, at high Froude numbers and large deflection angles, the shock undergoes a transition from the undular form just described to a regular jump form having a rather violent roller. This transition is directly analogous to that which has been observed (Ref. 25) for the normal hydraulic jump and which is quite familiar in hydraulic practice. In fact, a useful correlation is obtained if the oblique jump is treated as a "normal" hydraulic jump by basing the Froude number on the normal component of the velocity V_1 . Thus -

$$V_{n1} = V_1 \sin \beta \quad \text{and} \quad F_{n1} = \frac{V_{n1}}{\sqrt{gh_1}}$$

This Froude number is uniquely related to the depth ratio by Eq. (8),

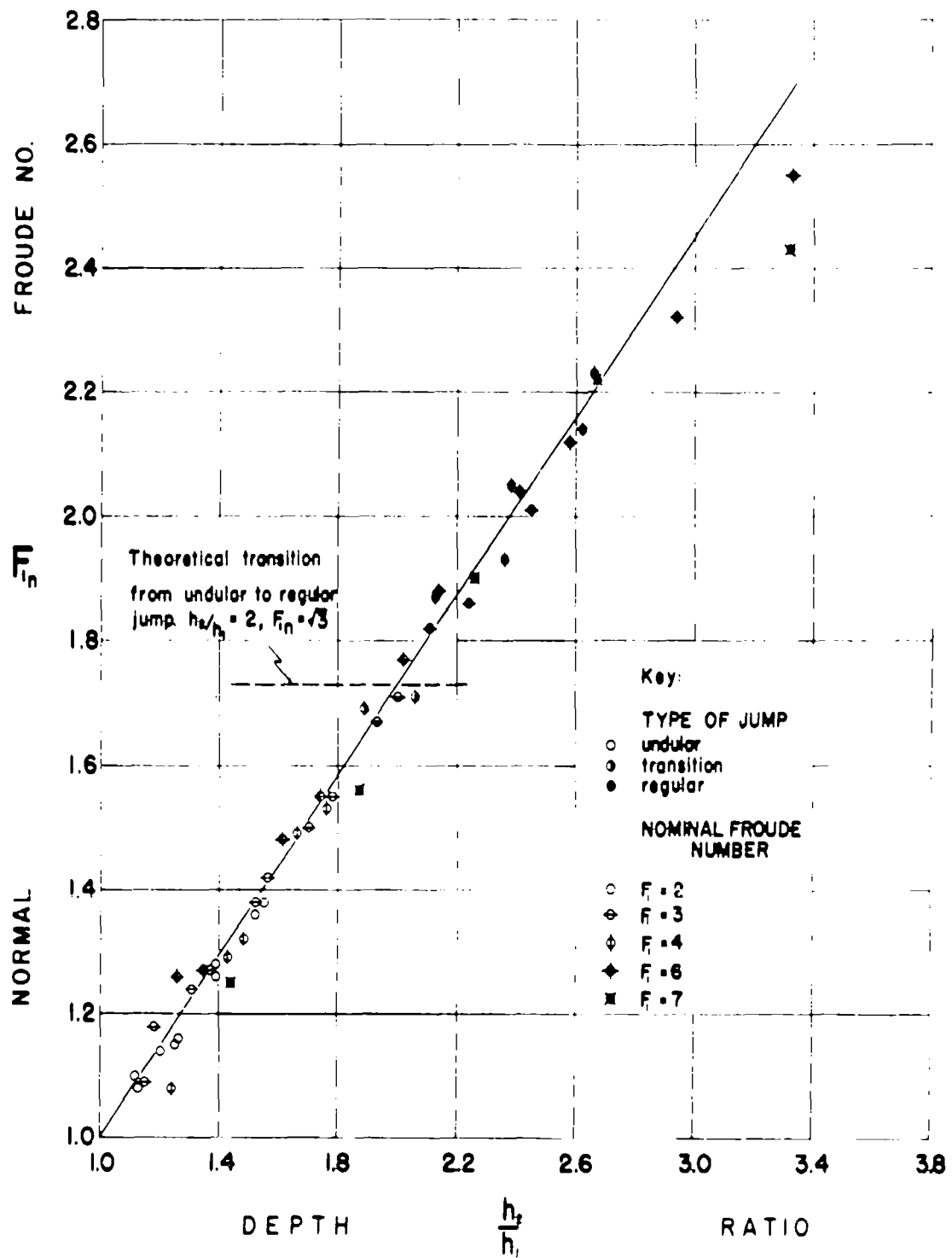
$$h_2/h_1 = \frac{1}{2} (\sqrt{8F_{n1}^2 + 1} - 1) \quad (8)$$

For each experimental run, Series B to J, the value of F_{n1} was determined from the experimental values for initial Froude number and wave angle and plotted for the corresponding experimental depth ratio. These points, together with the theoretical curve Eq. (8), are presented in Fig. 30. The experimental points were designated as undular, regular or "transition". These designations were obtained by looking at the wave profiles and deciding on the classification outlined above. For a few runs, the classification of undular or regular was not clear, and these were labeled as in "transition".

It is seen from Fig. 30 that the regions of undular and regular jumps are clear out, those jumps for which $h_2/h_1 < 2$ are undular, and for $h_2/h_1 > 2$ the jumps are regular. The depth ratio $h_2/h_1 = 2$ is the transition point according to an observation by Bakhmeteff (Ref. 25) in which it is noted that the ratio of h_2 to the total flow energy h_2/H_1 when plotted against F_{n1} reaches a maximum at $F_{n1} = \sqrt{3}$ which corresponds to a depth ratio $h_2/h_1 = 2$.

The jump form, whether undular or regular, appears to have little absolute effect upon the agreement of experiment and theory, although it is evident that as the jump becomes stronger (as measured by F_{n1}), the violent roller and accompanying fluctuations in depth make precise measurements more difficult. It seems reasonable to conclude that one useful limit of the analogy is reached for values of F_{n1} of the order of magnitude 2.5 as evidenced by the rather large deviations for points in this region in Fig. 30. This is not a serious restriction since $F_{n1} = 2.5$ requires, in general, large Froude numbers and large deflection angles. (For example $F_1 = 7.00$, $\Theta = 18^\circ$)

It is convenient at this time to discuss another physical limitation of the analogy applicable to low Froude numbers and large deflection angles. An inspection of Fig. 4 shows that for any given F_1 value, there is a maximum possible deflection angle Θ . If this value is exceeded in a channel of infinite width, theoretically the shock must detach itself and move upstream as a normal 90° jump. In a channel of finite width, this "choking" condition occurs before the limiting Θ angle is reached as described below. The initial shock wave strikes the right wall of the channel and is reflected back across the opening between the deflector vane and the wall. The flow behind the shock approaches the right hand wall with a Froude number F_2 and is directed at an angle, to this wall. If the value of Θ is below the maximum possible deflection angle corresponding to F_2 , a reflection is possible. However, a point is finally reached at which the required deflection of the flow is



CLASSIFICATION OF JUMP FORM BY USE OF
FROUDE NUMBER NORMAL TO WAVE FRONT

FIG.30

larger than is possible for F_2 and this second deflection produces a normal jump. This condition is illustrated in the photographs of the shock waves in Fig. 12(e).

The useful range of the channel can be extended slightly beyond the limit described above. Since the choking condition involves velocities near the critical, the reflections are sensitive to small changes in the flow energy. Therefore, the formation of the normal jump can be delayed by the addition of energy to the flow by means of a water jet applied near the reflection point along the right wall. This method, which does not affect conditions upstream of the reflection point, was used to obtain data for certain angles beyond the theoretical limit. Specifically, for Runs D and I corresponding to Froude numbers of 2.08 and 2.00 respectively, the jet was used to obtain a deflection angle of 12° and for Run F, ($F_1 = 3.20$), the jet was used to reach $\Theta = 21^\circ$ for the deflection vane.

It is clear, therefore, that the choking is governed by the values of F and Θ , in back of the shock. The downstream end of the deflector vane influences the conditions at the point of reflection by generating expansion waves. These expansion waves may or may not intersect the shock front upstream of the reflection point. If these expansion waves intersect the shock front, they will decrease the local values of F and the deflection Θ of the flow in back of the initial shock. Thus, the choking conditions can be governed within certain limits by reducing the length of the deflector vane.

7. Correlation of Experimental Results with Aerodynamic Theory

a. Mach Number Assumed Equal to Froude Number

The results of the hydraulic experiments on the shock characteristics for Series B through J are compared with the theoretical aerodynamic solutions for air ($\gamma = 1.4$) on the basis of the initial Mach number equal to the initial Froude number, i.e. $M_1 = F_1$. A summary of the correlation is presented in Tables VIII (a-d). Column 2 gives the Mach number equal to the initial Froude number; Column 3 lists the value of the wave angle determined from the hydraulic experiments; and Column 4 gives the calculated wave angle for air obtained from Eq. (49b) plotted in Fig. 8.

Column 5 are recorded the theoretical differences in wave angle for water and air for the same Θ and $F_1 = M_1$. In Column 6, the theoretical angle in air is compared with the experimental angle in water, and it may be noted that in practically all cases, the experimental percentage difference is less than the theoretical. The experimental deviation from the hydraulic theory is in the direction of the values expected from the aerodynamic theory. The results are illustrated in graphical

form in Fig. 31. A similar analysis is given in Columns 7 to 10 for the density ratio, and it is noted that in this case the theoretical and experimental differences are of the same order of magnitude. However, in some cases the experimental difference is larger. Figure 32 gives the latter results in graphical form.

b. On Basis of Modified Analogy

Figures 31 and 32 illustrate clearly the basis of the modification to the analogy as described in section II in which the Mach or Froude number is adjusted to produce similar geometry of flow. It is seen that if the initial Mach numbers were reduced slightly, both the shock angle and the density ratio would show better agreement with experimental points. Following the exact modification described previously for single shocks, an adjusted Mach number is obtained for each deflection angle Θ , and Froude number F_1 . The theoretical air curves would then become identical with the theoretical hydraulic curves shown in Figs. 19 and 20.

In effect, this procedure reduces the theoretical difference between water and air quantities to zero. Thus, the results of the hydraulic experiments may be interpreted as aerodynamic quantities with the same degree of accuracy as was originally obtained between experiment and hydraulic theory. The Mach numbers may be adjusted by using Fig. 7 and reading the F_1/M_1 value for each F_1 and h_2/h_1 or more conveniently from Fig. 33a in which the ratio F/M is plotted against F with Θ as the independent variable. For example in Run J, $F_1 = 4.18$ for $\Theta = 9^\circ$ the value of F_1/M_1 from Fig. 33a is $F_1/M_1 = 1.082$ and therefore $M_1 = 3.86$.

An experimental value for the F_1/M_1 ratio may be obtained for comparison with the theoretical value by calculating an "experimental" Mach number based on Θ and β_{exp} which will give the experimental flow geometry. For the above example $\Theta = 9^\circ$ and $F_1 = 4.18$, $\beta_{\text{exp}} = 21.45^\circ$ and the corresponding M_1 from Eq. (49b) is $M_1 = 3.97$. Therefore, the ratio $(F_1/M_1)_{\text{exp}} = 1.052$. These values have been calculated for Runs B through J and plotted in Fig. 33b. While the points scatter considerably, the dashed curves indicate the general trend. This scattering of experimental values is to be expected inasmuch as the ratio F/M is extremely sensitive to experimental error; it can be seen that the experimental curves have the same shape but indicate a smaller overall correction.

$$X = c_2/c_1$$

	(1) Wall Angle	(2) Mach Number	(3) Wave Angle	(4) Wave Angle	(5) Theor. % Diff.	(6) Exper. % Diff.	(7) Density Ratio	(8) Density Ratio	(9) Theor. % Diff.	(10) Exper. % Diff.
Run	Θ	M_1	β (Exp) Water	β (Calc) Air	β (Calc) Air vs β (Exp) Water	β (Calc) Air vs β (Exp) Water	X (Exp) Water	X (Calc) Air	X (Calc) Air vs Water vs X (Exp) Water	X (Calc) Air vs Water vs X (Exp) Water
I-1	3°	2.00	33.40°	32.50°	-2.1%	-2.8%	1.12	1.13	+0.9%	+0.9%
I-2	6°	2.00	35.25°	35.27°	-3.8%	-0.6%	1.25	1.26	0	+0.8%
I-3	9°	2.00	39.06°	38.27°	-5.3%	-2.0%	1.39	1.41	+0.7%	+1.4%
I-4	12°	2.00	42.96°	41.55°	-7.3%	-3.4%	1.52	1.56	+1.3%	+2.6%
D-1	3°	2.08	31.70°	31.19°	-2.3%	-1.7%	1.13	1.13	0	0
D-2	6°	2.08	33.86°	33.96°	-3.4%	+0.3%	1.26	1.27	+0.8%	+0.8%
D-3	9°	2.08	38.20°	36.77°	-5.3%	-3.9%	1.39	1.42	+1.4%	+2.1%
D-4	12°	2.08	41.56°	39.97°	-6.9%	-4.0%	1.55	1.58	+1.9%	+1.9%
B-1	3°	3.06	20.90°	21.30°	-2.3%	+1.9%	1.15	1.18	+0.8	+2.5%
B-2	6°	3.06	24.06°	23.60°	-4.2%	-1.9%	1.31	1.38	+1.4%	+5.1%
B-3	9°	3.06	27.00°	26.13°	-5.4%	-3.2%	1.52	1.59	+1.9%	+4.4%
B-4	12°	3.06	29.46°	28.88°	-6.1%	-2.0%	1.70	1.82	+3.3%	+6.6%
B-5	15°	3.06	33.26°	31.83°	-6.7%	-4.5%	1.93	2.05	+4.4%	+5.8%
B-6	18°	3.06	36.60°	35.10°	-6.7%	-4.3%	2.11	2.28	+4.8%	+7.5%

AIR CORRELATIONS SUMMARIZED
TABLE VIII-a

$$X = \rho_2 / \rho_1$$

	(1) Wall Angle	(2) Mach Number	(3) Wave Angle	(4) Wave Angle	(5) Theor. % Diff.	(6) Exper. % Diff.	(7) Density Ratio	(8) Density Ratio	(9) Theor. % Diff.	(10) Exper. % Diff.
	Θ	M_1	β (Exp) Water	β (Calc) Air	β (Calc) Air vs β (Calc) Water	β (Calc) Air vs β (Exp) Water	X (Exp) Water	X (Calc) Air	X (Calc) Air vs Water	X (Calc) Air vs X (Exp) Water
P-1	3°	3.20	21.76°	20.33°	-2.3%	-7.0%	1.18	1.19	+0.8%	+0.8%
P-2	6°	3.20	23.45°	22.63°	-4.3%	-3.6%	1.37	1.40	+1.4%	+2.1%
P-3	9°	3.20	26.20°	25.17°	-5.3%	-4.1%	1.56	1.62	+2.5%	+3.7%
P-4	12°	3.20	28.95°	27.93°	-6.0%	-3.7%	1.80	1.86	+2.7%	+3.2%
P-5	15°	3.20	32.35°	30.87°	-6.4%	-4.8%	2.00	2.10	+4.8%	+4.8%
P-6	18°	3.20	35.55°	34.08°	-6.4%	-4.3%	2.24	2.35	+5.5%	+4.7%
P-7	21°	3.20	39.00°	37.53°	-6.1%	-3.9%	2.45	2.58	+5.4%	+5.0%
C-1	3°	3.80	17.40°	17.30°	-2.9%	-0.6%	1.20	1.22	0	+1.6%
C-2	6°	3.80	19.85°	19.60°	-4.1%	-1.3%	1.43	1.47	+1.4%	+2.7%
C-3	9°	3.80	23.10°	22.13°	-5.3%	-4.4%	1.60	1.75	+3.4%	+5.1%
C-4	12°	3.80	26.45°	24.88°	-5.7%	-6.3%	1.89	2.02	+4.0%	+6.4%
C-5	15°	3.80	29.55°	27.83°	-6.0%	-6.2%	2.13	2.32	+5.6%	+8.2%
C-6	18°	3.80	32.65°	31.03°	-5.5%	-5.2%	2.88	2.61	+6.1%	+8.8%
C-7	21°	3.80	36.00	34.38	-5.0%	-4.7%	2.66	2.88	+6.3%	+7.6%

AIR CORRELATIONS SUMMARIZED
TABLE VIII-b

$$x = c_2/c_1$$

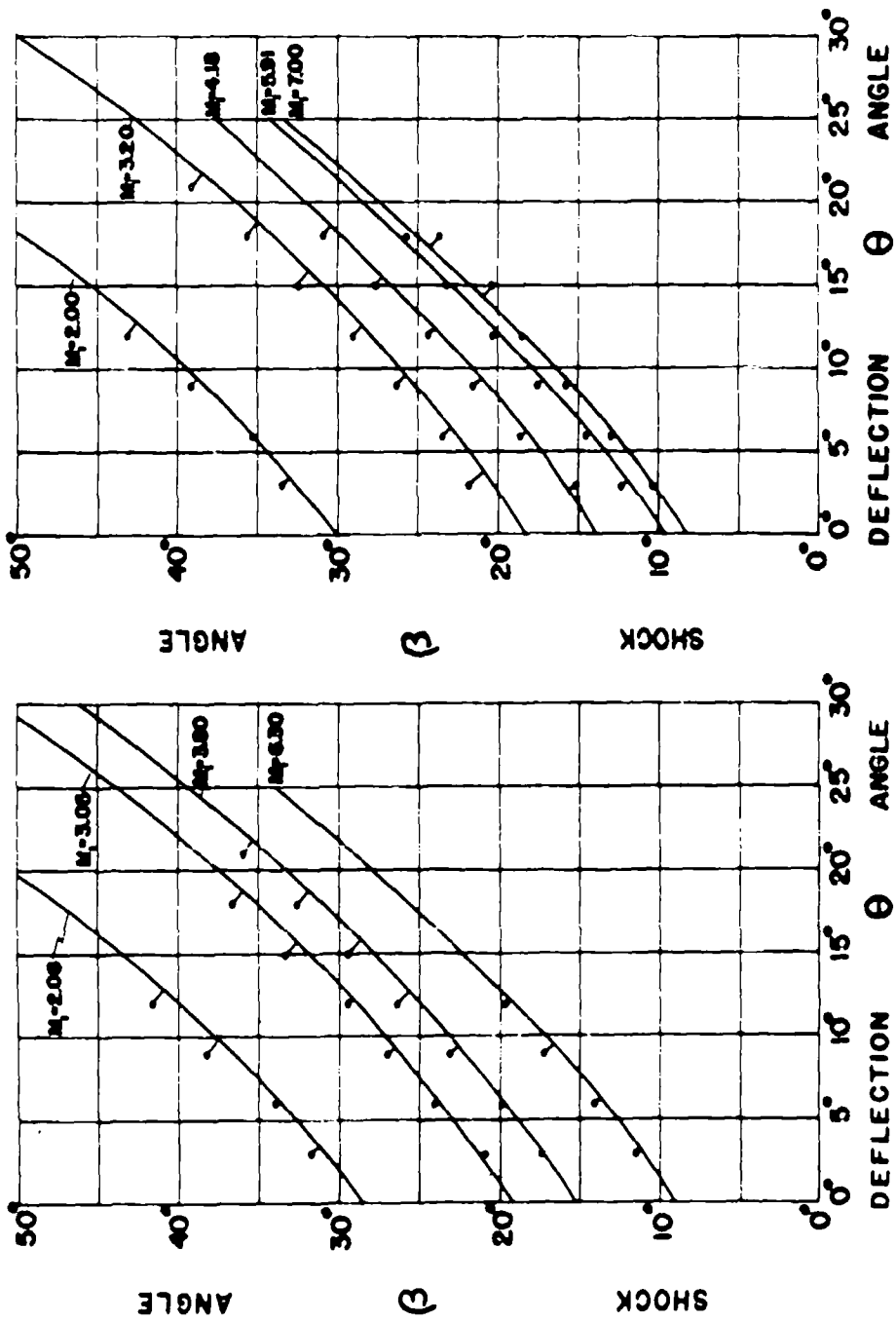
	(1) Wall Angle	(2) Mach Number	(3) Wave Angle	(4) Wave Angle	(5) Theor. % Diff.	(6) Exper. % Diff.	(7) Density Ratio	(8) Density Ratio	(9) Theor. % Diff.	(10) Exper. % Diff.
Run	Θ	M_1	β (Exp) Water	β (Calc) Air	β (Calc) Air β (Calc) Water	β (Exp) Water β (Exp) Water	X (Exp) Water	X (Calc) Air	X (Calc) Air vs Water	X (Calc) Air vs X (Exp) Water
J-1	3°	4.18	15.05°	15.83°	-3.0%	+4.9%	1.24	1.25	+0.8%	+0.8%
J-2	6°	4.18	18.50°	18.08°	-4.5%	-2.3%	1.48	1.53	+2.6%	+3.3%
J-3	9°	4.18	21.45°	20.67°	-5.5%	-3.8%	1.76	1.83	+3.8%	+3.8%
J-4	12°	4.18	24.25°	23.33°	-6.3%	-3.9%	2.06	2.16	+5.8%	+3.9%
J-5	15°	4.18	27.60°	26.42°	-5.4%	-4.5%	2.36	2.46	+5.7%	+4.1%
J-6	18°	4.18	30.85°	29.62°	-5.0%	-4.1%	2.62	2.76	+5.8%	+5.1%
G-1	3°	5.91	12.36°	11.75°	-3.8%	-5.1%	1.26	1.35	+0.7%	+6.7%
G-2	6°	5.91	14.50°	14.08°	-5.9%	-3.0%	1.61	1.77	+3.9%	+9.0%
G-3	9°	5.91	17.40°	16.75°	-5.1%	-3.9%	2.02	2.21	+5.0%	+8.6%
G-4	12°	5.91	20.25°	19.67°	-4.6%	-2.9%	2.41	2.64	+5.7%	+8.7%
G-5	15°	5.91	23.15°	22.75°	-3.5%	-1.8%	2.94	3.08	+5.8%	+4.5%
G-6	18°	5.91	25.60°	26.03°	-2.6%	+1.7%	3.33	3.46	+4.9%	+3.8%

AIR CORRELATIONS SUMMARIZED
TABLE VIII-c

$$X = \rho_2 / \rho_1$$

Run	(1) Wall Angle	(2) Mach Number	(3) Wave Angle (β Water)	(4) Wave Angle (β Air)	(5) Theor. % Diff. (β Calc) Air (β Calc) Water	(6) Exper. % Diff. (β Exp) Air (β Exp) Water	(7) Density Ratio	(8) Density Ratio	(9) Theor. % Diff. X (Calc) Air vs X (Exp) Water	(10) Exper. % Diff. X (Calc) Air vs X (Exp) Water
	θ	M_1								
H-1	3°	6.30	11.55°	11.17°	-3.9%	3.4%	1.35	1.37	+0.7%	+1.5%
H-2	6°	6.30	14.15°	13.53°	-5.5%	-4.6%	1.74	1.84	+4.9%	+5.4%
H-3	9°	6.30	17.25°	16.20°	-5.6%	-6.5%	2.14	2.31	+6.5%	+7.4%
H-4	12°	6.30	19.65°	19.17°	-4.3%	-2.5%	2.58	2.76	+6.2%	+6.5%
E-1	3°	7.00	10.30°	10.28°	-2.6%	-0.2%	1.44	1.41	+0.0%	-2.1%
E-2	6°	7.00	12.90°	12.67°	-5.8%	-1.8%	1.87	1.92	+4.9%	+2.6%
E-3	9°	7.00	15.70°	15.42°	-6.1%	-1.8%	2.26	2.46	+6.5%	+8.1%
E-4	12°	7.00	18.45°	18.42°	-3.7%	-0.2%	2.67	2.97	+6.4%	+10.1%
E-5	15°	7.00	20.30°	21.63°	-2.2%	+6.2%	3.32	3.42	+4.7%	+2.9%
E-6	18°	7.00	23.55°	24.98°	-0.9%	+5.7%	4.00	3.82	+2.6%	-4.5%

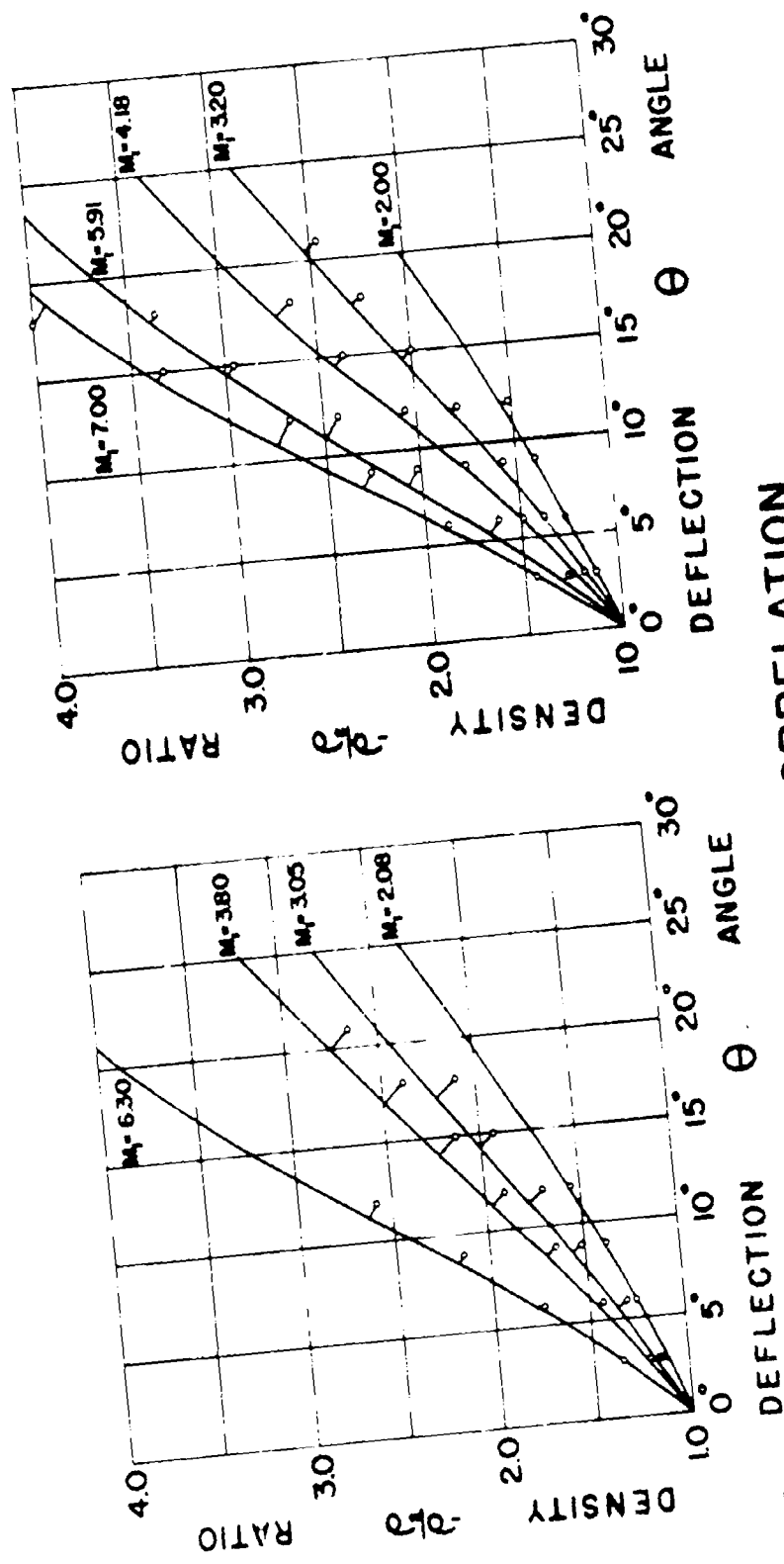
AIR CORRELATIONS SUMMARIZED
TABLE VIII-d



AIR CORRELATION

COMPARISON OF HYDRAULIC EXPERIMENTS WITH AERODYNAMIC THEORY BY DIRECT ANALOGY

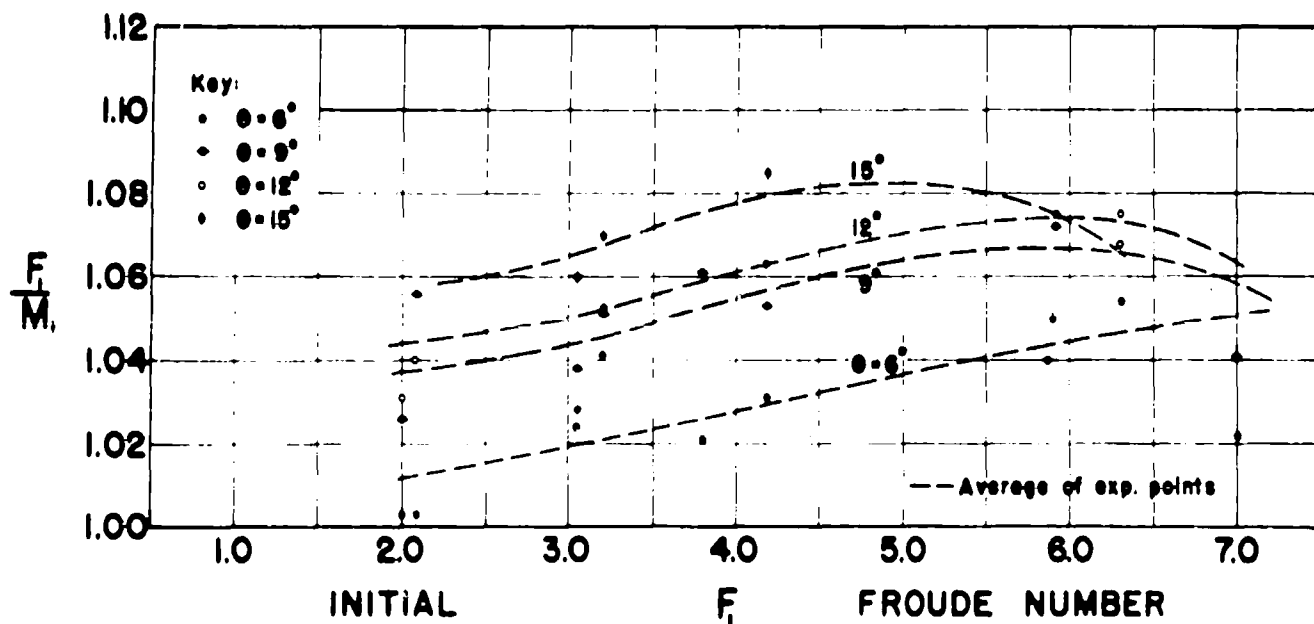
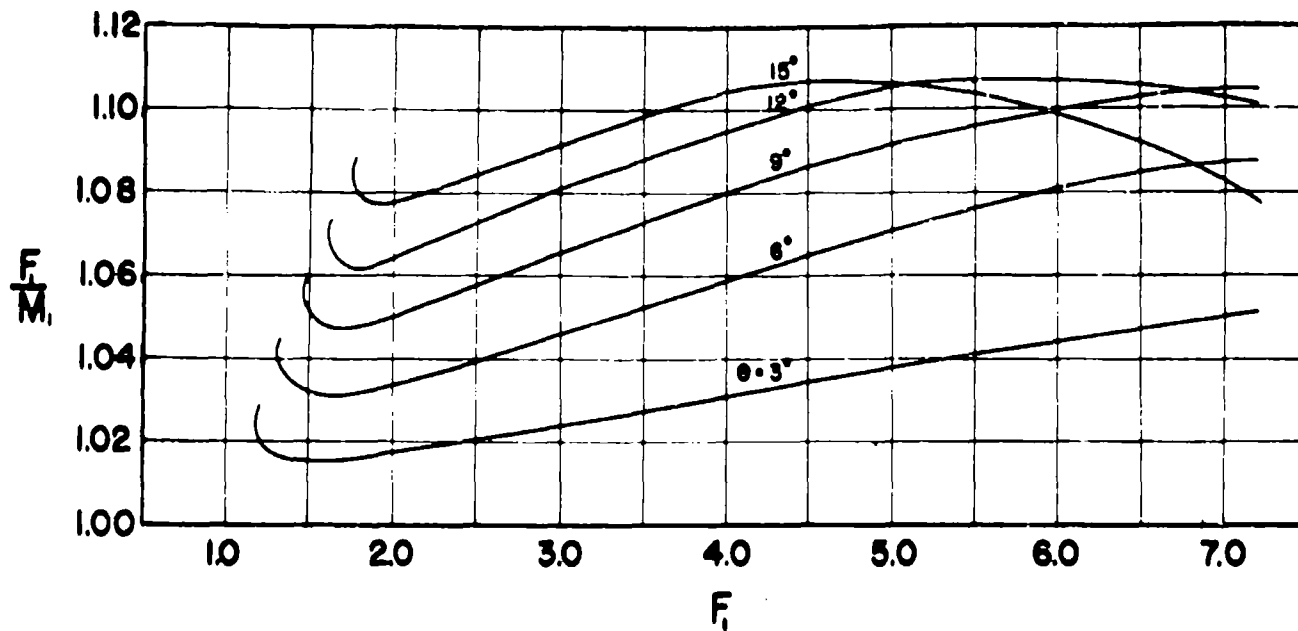
FIG. 31



AIR CORRELATION

COMPARISON OF HYDRAULIC EXPERIMENTS WITH
AERODYNAMIC THEORY BY DIRECT ANALOGY

FIG. 32



COMPARISON OF THEORETICAL AND EXPERIMENTAL VALUES
OF F_1 AND M_1 TO PRODUCE SIMILAR GEOMETRY OF FLOW

FIG. 33

SECTION V

SUMMARY OF CONCLUSIONS

1. The experimental program was primarily concerned with the verification of the theory of oblique shock waves in water. It has been demonstrated that there is satisfactory quantitative agreement between theory and experiment.
2. The non-uniform velocity distribution inherent in the experimental method has a negligible influence upon the results.
3. The geometric dissimilarity between aerodynamic and hydraulic shock waves can be largely compensated by selecting adequate model dimensions. Usually large ratios of longitudinal dimensions to depth should be employed.
4. The use of an induced initial boundary layer at a point of flow deflection is an effective means of reducing the initial distortion of the basic wave form and has no effect on final equilibrium conditions. This consideration may have an important bearing upon the size of the model.
5. The effect of surface tension can be made negligible by the use of reasonably large models, depths and velocities.
6. The practical limits of the analogy in regard to maximum Froude numbers and deflection angles are consistent with the range in which the supersonic flow theory applies.
7. By means of the so-called first modification of the analogy, satisfactory conversion from hydraulic measurements to aerodynamic quantities is possible.
8. The second modification of the analogy improves considerably the quantitative conversion from hydraulic measurement to corresponding aerodynamic quantities. The application of the method requires, however, a certain technique of interpretation and must be adapted to the problem at hand following the methods outlined.

Finally, it must be understood that no claim is made at this time as to the general applicability of the methods proposed towards a solution of complex problems of two dimensional supersonic flow. However, it is felt that these methods are promising if they are applied with a sound knowledge of all hydraulic factors involved in water channel operation and therefore of the resources which offer themselves to the experienced investigator. This latter restriction is, of course, not peculiar to this research tool alone, but applies to most experimental techniques.

BIBLIOGRAPHICAL REFERENCES

- (1a) A. T. Ippen and R. T. Knapp. A Study of High Velocity Flow in Curved Channels of Rectangular Cross Section. Transactions of the American Geophysical Union. 17th Annual Meeting, 1936. pp 516-521. (Unclassified, English)
- (1b) A. T. Ippen and R. T. Knapp. Experimental Investigations of Flow in Curved Channels. Abstract of results and recommendations. U.S. Engineer Office, Los Angeles, California, 1938. 2 Volumes. (Unclassified, English)
- (1c) A. T. Ippen and R. T. Knapp. Curvilinear Flow of Liquids with Free Surfaces at Velocities above that of Wave Propagation. Proceedings of the 5th International Congress of Applied Mechanics, 1938. pp 531-536. (Unclassified, English)
- (2) D. Riabouchinsky. Sur l'Analogie Hydraulique des Mouvements d'un Fluide Compressible. Compt. Rend. de l'Academie des Sciences. Volume 195, 1932, and Volume 199, 1934. (Unclassified, French)
- (3) T. von Karman. Eine praktische Anwendung der Analogie zwischen Uberschallströmung in Gasen and Überkritischer Strömung in Offenen Gerinnen. Zeitschrift für ang. Math. und Mechanik, No. 1, 1938 (Unclassified, German)
- (4a) E. Preiswerk. Application of the Methods of Gas Dynamics to Water Flows with Free Surface. Part I. Flows with no Energy Dissipation. Institut für Aerodynamik Eidgenössische, Technische Hochschule, Zurich. N.A.C.A. Technical Memo 934. (Unclassified, English)
- (4b) E. Preiswerk. Application of the Methods of Gas Dynamics to Water Flows with Free Surface. Part II. Flows with Momentum Discontinuities. Institut für Aerodynamik Eidgenössische, Technische Hochschule, Zurich. N.A.C.A. Technical Memo 935. (Unclassified, English)
- (5) Johnson & Witbeck. Water Analogy to Two-Dimensional Air Flow. General Electric Company. Report No. 55218, 1941. (Unclassified, English)
- (6) North American Aviation Inc. Application of the Water Channel - Compressible Gas Analogy. Report No. Na-47-87, March 3, 1947. (Unclassified, English)
- (7) North American Aviation Inc. An Experimental Investigation of Several Techniques for Obtaining Photographs of Waves formed in Water Channels. AL No. 129, March 7, 1947. (Unclassified, English)

BIBLIOGRAPHICAL REFERENCES

- (8) M. P. Barschdorf and H. G. Woodbury. Standing Waves in Supercritical Flow of Water. S.M. Thesis. Civil Engineering Dept., M.I.T., 1947 (Unclassified, English)
- (8a) J. C. Adams, Jr. Channel Transitions in Supercritical Flow of Water. S.B. Thesis. Civil Engineering Dept., M.I.T., 1948. (Unclassified, English)
- (9) K. Goldman & S. Meerbaum. Hydraulic Analogy of Supersonic Flow of Compressible Flow. S.M. Thesis. Mechanical Engineering Dept., M.I.T., 1948. (Unclassified, English)
- (10) N. S. Mumford, Jr. A Hydraulic Analogy of Supersonic Flow of Compressible Fluid. S.M. Thesis. Mechanical Engineering Dept., M.I.T., 1947. (Unclassified, English)
- (11) B. D. Langtry. A Study of Supersonic Diffusers - An Application of the Hydraulic Analogy. S.M. Thesis. Mechanical Engineering Dept., M.I.T., 1947. (Unclassified, English)
- (12) F. L. Giraud. Experimental Studies on Supersonic Cascades using Water Analogy. S.M. Thesis. Mechanical Engineering Dept., M.I.T., 1948. (Unclassified, English)
- (13) Gilmore & Flesset. The Analogy between the Flow of a Liquid with a Free Surface and the Two-Dimensional Flow of a Gas. Memo. Report No. M-54.1, California Institute of Technology, March 1949. (Unclassified, English)
- (14) H. E. Crossley, Jr. The Analogy between Surface Shock Waves in a Liquid and Shocks in Compressible Gases. Report No. N-54.1, California Institute of Technology, August 1949. (Unclassified, English)
- (15) J. W. Orlin, N. J. Lindner & J. G. Bitterly. Application of the Analogy between Water Flow with a Free Surface and Two-Dimensional Compressible Gas Flow. N.A.C.A. Technical Note 1186. (Unclassified English)
- (16a) A. T. Ippen. Mechanics of Supercritical Flow. Proceedings of the A.S.C.E., November 1949, Volume 75, No. 9. pp 1290-1317. (Unclassified, English)
- (16b) R. T. Knapp. Design of Channel Curves for Supercritical Flow. Proceedings of the A.S.C.E. November 1949, Volume 75, No. 9. pp 1318-1347. (Unclassified, English)

BIBLIOGRAPHICAL REFERENCES

- (16c) A. T. Ippen and J. H. Dawson. Design of Channel Contractions. Proceedings of the A.S.C.E. November 1949, Volume 75, No. 9. pp 1348-1368. (Unclassified, English)
- (16d) H. Rouse, B. V. Bhoota, E-Y. Hsu. Design of Channel Expansions. Proceedings of the A.S.C.E. November 1949, Volume 75, No. 9. pp 1369-1385. (Unclassified, English)
- (17) Ivey, Stickle & Schuettler. Charts for Determining the Characteristics of Sharp Nose Airfoils in Two-Dimensional Flow at Supersonic Speeds. N.A.C.A. Technical Note 1143. (Unclassified, English)
- (18) W. E. Moeckel & J. F. Connors. Charts for the Determination of Supersonic Air Flow against Inclined Planes and Axially Symmetric Cones. N.A.C.A. Technical Note 1373. (Unclassified, English)
- (19) Marie A. Burcher. Compressible Flow Tables for Air. N.A.C.A. Technical Note No. 1592, August 1948. (Unclassified, English)
- (20) Mary M. Neice. Tables and Charts of Flow Parameters across Oblique Shocks. N.A.C.A. Technical Note No. 1373, Aug. 1948. (Unclassified English)
- (21) Edmonson, Murnaghan & Snow. Theory and Practice of Two-Dimensional Supersonic Pressure Calculations. Bumble Bee Report No. 28. Johns Hopkins University, Applied Physics Lab., Dec. 1946. (Unclassified, English)
- (22) G. H. Keulegan & G. W. Patterson. Mathematical Theory of Irrotational Translation Waves. RP 1272, Journal of Research of National Bureau of Standards, January 1940. (Unclassified, English)
- (23) G. H. Keulegan. Laws of Turbulent Flow in Open Channels. RP 1161, Journal of Research of the National Bureau of Standards, December 1938. (Unclassified, English)
- (24) V. Vanoni. Velocity Distribution in Open Channels. "Civil Engineering", June 1941, p 366. (Unclassified, English)
- (25) B. A. Bakhmeteff & A. E. Matzke. The Hydraulic Jump in Terms of Dynamic Similarity. Transactions of the A. S.C.E., No. 101, 1938, p 830. (Unclassified, English)
- (26) A. T. Ippen. Gas Wave Analogies in Open Channel Flow. Bulletin 27, Proceedings of Second Hydraulics Conference, University of Iowa, 1943. pp 248-265. (Unclassified, English)

BIBLIOGRAPHICAL REFERENCES

- (27) J. J. Stoker. Formation of Breakers and Bores. Committee on Applied Mathematics, Volume 1, No. 1, January 1948. (Unclassified, English)
- (28) Air Materiel Command, Wright AF Base. Method of Characteristics in Compressible Flow. Technical Report No. W-TR-1178 (Unclassified, English)
- (29) A. Busemann. Compression Shocks in Two-Dimensional Gas Flows. N.A.C.A. Technical Memo 1189, 1949. (Unclassified, English)
- (30) Courant & Friedrichs. Supersonic Flow and Shock Waves. Interscience Publishers, Inc., 215 4th Ave., N.Y. 3, N.Y. (Unclassified, English)
- (31) A. H. Shapiro. An Appraisal of the Hydraulic Analogue to Gas Dynamics. Meteor Report No. 34, April 1949. Dept. of Mechanical Engineering, M.I.T. (Unclassified, English)

TITLE: Studies on the Validity of the Hydraulic Analogy to Supersonic Flow - Parts I and II (AF Technical Report)						ATI- 77 510
AUTHOR(S) : Harleman, Donald R. F. ORIG. AGENCY : Massachusetts Institute of Technology, Cambridge PUBLISHED BY : AMC, Wright-Patterson Air Force Base, Dayton, O.						REVISION (None) ORIG. AGENCY NO. (None) PUBLISHING AGENCY NO. AF-TR 5985 Parts I and II
DATE	U.S. CLASS.	COUNTRY	LANGUAGE	PAGES	ILLUSTRATIONS	PHOTOS, tables, diagrs, graphs
May ' 50	Unclass.	U. S.	English	101		
ABSTRACT: The design, construction, adjustment, calibration and instrumentation of a high velocity flow channel suitable for experimental investigations of the hydraulic analogy to supersonic flow is described. Method of setting up initial flow conditions is discussed. Previous experimental work both on supercritical flow and on the hydraulic analogy is reviewed, and abstracts of the pertinent investigations are presented. Experiments were carried out to determine factors affecting the frictional distortion of the basic wave form and to determine the influence of non-uniform velocity distribution and boundary layer development. The hydraulic analogy for supersonic flow with shocks is presented, and two possible modifications in the analogy are proposed which promise improvements in the method of obtaining quantitative aerodynamic information from water measurements for the simple shock wave patterns.						
DISTRIBUTION: Copies of this report obtainable from CADO.						
AD-A800 135				SUBJECT HEADINGS: Flow, Supersonic Boundary layer - Velocity distribution <i>CFSTI per ASD ltr 17 Mar 67</i>		
Central Air Documents Office Wright-Patterson Air Force Base, Dayton, Ohio				CADO 1. JICAL INDEX		USAF Contr. No. W33-038-ac-16703